Appendix 4

A Report on the Flight Dynamics of the Fokker F-28 Mk 1000 as They Pertain to the Accident at Dryden, Ontario, March 1989

J.M. Morgan
G.A. Wagner
R.H. Wickens

November 22, 1989

LIMITED
UNCLASSIFIED

Canada

A REPORT ON THE FLIGHT DYNAMICS OF THE FOKKER F-28 Mk 1000 AS THEY PERTAIN TO THE ACCIDENT AT DRYDEN, ONTARIO, MARCH 1989

Prepared by

J.M. Morgan
Flight Research Laboratory
National Aeronautical Establishment

G.A. Wagner
Air Canada and CALPA

R.H. Wickens
Low Speed Aerodynamics Laboratory
National Aeronautical Establishment

OTTAWA
NOVEMBER 22, 1989

NAE MISC 64

National Research Council Canada
Conseil national de recherches Canada

Copy # 12

Copy #12

A REPORT ON THE FLIGHT DYNAMICS OF THE FOKKER F-28 Mk 1000 AS THEY PERTAIN TO THE ACCIDENT AT DRYDEN, ONTARIO, MARCH 1989

Prepared by

J.M.Morgan
Flight Research Laboratory
National Aeronautical Establishment

G.A.Wagner
Air Canada and CALPA

R.H.Wickens
Low Speed Aerodynamics Laboratory
National Aeronautical Establishment

Ottawa
November 22, 1989

STATEMENT OF OWNERSHIP

F-28 FLIGHT DYNAMICS
TABLE OF CONTENTS

SECTION 1 - GENERAL INTRODUCTION

SECTION 2 - AERODYNAMICS

F-28 FLIGHT DYNAMICS
SECTION 1

OVERVIEW AND GENERAL INTRODUCTION

INTRODUCTION

In March 1989 a Fokker F-28 Mk1000, C-FONF, operated by Air Ontario crashed while attempting a take-off at Dryden, Ontario, under adverse weather conditions. The accident investigation is taking the form of a Judicial Enquiry and as such persons not normally a part of the Canadian aviation accident investigative group are assisting or participating in the enquiry. A sub committee of the full fact gathering team has been designated the Performance Sub Committee or the Performance Steering Group and has been charged with investigating the take off performance of the F-28 aircraft and the effects thereon of the environmental conditions existing at the time of the accident. This paper is a distillation of the work of three members of this Steering Group, namely:

J.M.Morgan	National Aeronautical Establishment
G.A.Wagner	Air Canada and CALPA
R.H.Wickens	National Aeronautical Establishment

The three authors represent considerable expertise in a variety of appropriate disciplines. Mr Wickens is a specialist in low speed aerodynamics, Mr Wagner is a practising airline pilot who is also a qualified aeronautical engineer and assistant university professor, while Mr Morgan is a physics graduate and an engineering test pilot with extensive experience in real-time software and mathematical modelling techniques.

DOCUMENT ORGANISATION

The document has been divided up into Sections describing the various aspects of the work conducted, namely:

Section 1. This section is a general introduction and gives a brief overview of information available to the group and the kinds of investigations carried out in support of the enquiry.

Section 2. This section provides in depth background information into the aerodynamics of lift and drag, the effects of surface roughness (contamination) on the performance of an aerofoil and some detailed analysis of the F-28 wing.

Section 3. In Section 3 dynamic man-in-the-loop simulations carried out during a visit to the Fokker plant are described together with tentative conclusion drawn from them.

Section 4. Here analytical mathematical modelling of the F-28 is described in detail and sample trajectories for a F-28 aircraft attempting take off in the presence of flying surface and runway contamination are presented. The results are interpreted and conclusions based on the off-line modelling are discussed.

Section 5. This section deals with validation of the mathematical models described in Section 4.

Section 6. This section completes the document with a brief discussion of the results and offers conclusions as to the engineering reasons for the trajectory observed at the Dryden accident.

OBJECTIVES

The objective of the simulation work was to develop a range of possible flight path scenarios which were similar to that flown by the crew of the F28-MK1000 in the Dryden accident and from that determine a range of conditions which could have caused such a trajectory. The aerodynamic analyses were performed to support the simulation efforts and to provide enhanced background for the accident analysis and investigation.

THE INVESTIGATIVE PROCESS

For some decades now, civil transport aircraft have been required to carry Flight Data Recorders (FDR) and Cockpit Voice Recorders (CVR), devices that record a variety of aircraft state, configuration, power plant and crew activity parameters. These devices are built to withstand high levels of impact and certain exposure to fire while retaining their data in a recoverable fashion. When these recorders are recovered intact and useable after a crash, flight path re-construction is usually possible with a high level of confidence and such re-constructions can be invaluable in determining possible or probable causes of the accident.

Unfortunately the FDR aboard the Dryden aircraft did not survive in a readable state due to an intense post-crash fire. This meant that the group had only the accounts of eye witnesses on which to base any assumptions as to the aircraft's pre-crash behaviour. Luckily there were a comparatively large number of witnesses, including survivors and amongst the latter were several professional pilots, whose recollections have proved very valuable. There was also reasonable agreement among the witness reports as to the trajectory of the aircraft prior to crash, while analysis of tree impacts conducted by personnel of the Canadian Aviation Safety Board (CASB) shed some light on the flight path just prior to the final impact.

GENERAL CONDITIONS OF ACCIDENT

From witness's statements or interviews and the impact swath through the trees, there are some general prima facie conclusions which can be drawn, these are:

The aircraft's wing was, to some extent or other contaminated with snow and or slush at the start of the take-off run, and was at least partially contaminated up to the point of rotation.

The wing trailing-edge flaps were set to 18 degrees at the start of the take-off run and were at or near 25 degrees at the point of impact.

The engines functioned normally throughout the take-off attempt.

The aircraft rotated for the first time rather later than normal, either became briefly airborne or partially so, un-rotated temporarily, re-rotated and became airborne at very low level at or close to the end of the runway. It remained at very low level (failed to climb) until impact.

There is a very high probability that the runway was contaminated with snow or slush at the time of the take off attempt.

ASSUMPTIONS

In this case due to the lack of factual numerical data, the only way to attempt to re-create the flight path was by assuming certain details about the aircraft's mechanical and operational status, and then using a mathematical simulation and varying parameters which were possibly related to the reason the aircraft failed to fly.

The resulting flight paths were then compared with witness reports and other analyses of the aircraft's trajectory. These simulator studies were set up to produce the same forms of numerical and graphical output as would be obtained from a FDR analysis. Simulator studies were conducted both in a real-time dynamic engineering simulator at Fokker in Holland and by the use of mathematical flight path simulations based on aircraft performance data supplied by the manufacturer. The off-line simulations were written and developed by members of the sub-committee on performance.

These studies assume, based on information provided to us by other groups involved in this investigation, that:

- The aircraft powerplants generated normal thrust throughout the takeoff (although we do consider a single powerplant failure for completeness).
- There were no structural failures prior to impact.
- There were no brake failures or seizures, or tire failures which would have extended the ground roll portion of the takeoff or rendered the aircraft incapable of achieving Vus (unstick speed).
- There were no flight control system failures.
- There was no interference in the flight control system from any source.
- The flight crew handled the aircraft with normal handling techniques.

- There were no system/instrument failures such that the flight crew was unable to fly the aircraft with the precision required for instrument flight. (An example would be failure of pitot heat so that the pilots would not have airspeed information available).

- There were no adverse wind conditions which would have affected the aircraft's performance.

Based on the above assumptions, these simulations attempt to recreate the flight profile of the aircraft by assuming a range of wing snow/ice contamination levels and runway water/slush/wet snow contamination. These simulations and the results should NOT be interpreted as defining what actually happened to the accident aircraft. Rather, the material presented in this study should be interpreted as follows:

If the aircraft suffered no other operational or technical problems other than wing contamination combined with a certain degree of rolling resistance contamination on the runway, then the results of this simulation are possibly representative of the Dryden accident flight profile. In effect, this simulation and analysis is examining a subset (primarily aerodynamic and handling parameters) of all possible factors which may have been related to this accident.

CONTAMINATED WING TAKE OFFS

There is a long history of aircraft accidents related to flight in icing conditions. Specifically, there have been a number of accidents of aircraft which took off with ice/snow contaminants adhering to the wings and other parts of the aircraft. In these cases, either the aircraft were not de-iced prior to takeoff or the time between de-icing and departure was so long that the aircraft wings were again contaminated at takeoff time.

Additionally, there have been a number of events with F28-1000 aircraft which indicated that this aircraft was no different than others of similar configuration; it is sensitive to ice and snow contaminants on the wing, especially on the first 15% of chord. Experience with the F28 indicated that early flow separation and stalling was a characteristic effect of ice and snow contaminants on the wings. Furthermore, the premature separation on F28 aircraft typically caused wing drop as a result of outer panel flow separation and wing tip stall prior to inboard wing stall. (See Section 2 for details on this characteristic). There were two F28 accidents a number of years ago, one in Turkey and the other in Hanover, Germany, which are similar in a number of characteristics to the Dryden accident.

In the Dryden accident, the witness reports of contaminant on the wings of the aircraft during the takeoff roll, combined with descriptions of the aircraft's flight characteristics during takeoff roll, rotation, liftoff, and the short airborne segment were, in general terms, similar to reports of other ice/snow related accidents. This is true of events involving both the F28 and other aircraft.

These facts, combined with the lack of FDR data, provided the rationale for a requirement to simulate the flight path of the F28-MK1000 while considering significant amounts of wing contaminant and runway contamination. The engine failure case considered in this section was studied not because we had any indication to date that one of the powerplants had failed, but rather for completeness.

GENERAL APPLICABILITY

In this study, great care has been taken to model specifically the performance of the Fokker F-28 in the presence of contamination of both the flying surfaces and the runway. The results obtained, though, should never be interpreted in any way as indicating that this specific aircraft has shortcomings in this respect to any greater or lesser extent than any other aircraft in this class. Such sensitivity to contamination as has been demonstrated in this exercise might reasonably be expected to pertain in any aircraft of this class (ie, swept wing, jet propelled) in far greater measure than is seen in other classes of aeroplane. This is vividly portrayed in Figure 1, taken directly from a Fokker publication [1], which shows the markedly more severe penalties paid for contamination by a jet as opposed to a propeller powered aircraft. Not only does the shallower lift curve slope and reduced $C_{L_{max}}$ of the swept wing make the performance more readily degradable, but the jet powered machine does not have the advantage of a relatively large area of its wing being immersed in high velocity air from the propeller slipstream, its only lift producing capability being a result of its motion relative to the air.

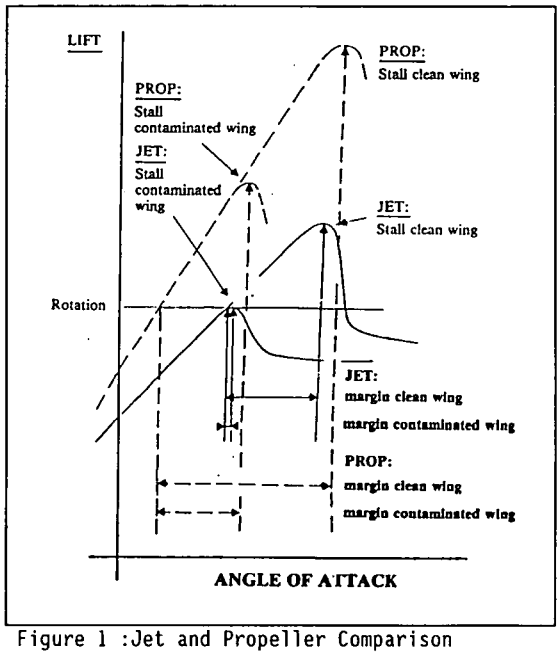

Figure 1 :Jet and Propeller Comparison

F-28 FLIGHT DYNAMICS
SECTION 2

AERODYNAMIC NOTES AND A DISCUSSION OF THE STALL AND POST STALL BEHAVIOUR

INTRODUCTION

This section of the report on flight dynamics presents a brief survey of the aerodynamic principles which are relevant to the Fokker F-28 transport aircraft, during ground roll and initial climb phase, and to degrees of wing contamination which affect that portion of the flight envelope.

Icing contamination of the lifting and control surfaces is not specifically addressed in this discussion, except in the context of roughness-induced changes to the wing characteristics, including stall and trim changes.

LIFT

The production of lift and drag on a conventional wing is a consequence of the streamline flow around the aerofoil and its smooth departure from the trailing edge. The lift force originates from the circulation and curvature of the flow over the profile and drag is a result of fluid viscosity and span loading.

The flow accelerates over the top and bottom of the aerofoil, especially near the leading edge. The pressures on both surfaces fall below ambient static pressure and the differential between these values, taken over the entire wing surface, results in a net lifting force.

The lift force is the product of flow dynamic pressure, wing area and lift coefficient, it expressed as follows:

$$L = (\tfrac{1}{2}\rho V^2) \times (S) \times (C_L) \qquad (1)$$

The lift coefficient, C_L depends on the angle of attack of the wing or aerofoil, where angle of attack is defined as the inclination of the aerofoil chord line to the oncoming flow. A similar expression for drag is:

$$D = (\tfrac{1}{2}\rho V^2) \times (S) \times (C_D) \qquad (2)$$

Lift is always at right angles to the direction of flight and drag is directed rearwards along the direction of flight. Figure 1 shows the forces on an aerofoil section in conditions of attached flow and also for separated flow, or stall. For normal attached flow the lift force can be decomposed into two components: a normal force and a force in the plane of the chord line, directed upwind. This latter force is known as leading edge suction and is caused by the curvature and acceleration of the flow around the leading edge. Achieving the full value of leading edge suction is crucial to the efficient operation of the aerofoil. If the value of the leading edge suction is reduced, or lost completely (as may be the case

when the wing is stalled) then the main force on the aerofoil, in addition to friction drag, is the normal force, whose components are a reduced lift and a significant drag component (Figure 1b).

The basic characteristics of an aerofoil can be altered by the use of camber and high lift devices.The effect of camber is to change the relationship between lift coefficient, C_L, and angle of attack (α), see Figure 2. With a cambered aerofoil, C_L has a finite value when α is zero; however, the slope of the lift curve remains unchanged. High lift devices consist of trailing edge flaps, which extend rearwards and downwards and may have complex geometries, and leading edge slats, which extend forwards and downwards and enable the flow at the leading edge to remain attached at higher angles of attack than would otherwise be the case.

The main effect of flaps is to displace the lift curve upwards by an amount which depends on flap angle and geometry (Figure 3a). Maximum C_L is increased but still occurs at an angle of attack similar to that of the unflapped wing. Flap deflection also results in a sizeable drag increment (Figure 3b).

The increment in lift achieved by flap defection results in increased flow acceleration and suction on the nose of the aerofoil. To avoid leading edge separation and to achieve the potential gains in maximum lift, special attention must be paid to the leading edge design. This is done by the use of a generous nose radius (as in the case of the F-28 wing) or by the use of a leading edge slat. Figure 3a shows the effect of the extension of leading edge devices on the lift characteristics of the basic and flapped wing. Maximum C_L is increased significantly and occurs at a greater angle of attack than with the device retracted. Drag also increases as a result of slat extension but not as much as for the extension of flaps.

The pitching moment on the aerofoil is also affected by camber and the deflection of flaps. As angle of attack increases the aerofoil pitching moment is approximately constant until the stall. After the stall the tendency is to pitch nose down. Flap extension produces a further nose down increment in the pitching moment. Pitching moment is expressed as:

$$M = (\tfrac{1}{2}\rho V^2) \times (S) \times (c) \times (C_M) \qquad (3)$$

where (c) is the characteristic length, (ie the chord length for an aerofoil) and C_M the pitching moment coefficient.

The foregoing discussion relates to the origins of lift on the wing section, or aerofoil. The lift of the complete wing is more complex, and depends upon the shape of the planform, principally the aspect ratio, (span squared/area). The vortex flow that is a fundamental characteristic of the aerofoil section, extends along the span, and leaves the wing tips in the form of wing tip vortices which stream downwind. Actually, vorticity is shed along the entire wing span in the form of a vortex sheet that subsequently rolls up at the side edges into concentrated free vortices.

For the purpose of analysis the wing can be replaced by a vortex system consisting of a bound vortex travelling with the wing, and free vortices that emanate from the wing tips and stream down wind. A schematic representation of this flow model is shown in Figure (4).

This simple concept has allowed all conventional lifting surfaces to be compared on the same basis; aerodynamic theory shows that aspect ratio is the governing physical parameter that determines lifting performance and induced drag. The slope of the lift curve is linear over the operating range of the wing, and decreases as wing aspect ratio decreases. The upper bound of the relationship is the lift curve slope of the airfoil section, corresponding to an infinite aspect ratio and it is evident from Figure 4b that a high aspect ratio is desirable for efficient flight. Conversely, a disturbance in the distribution of spanwise load, such as that caused by the deflection of trailing edge controls, or a partial stall, corresponds to a lower equivalent aspect ratio, lower lifting effectiveness and higher induced drag as compared to the undisturbed span loading.

The free vortex system behind the wing gives rise to an induced flow, the vertical component of which is termed "downwash". The momentum of this flow is imparted to the undisturbed air per unit time as the wing advances, and is directly related to lift. The energy of the complete downwash field represents the price to be paid for the generation of lift. The downwash flow in the region immediately behind the wing is important for the operation of the tail plane, and the longitudinal stability of the aircraft. Thus if aspect ratio changes, or if a local disturbance occurs on the wing surface, the downwash will be altered, the load on the tail plane will change, and the aircraft trim equilibrium will be disturbed.

DRAG

Drag forces acting on an aircraft consist of two components: pressure drag and friction drag. Pressure drag, which is parallel to the direction of motion, results from the pressure forces acting on the body. Friction drag is the sum of all the tangential forces taken in the same direction, and is the viscous component.

Pressure drag has two components: induced drag, which is dependent upon lift and wing aspect ratio; and wake or form drag, which is dependent upon the shape of the wing section, and the growth of the unseparated boundary layer. Form drag originates from a balance of the pressures over the front and rear portions of the airfoil section, and can be thought of as a buoyancy force directed rearwards.

Form or wake drag is zero if the flow is frictionless, and the external flow closes around the wing (ie. no separation). This is known as D'Alembert's paradox. In a real flow, however, where viscosity consumes the momentum next to the wing surface, the pressure over the rear portion of the airfoil is altered, and therefore no longer balances the forward pressure force. The resulting imbalance is a pressure drag and depends upon the form or profile of the airfoil. If separation, or any other disturbance occurs on the rear portion of the airfoil, this imbalance becomes very large and constitutes a significant increase in drag. Form drag and friction drag, taken together, are called profile drag, and depend on the local cross-section or profile of the wing.

The induced drag of the lifting system arises from the bound and streamwise arrangement of vorticity. In its simplest form, the wing can be thought of as a device which advances into still air, and continuously deflects downwards, a finite mass of air in the wake. This idealization, known as the streamtube concept, suggests that the trailing wake and its circulating flows are contained within a circular tube spanning the wing tips, that contains all of the momentum associated with the production of lift.

Similarly, the work done in producing this deflected streamtube, its internal flows and its downward motion, results in a drag which is dependent upon lift, and is termed induced drag.

A simple formula for total drag is as follows:

$$C_D = C_{D_o} + C_L^2/\pi(Ae) \qquad (4)$$

C_{D_o} is the viscous drag coefficient, and (Ae) is the effective aspect ratio. Lift/drag ratio, a measure of wing performance, depends upon effective aspect ratio, and profile drag.

A secondary, but important parameter in the relationship between lift and induced drag, is the distribution of aerodynamic load along the span of the wing. Induced drag is a minimum when the distribution of lift over the span is elliptic in shape and the value of the wing efficiency factor e is 1.0. Any departure from this shape, due to local separation, or deflection of controls, results in a non-optimum load distribution, a value of e less than 1.0, and higher induced drag for the same lift.

SKIN FRICTION AND THE BOUNDARY LAYER

Viscous drag resulting from the frictional force on the wing arises from the loss of momentum of the fluid that has passed over the surface. This phenomenon is confined to a thin layer adjacent to the surface, in which intense shearing takes place. The shearing stress, or frictional force per unit area, is measured by the product of the coefficient of viscosity and the velocity gradient next to the surface. Thus a gas of low viscosity can produce significant frictional drag on a smooth surface. The boundary layer, as this thin region is called, may be composed of either laminar or turbulent flow and its behaviour determines the limits of efficiency and stability of the airflow over the range of operation of the aircraft.

The initial flow in the boundary layer on a smooth surface will be smooth and orderly (ie. laminar), and the velocity increases from zero to its full value across the thin layer of the viscous region. This layer, in which momentum loss occurs, increases in thickness with distance from the leading edge; the frictional force, which depends upon the velocity gradient, diminishes in the same distance. Figure 5 shows, schematically, the main elements of the laminar and turbulent boundary layer.

Viscous drag is the sum of the frictional force over the length of the surface. Thickening of the laminar boundary layer with distance implies a continuous loss of kinetic energy dissipated by viscosity, and at some point separation will occur when the kinetic energy of the flow is sufficiently reduced. This will occur more rapidly if the flow is advancing into an adverse (positive) pressure gradient.

Transition from laminar to turbulent flow in the natural boundary layer is inevitable, and has both beneficial and adverse effects. As is known for the dimpled golf ball, a turbulent flow resists the tendency to separate with a corresponding reduction of form drag. The same observation can be made for the airfoil in which the boundary layer flow is turbulent. The tendency to separate is resisted, and the maximum lift coefficient at which the airfoil will stall is increased. The negative effect is that as far as viscous forces are concerned, the turbulent boundary layer will have a higher skin friction, and hence a higher drag than the laminar layer, even on a smooth surface.

The main criterion which determines whether or not the boundary layer is turbulent is a parameter which expresses the ratio of fluid inertial and friction forces. The parameter is the Reynold's Number[1] and it determines the relationship between the flows on similar bodies, such as the wing boundary layer flow on a full size aircraft, and its scaled-down model counterpart. Reynold's Number also determines, in both cases, when the boundary layer makes the transition from laminar to turbulent flow. Research has shown that for flow on a smooth flat plate, transition to turbulence will occur at a Reynold's number of about one million. This is well below the value for typical transport aircraft on take off, so unless the aircraft wing is designed specifically to have extensive laminar flow, it will be fully turbulent over most of its length, and therefore its flight envelope.

The turbulent boundary layer is characterized by a thick layer of turbulent mixing and dissipation. Embedded below the turbulent region is a thin laminar layer next to the surface, called the laminar sub-layer. It is in this sub-layer where the velocity gradients are high, and the frictional drag originates (Figure 5b). The flow on the airfoil at full scale Reynold's numbers is turbulent except at the nose, near the leading edge attachment point, where the boundary layer is initially laminar. Transition to turbulence occurs within a short distance, however, due to local pressure gradients and the condition of the surface.

The laminar sub-layer over the forward portion of the aerofoil chord has high levels of frictional drag, but its thickness is gradually reduced by the turbulent region adjacent to it, as the flow progresses along the chord. The initial thickness of the sub-layer is important in determining whether or not the surface can be considered aerodynamically "smooth", or "rough". This is especially critical near the nose of the airfoil, where any protuberances or roughness elements will have a serious effect further downstream: further aft on the chord

[1] Reynold's Number is defined as:

$$R_e = (\text{velocity}) \times (\text{chord}) / (\text{kinematic viscosity})$$

the rising turbulence intrudes into the sub-layer, the surface is always considered "rough", and the energy loss is due mainly to turbulent dissipation.

Because the flow at the trailing edge is theoretically a stagnation point, the external flow must decelerate before coming to rest, resulting in an adverse pressure gradient. If upstream roughness or excessive turbulent dissipation has consumed momentum in the boundary layer, it may separate, and the stall begins. As the wing incidence increases, separation becomes more wide spread until the wing is said to have stalled.

If the surface contamination elements (rivet heads, frost etc.) lie within the laminar sublayer they have virtually no effect on the total resistance. If, however, the roughness elements protrude beyond the laminar sublayer, the result is a noticeable increase in skin friction, and production of more turbulence. An increase of Reynold's number aggravates this problem since the laminar sub-layer becomes thinner at high Reynold's numbers. If the roughness height is large in comparison with the laminar sub-layer, then the frontal drag of these elements determines the average skin friction, and their shape, orientation and distribution become important. The increased turbulence and dissipation in the roughened boundary layer also leads to a premature flow separation and stall for Reynold's numbers above one million. At high Reynold's numbers nearly all of the loss of energy is due to wake formation; the resistance is independent of viscosity, and proportional to the square of the velocity. Figure 5c shows the effect of Reynold's number on drag coefficient in laminar and turbulent flow. If the surface is rough, the curve representing turbulent flow indicates an increase in skin friction drag.

Figure 6a shows the critical roughness size (in terms of percent chord) below which there is no increase in drag on a flat surface. The working range of Reynold's number for the F-28 is also indicated in this Figure. For distributed roughness greater than the critical size, Figure 6b shows the drag increase experienced by both wings and bodies, for a range of Reynold's numbers.

CHARACTERISTICS OF THE STALL OF AEROFOILS

Separation of the turbulent boundary layer is followed by partial or complete detachment of flow over the airfoil, a dramatic decrease in lift, and an increase in drag. The trailing edge no longer completely governs the strength of the circulation and vorticity is shed downwind as a turbulent wake. The chordwise distribution of pressure is greatly altered, and the resulting change in airfoil pitching moment will disturb the aircraft trim conditions. Since the pressure distribution of the stalled airfoil no longer conforms to that of attached flow, form drag will increase. Friction drag is indeterminate over the separated region, but will be active on the lower surface of the airfoil. For the complete wing, induced or vortex drag will be less, since lift is lower.

There are basically three types of aerofoil stall (illustrated in Figure B-1), and the characteristics of each are governed mainly by airfoil geometry and Reynold's number.

Type 1: Trailing Edge Stall

The trailing edge stall is the most common and desirable type of stall for airfoils with thickness/chord ratios 15% and above. At high angles of attack, flow on the upper surface is characterized by a thickening of the turbulent boundary layer, followed by an initial separation at the trailing edge. The separation gradually moves forward, with a corresponding decrease in lift. Maximum lift occurs when the separation reaches mid-chord. The resulting collapse of lift is gradual, drag continues to rise rapidly, and pitching moment becomes less nose down. Flow at the leading edge remains attached, and the leading edge suction force is active to a high angle of attack.

Type II: Leading Edge Stall

As thickness/chord ratio decreases below about 10%, the airfoil experiences an abrupt separation of flow near the leading edge. Separation of the laminar portion of the boundary layer occurs well before maximum lift, and transition to turbulent flow will occur in the separated shear layer. The flow will reattach in the form of a small bubble just aft of the airfoil nose. At moderate angles of attack, the pressure distribution is not seriously altered, and the lift, drag and moment characteristics of the airfoil are not greatly changed.

As angle of attack increases, however, the bubble enlarges and moves aft until reattachment of the turbulent shear layer is no longer possible.The flow then separates over the entire airfoil surface, the leading edge suction collapses, and the pressure distribution along the chord remains nearly constant with low negative values. Lift drops abruptly with no gradual transition; pitching moment becomes significantly less nose down.

Type III: Thin Aerofoil Stall

Separation and stall on very thin sections (<6% t/c) consists mainly of the gradual lengthening and ultimate breakdown of the upper surface short bubble. The breakdown of the bubble with resulting flow separation occurs at moderate angles of attack. The lift curve is characterized by a gradual reduction in lift slope, and a stall which occurs at a low maximum lift coefficient, but with a gradual decline. Pitching moment undergoes a large but gradual negative change. The pressure distribution exhibits negative values, which extend over the length of the bubble, as long as it is attached to the surface. When flow breakdown occurs the long bubble detaches from the trailing edge, and a trailing wake is shed from the leading edge.

In general, modern airfoils do not conform precisely to these three distinct categories of stalling behaviour; rather, combinations of the different stall characteristics may be exhibited, and may be sensitive to minor variations of shape, Reynold's number, leading and trailing edge devices etc. For Reynold's numbers appropriate to the operation of typical transport aircraft, a large nose radius is desirable to delay the breakdown of leading edge suction and to achieve the trailing edge separation (type I) and high maximum lift. Conversely, as Reynold's number diminishes, all airfoils tend to stall from the leading edge (type III). Observations from both wind tunnel and flight test indicate that the aerofoil section of the F-28 wing lies well within the region for TYPE I (Trailing Edge) stalls and, as such, may be considered a conservative design. The reason for this may be attributed mainly to the generous nose radius of the aerofoil.

STALLING CHARACTERISTICS OF ROUGHENED AIRFOILS

The previous remarks regarding airfoil stall relate to flow over a smooth surface. When the airfoil has a roughened surface, transition to turbulence occurs earlier, friction drag increases, and flow separates prematurely from the upper surface.

The effect of distributed roughness on the premature stall of airfoils is shown in Figures 7 and 8 which are from Reference [2]. The roughness was distributed uniformly over part or all of the airfoil, and Reynold's number was varied from about 10^5 to 10^7. Maximum lift coefficient is considerably reduced by roughness for the two airfoils which were tested, and the critical Reynold's number at which this occurs decreases as the magnitude of the roughness increases. The results of Reference [1], for the higher Reynold's numbers, indicate that roughening of the entire wing upper surface results in a loss of maximum lift of as much as 50%. Drag under conditions of premature stall would be due mainly to form drag, and would be high. The size of the distributed roughness in these experiments corresponded to 0.01 in. and 0.004 in. on a wing the size of that of the F-28. Most studies of the effect of roughness on the performance of airfoils deal with the uniform distribution of contamination over the entire upper surface. The importance of preserving smooth attached flow around the nose is important; if the nose contamination is removed, the wing is restored to its original unstalled state. Conversely, the contamination may take the form of a single roughness element, or ridge which extends across the span on the upper surface. The drag of such a protuberance depends upon the degree to which it extends above the sub-layer, and the sharpness of its edges. Maximum lift will be reduced and if the flow over the nose is critical, separation will occur abruptly from the leading edge. Figure 7b shows a comparison of the loss of lift due to uniformly distributed roughness to that due to a single, spanwise ridge extending along the wing upper surface.

STALLING OF COMPLETE WING

Stall characteristics of the complete wing depend upon which portion stalls first, and how the separation spreads along the span. Initial stalling at the wing tip is undesirable since it may induce a violent roll, and a loss of aileron control.

If the boundary layer is encouraged to stall first at the wing root, then the tendency to wing drop is lessened, but the turbulence and low total pressure which results from the separation may result in buffeting of the tailplane and poor quality flow in the engine intakes for fuselage-mounted fan engines. Stall management on wings of current transport aircraft is usually achieved by precipitating the separation at a particular spanwise location. This may be accomplished by the use of various devices at the leading edge, eg; kinks in the leading edge, notches, fences or vortilons. These devices not only result in stall at a particular lift coefficient, but ensure a symmetric stall.

GROUND EFFECT

Ground effect is perceived as a cushioning of the aircraft when landing with a resulting tendency to "float" before touchdown. Ground effect also has a significant effect during take-off, although the physical sensation may not be as obvious.

The phenomenon originates from the interaction of the wing and fuselage with the ground plane and is composed of three different phenomena, which affect both lift and drag. They are usually applied as corrections to design and performance data.

The first effect is due to the volume or displacement of the airplane and the low pressures that will be induced between it and its image. These negative pressures act to suck the aircraft on to the ground, and therefore constitute an effective loss of lift.

The second effect occurs only when the wing is lifting and the resulting interaction results in an increase in lift per unit angle of attack. The sensation experienced on landing is due to this increase of lifting effectiveness. This increase is, in some cases, cancelled or reduced by the displacement effect of the aircraft volume, already described.

The third ground effect results from the interaction of the trailing wake behind the wing with the ground plane. The most important result of this is that the upwash at the wing diminishes, so that the effective angle of attack is lower. This causes a significant reduction of induced drag, thereby lengthening the final flight path before touch down.

The beneficial value of ground effect during take-off is reduced drag and increased lift, however these benefits diminish rapidly as the aircraft climbs. At approximately one wing span above the ground, the ground effect has essentially vanished.

AERODYNAMIC CHARACTERISTICS OF THE FOKKER F-28, MK. - 1000

FOKKER F-28 MK. - 1000 - SPECIFICATIONS

The Fokker F-28 (Mk.1000) is a twin-turbofan short range airliner. It is a swept, low-wing configuration, with a T-tail, and rear mounted engines. The version of the present

investigation seats 65 passengers, and cruises at a maximum speed of 455 kt at 23000 ft (a Mach number of 0.75).

A full technical specification of the Fokker F-28, (MK.-1000) can be had from Reference [3] and is presented in Appendix A. Some of the geometric, weight and performance parameters relevant to the present investigation are listed as follows. A general arrangement of the aircraft is shown in Appendix A.

TABLE I

Wing Span	77'-4 1/2"
Wing Area	822 ft^2
Aspect Ratio	7.27
Mean Aerodynamic Chord (MAC)	11.5 ft.
Engine Thrust[2]	9850 lb.
Max. take-off weight	65000 lb.
Operating weight empty	35,464 lb.
Max cruise speed (23000')	455 kt.

Rotation speed for the F-28 ranges from 100 to 130 kt. depending on weight and environmental factors.

The flow on the wing changes from a high lift condition at lift off using slotted Fowler flaps, to low transonic flow at cruise. The lift coefficients of the mean chord section based on maximum weight and the above speeds are 1.38 and 0.24 at lift-off and cruise respectively. The maximum lift coefficient for the F-28 wing is about 2.1. The wing is not equipped with leading edge devices (Slats, Kreuger Flaps etc.)

The Reynold's number of the flow at the mean chord ranges from 12 million at sea level (lift off at 130 kt) to 29 million at 23000 ft. (455 kt.). The boundary layer flow is turbulent over the main wing component under normal operating conditions.

AERODYNAMIC DATA FOR THE FOKKER F-28, MK.-1000

Relevant aerodynamic data which was made available by Fokker comes from several sources:

[2] Sea Level Static, ICAO Standard Day

1) Results of a wind tunnel test at the NLR[3] in which the effects of simulated ice contamination of the wing were measured.

2) A description of the aerodynamics of wing stall, including flight experience with the airplane.

3) Computed values of pressure distribution, skin friction and displacement thickness of the boundary layer, for the F-28 airfoil section.

4) An official database from which the F-28 simulator model was assembled.

F-28 WIND TUNNEL TEST DATA

Figure 9 shows the results of wind tunnel tests on a complete model of the Fokker F-28. The test Reynold's number of the Mean Aerodynamic Chord (MAC) was 2.85 million, and the wing flaps were set at 30 degrees. The model angle of attack range was from -2 to +20 degrees. The test was conducted in the NLR wind tunnel and the model was positioned on a mounting which allowed a range of pitch angles to be used.

Data are also shown in which the upper surface of the main wing component is treated uniformly distributed carborundum roughness elements. The wing roughness was intended to simulate ice deposits of 1 and 2 mm thickness full scale, uniformly distributed on the upper wing surface at one element per sq cm. Tests were also done with the first 15% of the wing component cleaned off. Figure 9 presents C_L and C_M plotted against angle of attack, and also C_L against C_D.

The lift slope in the linear part of the lift curve is 0.100. For angles above about 8 degrees, the lift curve becomes non-linear, due to a thickening and deceleration of the trailing edge boundary layer. Maximum lift occurs at 14 degrees, and has a value of C_L = 2.13. The top of the stall is rounded, but lift falls rapidly to a value of 1.55 as the wing pitches to 16.5 degrees. Lift continues to diminish to a value of C_L = 1.46 at 20 degrees angle of attack.

The wing exhibits a characteristic hysteresis in lift, as the angle of attack reverses. Maximum lift is not achieved, and the data returns to the linear part of the lift curve at an angle of attack of 7.5 degrees and at a lift coefficient of 1.75. Hysteresis is an entirely viscous phenomenon, and is a common occurrence on wings and airfoils. It is associated with flow fluctuations, particulary during reattachment at the stall. Hysteresis does not occur when the wing upper surface is roughened; the maximum lift coefficient under these conditions is 1.6.

---

[3] Nationaal Lucht- en Ruimsevaartlaboratorium, the Dutch National Aerospace Laboratory.

Pitching moment C_M, is nose down relative to the quarter chord of the MAC, for values of lift before and after the stall. There is little hysteresis.

Drag rises slowly with lift until maximum lift is reached, as is shown in the drag polar Figure 9. Drag at C_{LMax} is about triple the drag for small values of lift, and is attributed to induced or vortex drag.

As lift falls, after flow separation, the drag rise is due mainly to form drag from the altered wing pressure distributions. Hysteresis also occurs in drag, since the pressure distribution is also affected by the flow separations. As with the lift curve, roughness reduces the hysteresis effect.

The effect of roughness on the wing upper surface is dramatic. Maximum lift occurs some 7 degrees earlier at an angle of attack of 7.5 degrees, and reaches a value of 1.6. At higher angles lift diminishes to C_L = 1.4, and thereafter remains constant.

With roughness applied, pitching moment begins to decrease rapidly beyond 8.5 degrees, and thereafter becomes strongly nose down at maximum lift.

Drag at maximum lift for the roughened wing is less than that for the clean wing, but lift is also less: the drag continues to rise rapidly as lift falls. At angles of attack above 11 degrees, there is a rapid rise in drag, to a value of C_D = 0.6, with essentially no change in lift.

With the entire wing upper surface roughened, the levels of turbulence in the boundary layer that is developing on the nose are higher than normal and kinetic energy is being exchanged for pressure at a higher rate than for the clean surface. If the roughness elements are large enough the result is higher local drag and turbulence; the sublayer itself is annihilated by the wake turbulence of the roughness elements. This factor and also the fact that the flow is subjected to a rising pressure aft of the nose suction peak, provide the potential for early boundary layer separation and wing stall.

Conversely, if the wing nose is clean over the first 15% of chord, the boundary layer, and particularly the laminar sublayer, develops naturally and is able to negotiate the adverse pressure gradient on the rear half of the wing successfully. If roughness is present on the rear portion of the wing surface only, the potential for flow separation is modified by a weakening of the adverse pressure gradient and the additional roughness-induced turbulence plays a more active role in resisting the tendency to separation. Friction drag, however, will be higher, due mainly to the drag of the roughness elements themselves.

EFFECT OF ROUGHNESS ON DRAG IN UNSEPARATED FLOW

Roughness elements on a smooth surface will affect skin friction drag and if the local flow is still laminar, roughness will cause an immediate transition to turbulent flow. The resistance formulae of Reference [4] can be used to estimate drag theoretically, resulting

from simulated roughness contamination, assuming separation does not occur. For a chord Reynold's number of 12 million, and a smooth surface of the same length as the F-28 mean chord, the total skin friction drag coefficient is estimated to be 0.0029. When roughened, the drag coefficient rises to 0.0065 and 0.0079 for roughness heights of 1 mm and 2 mm respectively. The wind tunnel results obtained by Fokker indicate that, for angles of attack below the stall, roughness causes a drag rise of about 6% in the complete airframe model compared to the smooth wing configuration.

The wind tunnel data for the F-28 model show very clearly the effects of wing contamination on aerodynamic characteristics. They do not, however, conform precisely to the airplane configuration in the present investigation, since the flap setting on the model was 30 degrees, compared to the 18 to 25 degree settings which the actual aeroplane was thought to have had during the takeoff run. The test Reynold's number was 2.85×10^6, compared with 12×10^6 for the aircraft at take-off. The main effect of these differences will be on maximum lift. The lift curve to C_{LMax} for attached flow for a flap angle of 18 degrees is available from the Fokker data base, and it can be assumed that appropriate Reynold's number corrections have been made. Similar information is available for C_D and C_M beyond stall; the correction process is more uncertain, but it is assumed that the incremental changes in the aerodynamic characteristics due to both stall and contamination can be applied from the wind tunnel data directly to the data base.

STALLING CHARACTERISTICS OF THE F-28 WING

The Fokker F-28 has a wing of aspect ratio 7.27, swept 16 degrees at the quarter-chord line. The leading edge profile has a kink at wing station 4700 (40.7% semi-wing span), and a leading edge fence at station 3784 (32.8% semi-wing span). The mean aerodynamic chord, to which Reynold's numbers are referred, is at wing station 4940 (43.8% of wing semi-span). Investigations by Fokker of the maximum lift, and wing stall aerodynamic characteristics using wind tunnel investigations and flight test, are presented in Reference [5].

An important design objective for the F-28 was the achievement of a high maximum lift coefficient, and satisfactory stall characteristics. The wing sections are characterized by a large nose radius in order to improve maximum lift capabilities. Further improvements were achieved by the use of Fowler flaps, which are single slotted at the 18 degree take off position, and double slotted at higher extensions.

In addition to attaining high values of C_{LMax}, it was desirable to produce airplane stall characteristics that resulted in definite nose down pitching. This avoids large attitude changes, high drag levels and losses in height when the aircraft stalls. The pitching moment curve in Figure 9 for the clean wing attests to the fact that this goal was achieved.

Initial wind tunnel testing of the F-28 prototype was performed on both full and half models at Reynold's number 3 and 5 million respectively. Wing stall was characterized by a rapid spanwise spread of the separation. Initiation of the stall at a particular point along the wing was done using a small leading edge fence. The stall progresses in a wedge-

shaped configuration in both outboard and inboard directions. The outer portions of the wing, and the wing root junction stall last, thus enabling full retention of lateral control, and avoidance of flow distortion into the engine intakes until after maximum lift has been achieved. Flight test observations confirmed the wind tunnel test results with regard to stall progression and maximum lift, but also disclosed an initial, strong buffeting which preceded the fully stalled condition. Figure B-2 shows the main features of the stall patterns and vortex wake of the F-28 wing, inferred from wind tunnel and flight test data.

Observations were also made, during flight test of the F-28, of differences in the stall in free air (at altitude) and in ground effect. It was observed that in free air the stall progresses along the wing in the manner already described, while in ground effect however and with the mainwheels in contact with the surface, it was noted that separation occurred on the inboard wing panels only (Reference [3]): the outer wing panels did not stall. Maximum lift was essentially unchanged, but occurred at an angle of attack some 4 degrees lower than in free air. These observations conform to the results of other research into ground effect (Reference [6]): Similar observations are not available for the effect of ground proximity on the stall characteristics of a roughened wing.

The rate and progression of the stall over the artificially roughened wing surface is not precisely known, although the measured lift and drag coefficients supplied by Fokker indicate a complete breakdown of the flow. Since the entire upper wing upper surface of the wind tunnel model, including the leading edge, was roughened, and recalling the basic research on the effects of roughness on lift (Reference [1]), it is likely that separation occurs simultaneously along the entire span. In this situation, the leading edge fences may be less effective in fixing the initial spanwise location of the stall, and also in ensuring a symmetrical stall across the span. Even when complete stall has not occurred on the outer wing panels, the aileron effectiveness may be adversely affected by roughness. No data were available on this point. Figure B-3 shows a representation of the stall pattern and wake on a contaminated wing.

COMPUTED DATA FOR FOKKER F-28 AIRFOIL

The airfoil section of the Fokker F-28 is a modified NACA 4-digit profile, with a large nose radius. The design cruise Mach number of the Mean Aerodynamic Chord is 0.75, and the dive Mach number is 0.83. Airfoil thickness at the M.A.C. is 14%. The generous nose radius, although a limiting factor in high sub-sonic flight, enables flow around the leading edge to remain attached, and the suction force to reach its full value when trailing edge flaps are used during take-off and landing. The graphs shown in Figure 10 give the top and bottom surface pressures, and boundary layer parameters for a flap angle of 18 degrees, and angles of attack of -2 degrees and 5 degrees. The computation method included viscous effects, and used the code VSWAKE.

The maximum nose suction peak at these angles is about -1.2 for α=-2 degrees; and -5.34 at α=+5 degrees. Reynold's number in both cases was 15 million. The lift coefficients were 0.6515 and 1.5100 respectively, and the moment is nose-down.

Calculations include local values of skin friction C_F and boundary layer displacement thickness δ^*. The displacement thickness represents the distance by which the outer streamlines have been displaced by viscous retardation of the fluid in the inner streamlines. It is a measure of viscous drag.

AERODYNAMIC DATA BASE

The performance group was supplied with a complete data base of aerodynamic, stability and control information. This data base was originally used by Fokker to construct their F-28 dynamic simulator. It is corrected for the variable effects of Reynold's number, Mach number and altitude; so that the data, when applied to the complete equations of motion, produces the real airplane performance in the simulator. The utility of these data in the context of the present investigation is that it is standardized and credible, and can be used to create a realistic scenario for take off and initial climb.

The data which are of initial interest are lift, drag and moment for the aircraft in free flight and also in ground effect. The data do not go beyond C_{LMax} into the post-stall regime. The effects of wing contamination are presented in the form of incremental changes of lift, and it is believed that these are derived from the single wind tunnel test which has already been described Figure 9 for uniform roughness heights of 1 and 2 mm. Incremental corrections for roughness heights smaller than these values were not available in experimental form, although arbitrary factors could be applied to the data (Figure 14).

The aerodynamic effect of the ground cushion during take off and climb, particularly at high lift coefficients, acts to change the angle of attack necessary to produce a certain lift coefficient. With flaps extended, below a lift coefficient of about 1.5, ground proximity increases lift; particularly when the trailing edge approaches the ground. This is particularly relevant to swept-wing aircraft, where the tips may come close to the ground during rotation. An additional phenomenon, which reduces lift and induced drag, arises from a reduction of the wing upwash and induced angle of attack. This is due to the presence of the ground plane, which does not allow vertical velocities.

The F-28 data base also includes the effects of ice accretion on the leading edges of the wings, tailplane and fin, to a thickness of 2 in. Graphs in Figure (12) show the incremental changes in lift, drag and pitching moment which would occur during flight operations in icing conditions.

In the context of the present investigation, these data may not represent precisely the type of uniform contamination which was simulated in the NLR wind tunnel, nor ice that is deposited by freezing rain or snow.

CONCLUSIONS

The following conclusions are based on the various F-28 aerodynamic data which were given by Fokker to the performance group. They do not specifically address or explain the circumstances of the Dryden accident at this time.

The F-28 wing section is designed for a cruise mach number of 0.75, and a high maximum lift coefficient at low speeds. A generous nose radius minimizes the likelihood of separation under high lift conditions and promotes stall from the trailing edge.

Stalling of the basic smooth wing is from the trailing edge. It then spreads outward from the leading edge fence location in a fan-shaped manner toward the tip and wing root regions. These regions separate last, allowing lateral control and engine intake flow to remain effective to high angles of attack.

In ground effect, with the main wheels on the ground, stalling occurs 4 degrees earlier, but only the inner portion of the wing stalls. C_{LMax} is unchanged.

Artificial roughness on the upper surface of the wing of a wind tunnel model caused a premature stall in which boundary layer separation may have occurred all along the leading edge. The roughness corresponded to an element size of about 1 to 2 mm on the full scale F-28 wing while the distribution corresponded to approximately one element per square centimetre on the same wing. With flaps set to 30 degrees on the model the wing stalled at an angle of attack 7 degrees lower than for the clean wing. There was a 33% loss of maximum lift compared to the clean wing.

Research on wing sections at Reynold's numbers ranging from 100,000 to 10,000,000 shows that roughness not only increases drag below the stall but also increases the likelihood of a premature stall, particularly if the nose is roughened. As Reynold's number increases towards the values experienced by the F-28 wing during take-off (greater than 10,000,000) the loss in maximum lift can be as high as 50% compared to a clean surface (Reference [1]).

In some cases the aerofoil is sensitive to the size of the roughness elements; the loss of maximum lift being less for very small roughness heights. Most aerofoil sections, however, respond to roughness of any scale by stalling prematurely and incurring the maximum loss of lift. Removal of roughness on the nose and over the first 15% of chord restores the aerofoil close to its original performance.

LIST OF SYMBOLS

A	Aspect Ratio
b	Wing Span
c	Wing Chord
c (MAC)	Mean Aerodynamic Chord
D	Drag
e	Wing Efficiency Factor
L	Lift
M	Moment
Re	Reynold's Number (Vc/ν)
S	Wing Area
V	Flight Velocity
α	Angle of Attack
ρ	Air Density
ν	Kinematic Viscosity
C_L	Lift Coefficient
C_D	Drag Coefficient
C_M	Moment Coefficient
C_p	Wing Surface Pressure Coefficient
C_F	Boundary Layer Friction Coefficient
δ^*	Boundary Layer Displacement Thickness
SLS	Sea Level Standard Conditions

AERODYNAMIC FORCES ACTING ON A WING SECTION

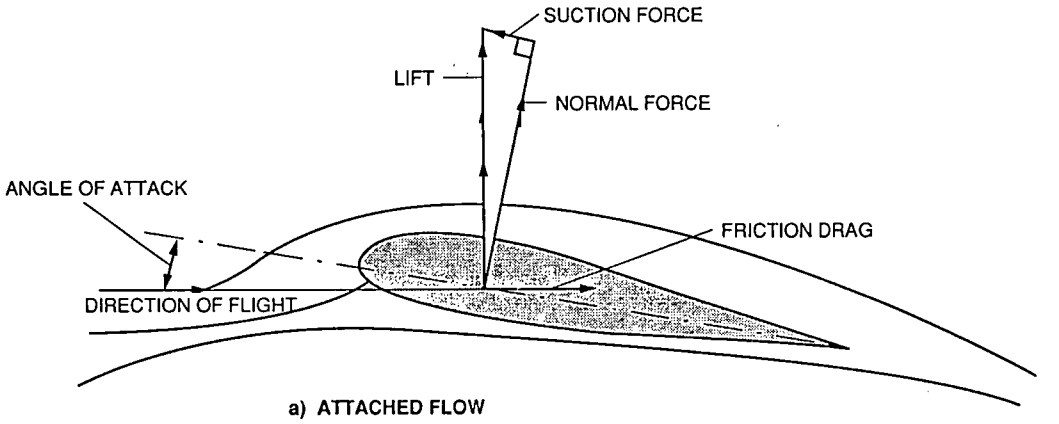

a) ATTACHED FLOW

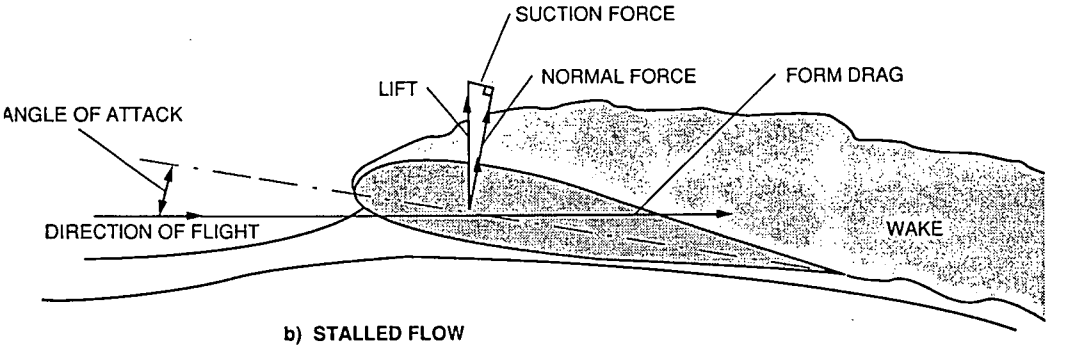

b) STALLED FLOW

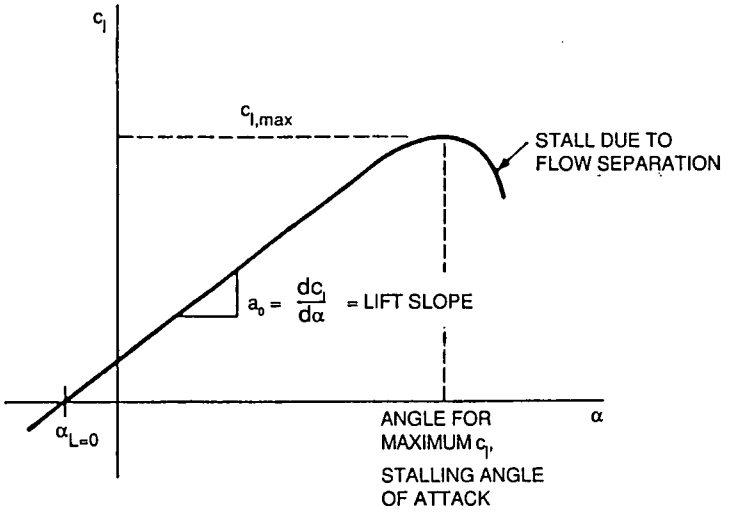

SKETCH OF A TYPICAL LIFT CURVE

(a)

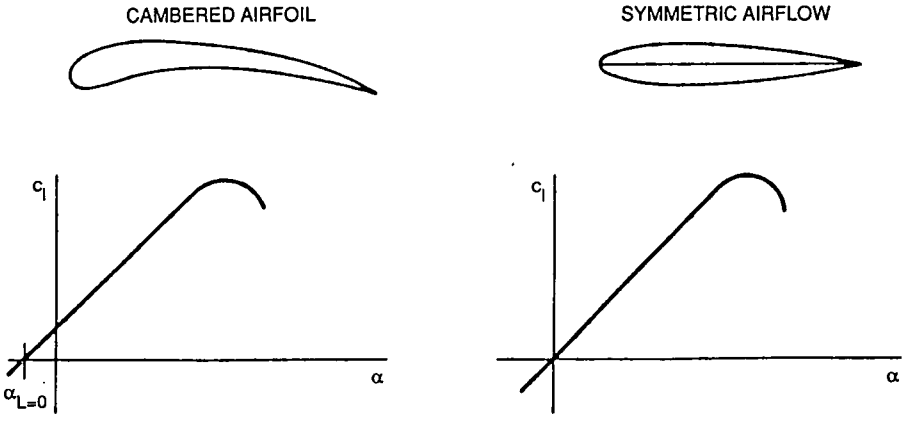

COMPARISON OF LIFTS CURVES FOR CAMBERED AND SYMMETRIC AIRFLOWS

(b)

AIRFOIL LIFT AND DRAG CHARACTERISTICS WITH HIGH-LIFT DEVICES

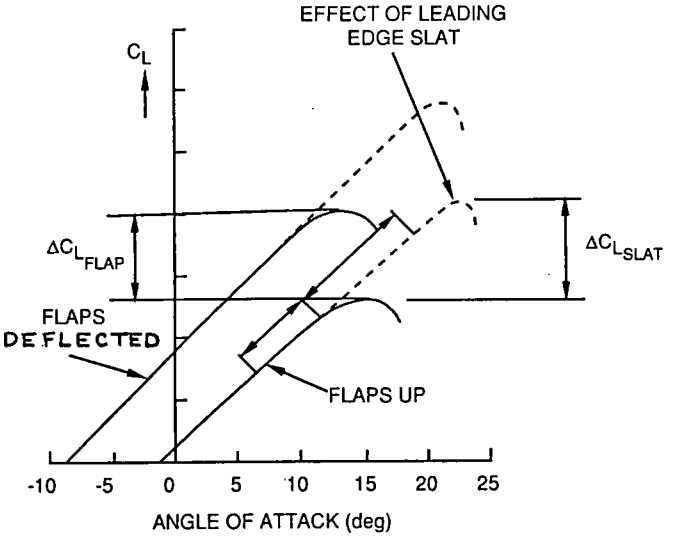

LIFT CURVES WITH AND WITHOUT HIGH-LIFT DEVICES (REF. 3)

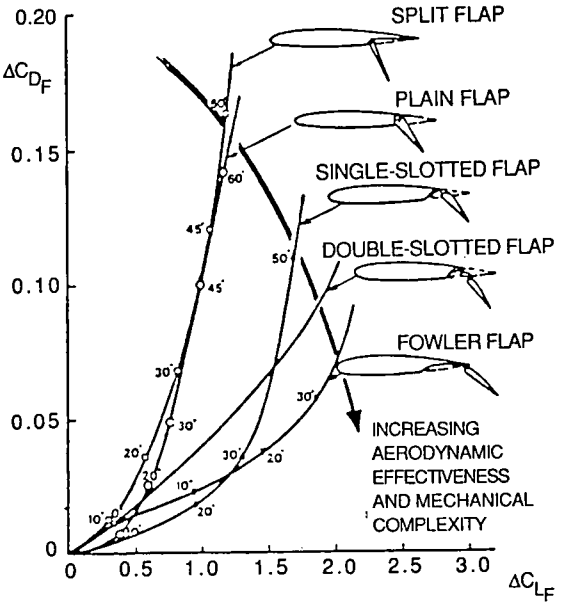

TRENDS IN PERFORMANCE OF TRAILING-EDGE FLAPS (REF. 3)

F-28 FLIGHT DYNAMICS Section 2 - Aerodynamics Figure 4 Page 26

TRAILING VORTEX SYSTEM AND LIFT FOR FINITE WINGS

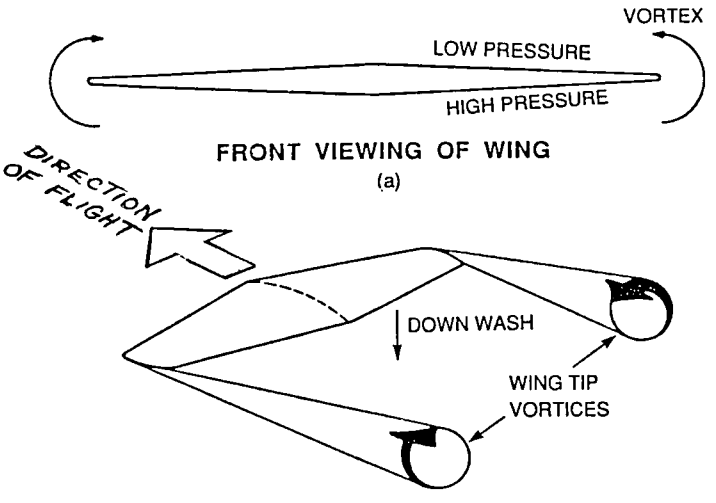

ORIGIN OF WING TIP VORTICES
ON A FINITE WING

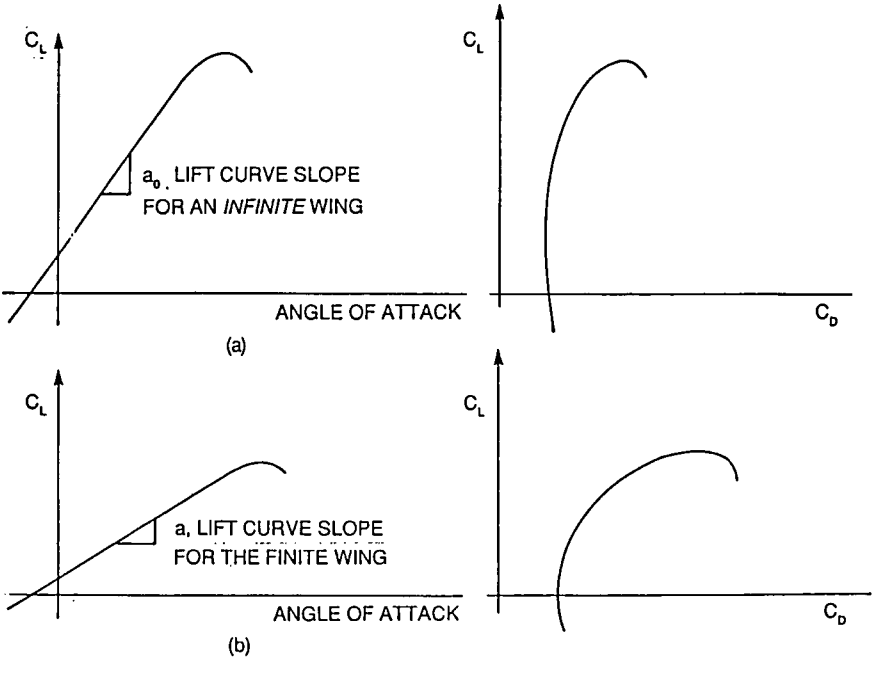

DISTINCTION BETWEEN THE LIFT CURVE SLOPES
FOR INFINITE AND FINITE WINGS

CHARACTERISTICS OF BOUNDARY LAYER FLOW

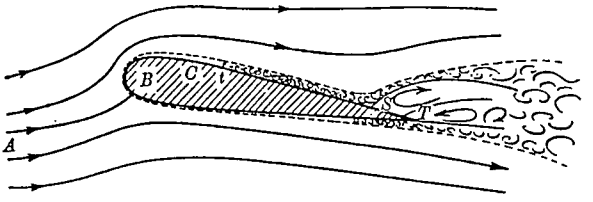

A SKETCH (not to scale) ILLUSTRATING THE NATURE OF THE FLOW OF A UNIFORM STREAM PAST AN AEROFOIL WHEN SEPARATION OCCURS NEAR THE TRAILING EDGE.

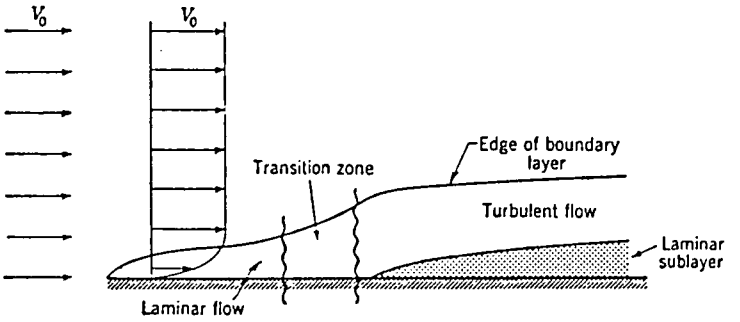

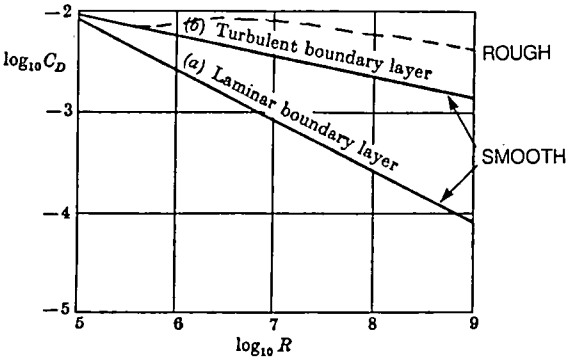

THE SCALE EFFECT ON THE DRAG COEFFICIENT OF A FLAT PLATE IN A UNIFORM STREAM WITH (a) A LAMINAR AND (b) A TURBULENT BOUNDRY LAYER OVER THE WHOLE SURFACE.

EFFECT OF ROUGHNESS ON DRAG

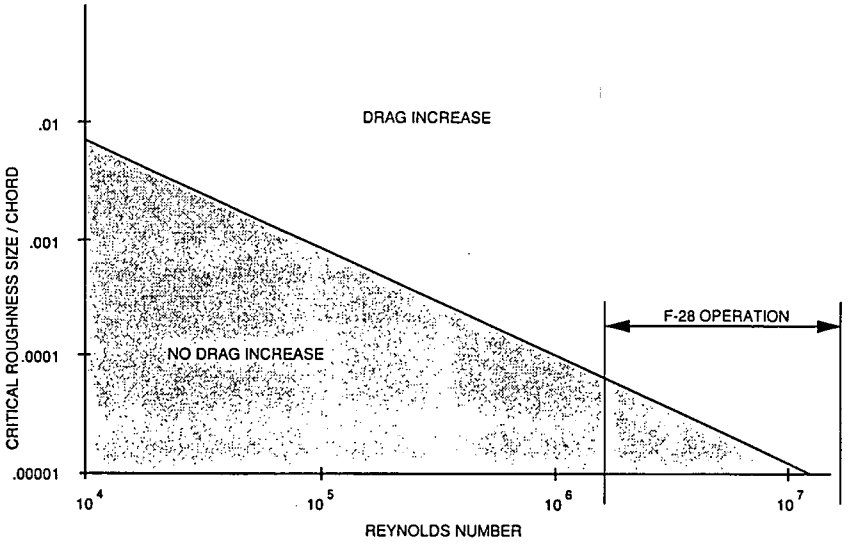

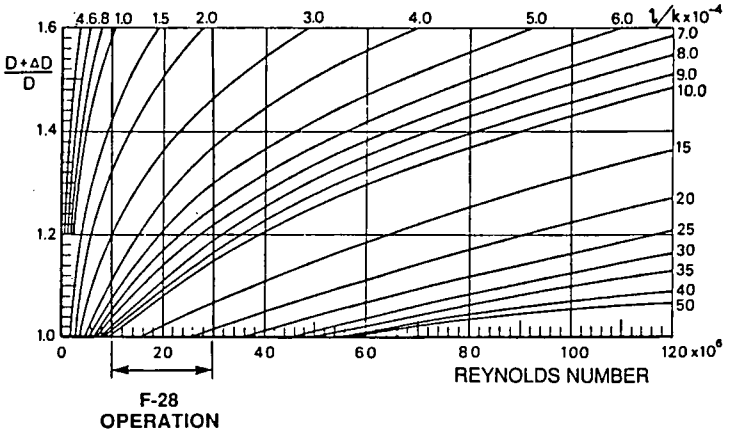

(b) WING OR BODY DRAG DUE TO SURFACE ROUGHNESS (REF 3)

ROUGHNESS EFFECTS ON WING CHARACTERISTICS

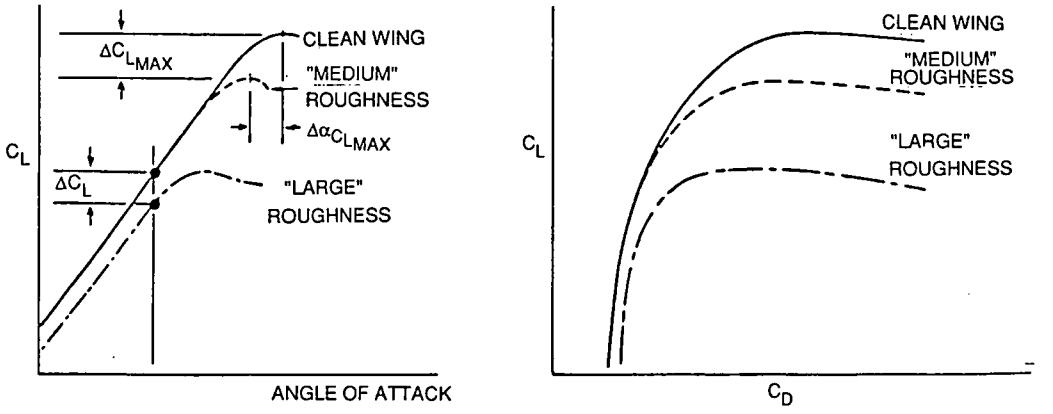

TYPICAL EFFECT OF SURFACE ROUGHNESS AT THE LEADING EDGE ON AERODYNAMIC CHARACTERISTICS (REF. 12)

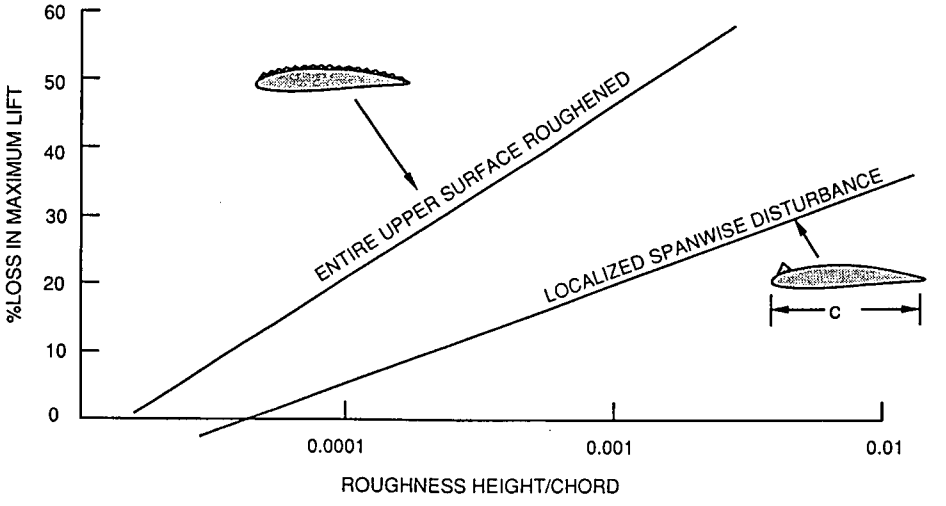

b) EFFECT OF DISTRIBUTED AND ISOLATED ROUGHNESS ON MAXIMUM LIFT LOSS (REF. 12)

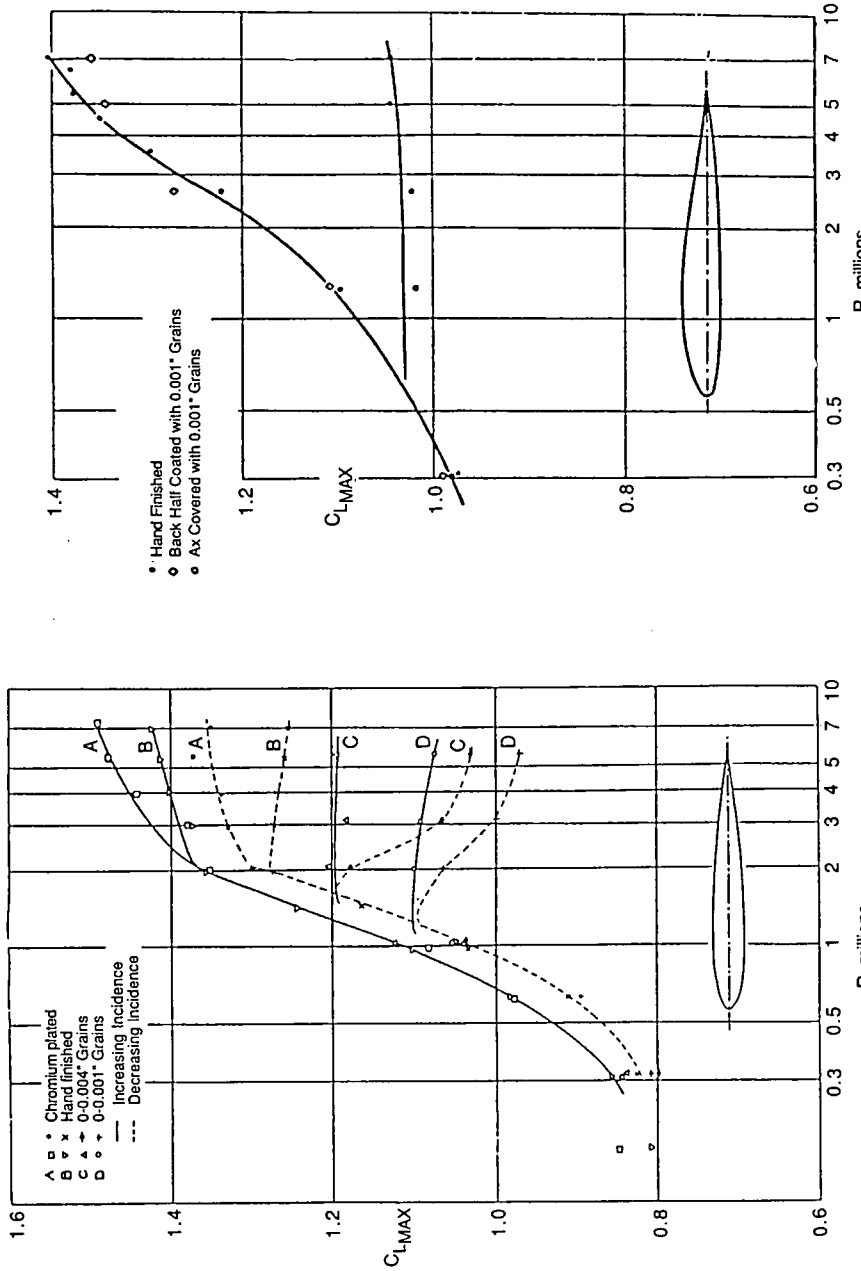

EFFECT OF UNIFORM ROUGHNESS DISTRIBUTION ON THE MAXIMUM LIFT OF WINGS (REF. 9)

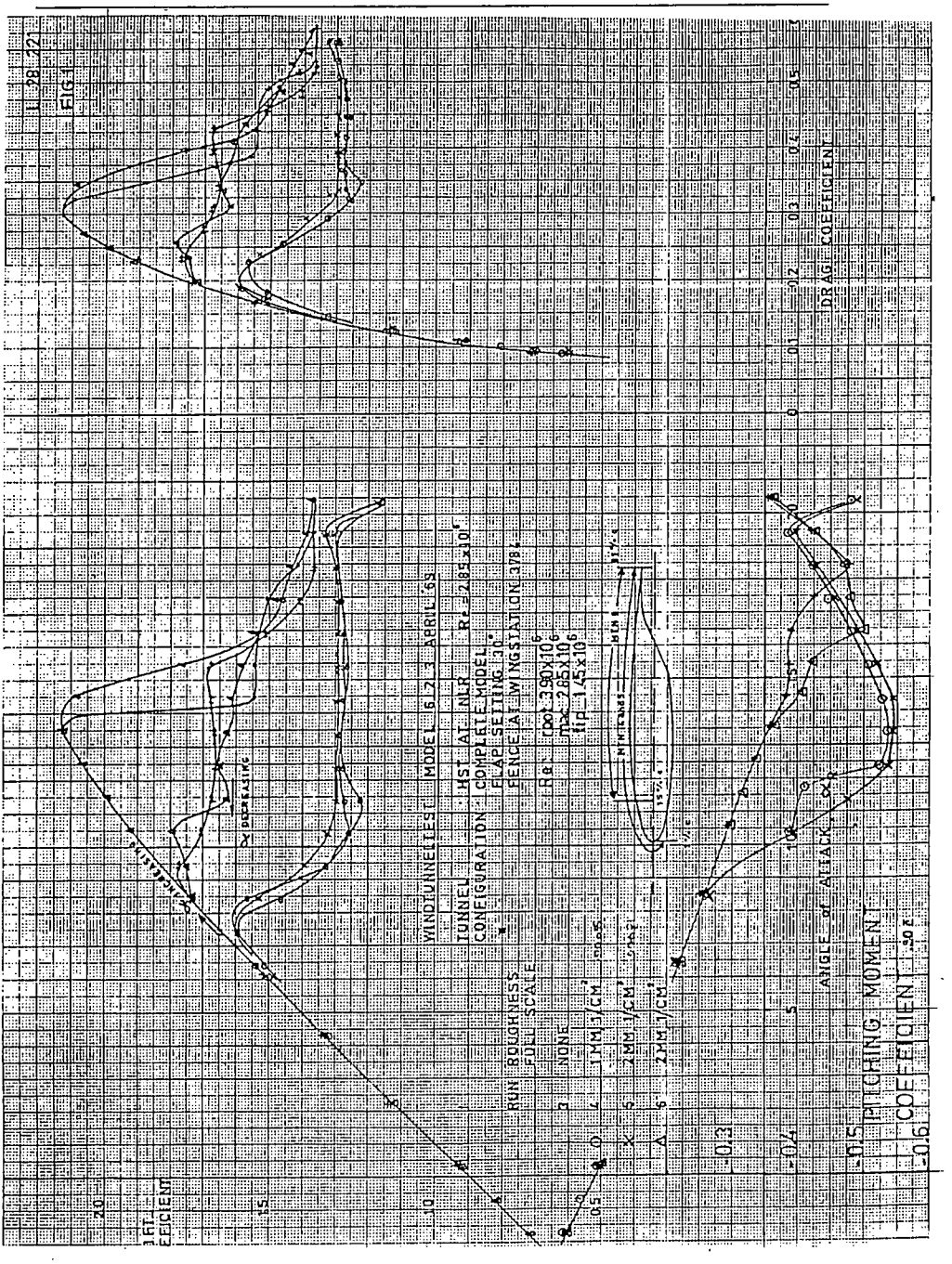
FIG 1
WINDTUNNELTEST MODEL 6.73 APRIL '65
TUNNEL LST AT NLR
CONFIGURATION COMPLETE MODEL
FLAP SETTING 30°
FENCE AT WINGSTATION 378
RUN ROUGHNESS
FULL SCALE
NONE
DRAG COEFFICIENT
ANGLE of ATTACK
PITCHING MOMENT COEFFICIENT

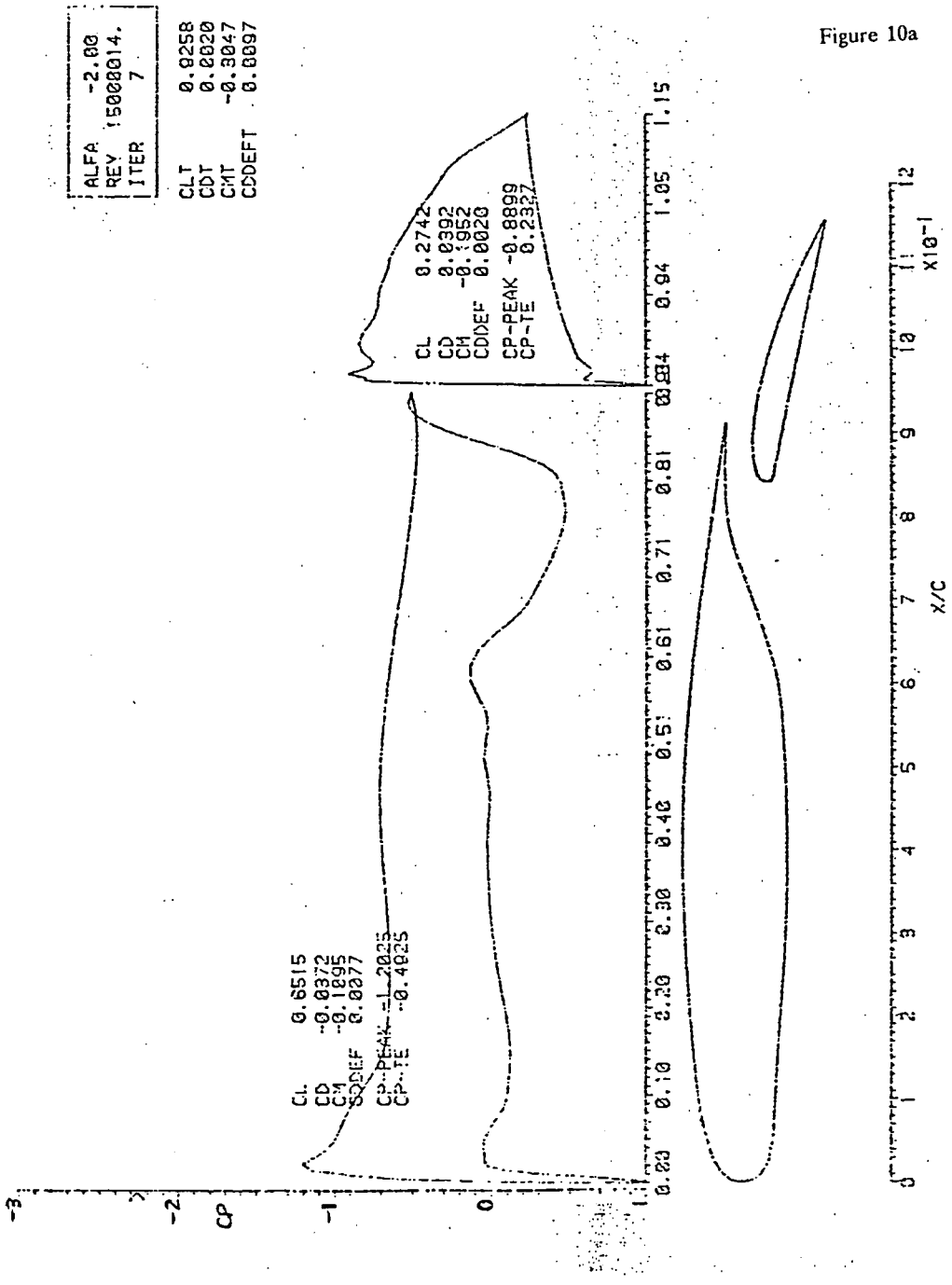

Figure 10a

Section 2 FIGURE 10a Theoretical Flow and Pressure Data for F-28 Aerofoil

Section 2 FIGURE 10b

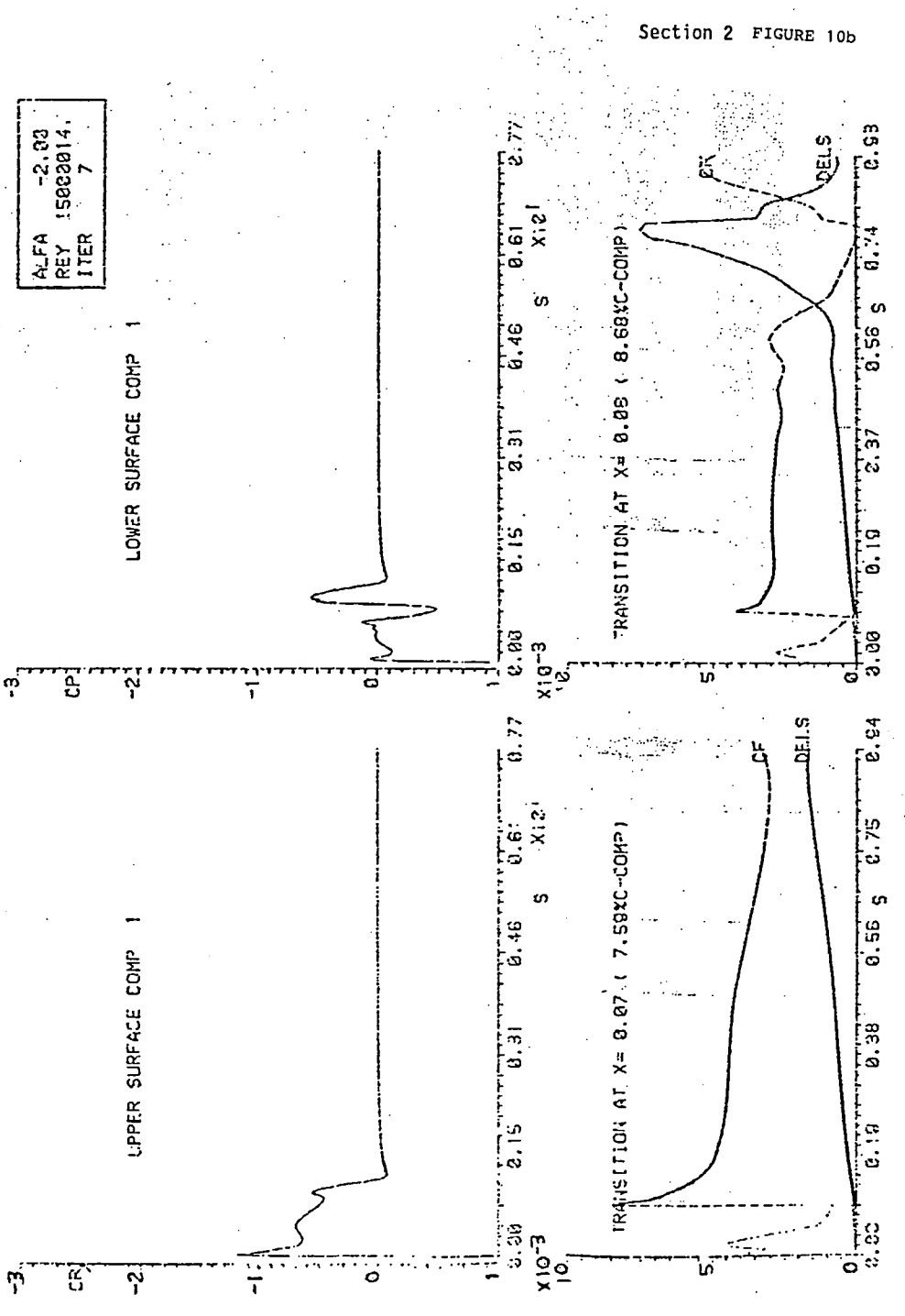

FIGURE 10c

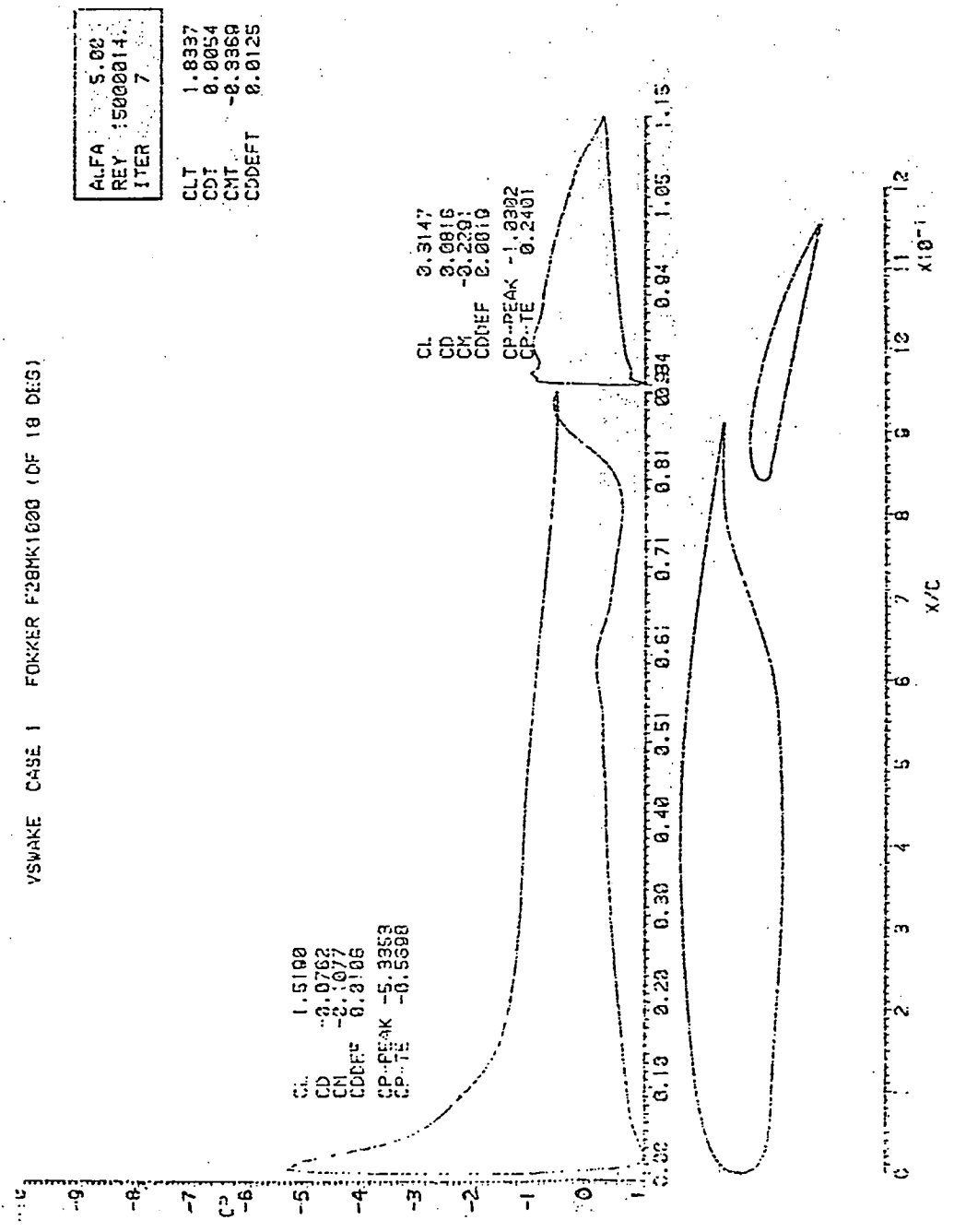
VSWAKE CASE 1 FOKKER F28MK1600 (OF 10 DEG)
ALFA 5.00
REY 15000014.
ITER 7
CLT 1.8337
CDT 0.0054
CMT -0.3369
CDDEFT 0.0125
CL 1.5100
CD -0.0762
CM -2.1077
CDDEFT 0.3106
CP-PEAK -5.3353
CP-TE -0.5698
CL 0.3147
CD 0.0816
CM -0.2291
CDDEF 2.0010
CP-PEAK -1.3302
CP-TE 0.2401
Cp
X/C
X10⁻¹

FIGURE 10d

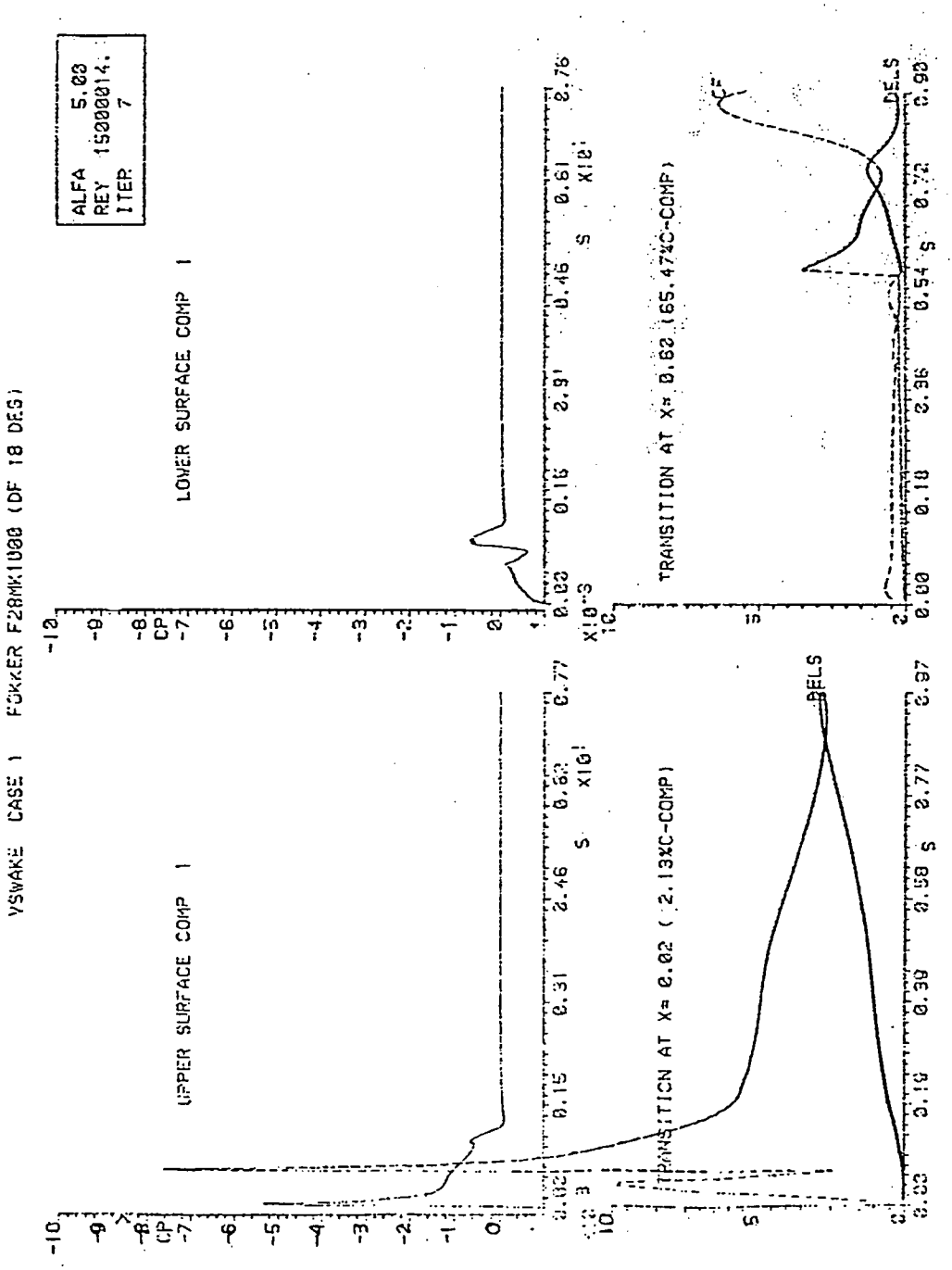
VSWAKE CASE 1 FOKKER F28MK1000 (DF 18 DEG)
ALFA 5.00
REY 15000014.
ITER 7
LOWER SURFACE COMP 1
UPPER SURFACE COMP 1
TRANSITION AT X= 0.62 (65.47%C-COMP)
TRANSITION AT X= 0.02 (2.13%C-COMP)
BELS
CP
S X10¹
X10⁻³

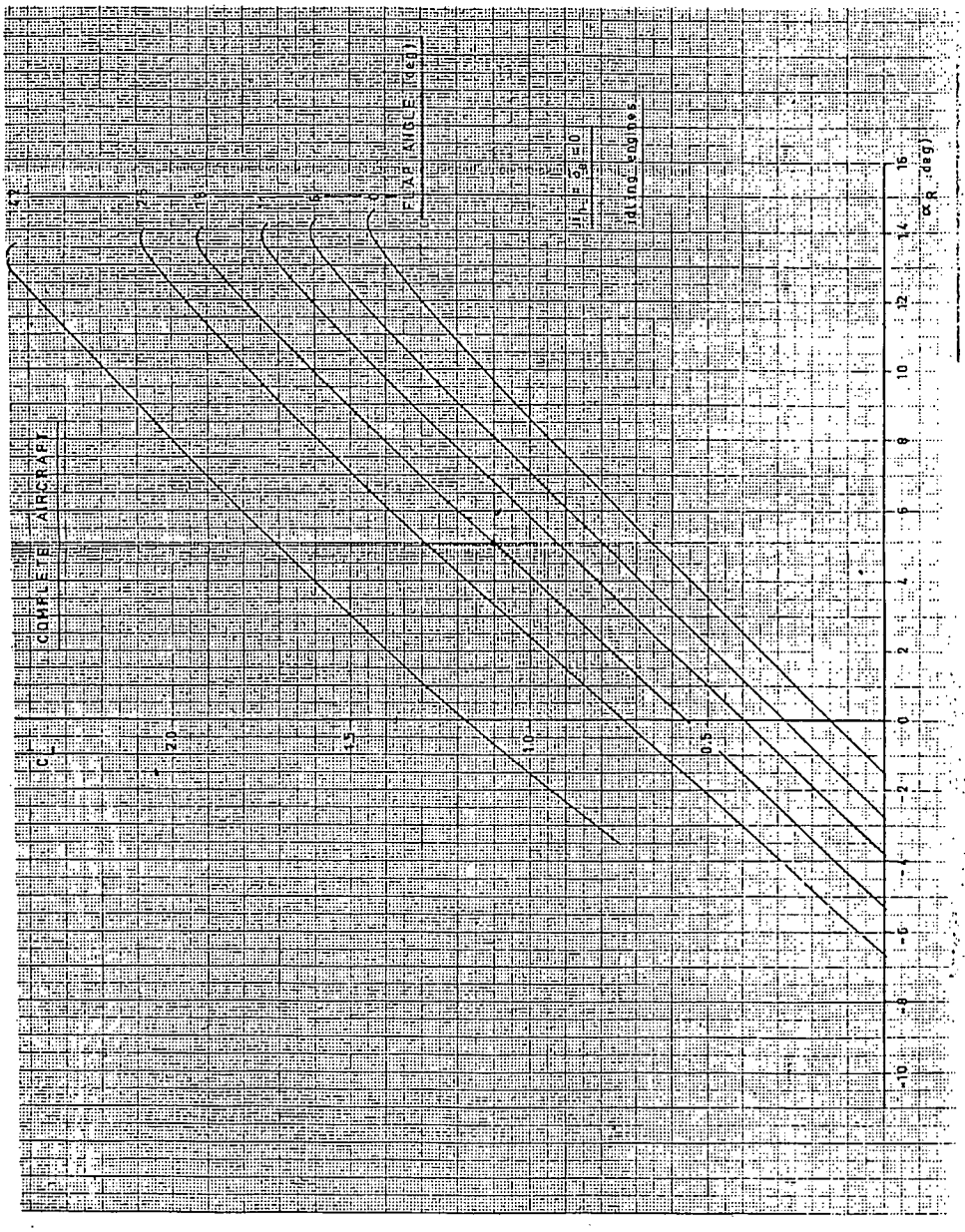

FIGURE 11 F-28 LIFT COEFFICIENT vs ANGLE OF ATTACK (FREE AIR)

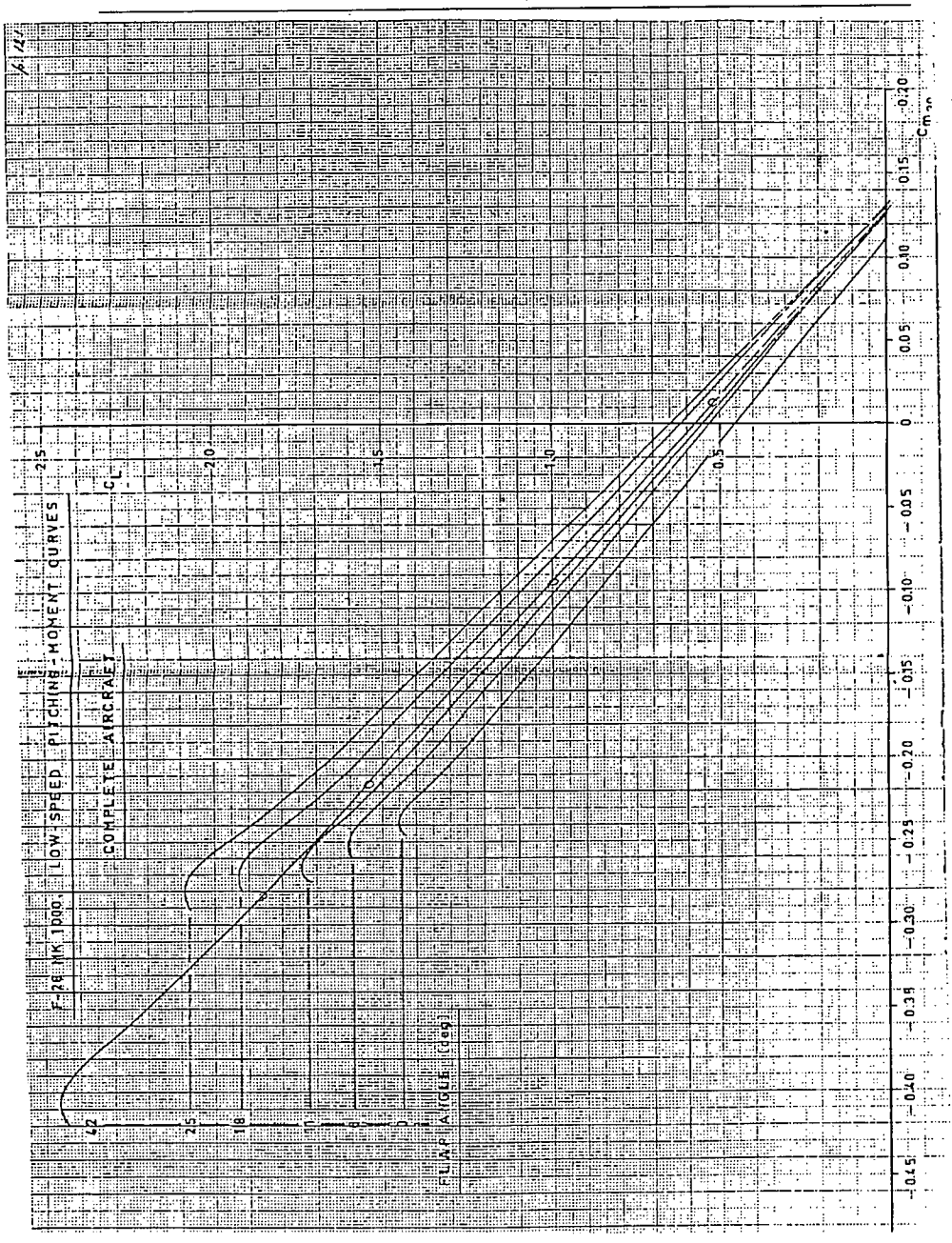

FIGURE 12 F-28 MOMENT COEFFICIENT vs LIFT COEFFICIENT (FREE AIR)

Fokker **FOKKER-VFW B.V.**

NETHERLANDS AIRCRAFT FACTORIES FOKKER-VFW

RAPPORT NR.+REPORT NR.

L-28-269

BLAD,PAGE 107

F-28 Mk.1000 Basic low speed drag polars (FREE AIR)

Flap angle (deg.)	Drag polar
0	$C_D = 0.0195 + 0.0535\ C_L^2$
6	$C_D = 0.0270 + 0.0515\ C_L^2$
11	$C_D = 0.0325 + 0.0486\ C_L^2$
18	$C_D = 0.0405 + 0.0470\ C_L^2$
25	$C_D = 0.0600 + 0.0470\ C_L^2$
42	$C_D = 0.1340 + 0.0400\ C_L^2$

Section 2 FIGURE 13 Low Speed Drag Polars, Free Air

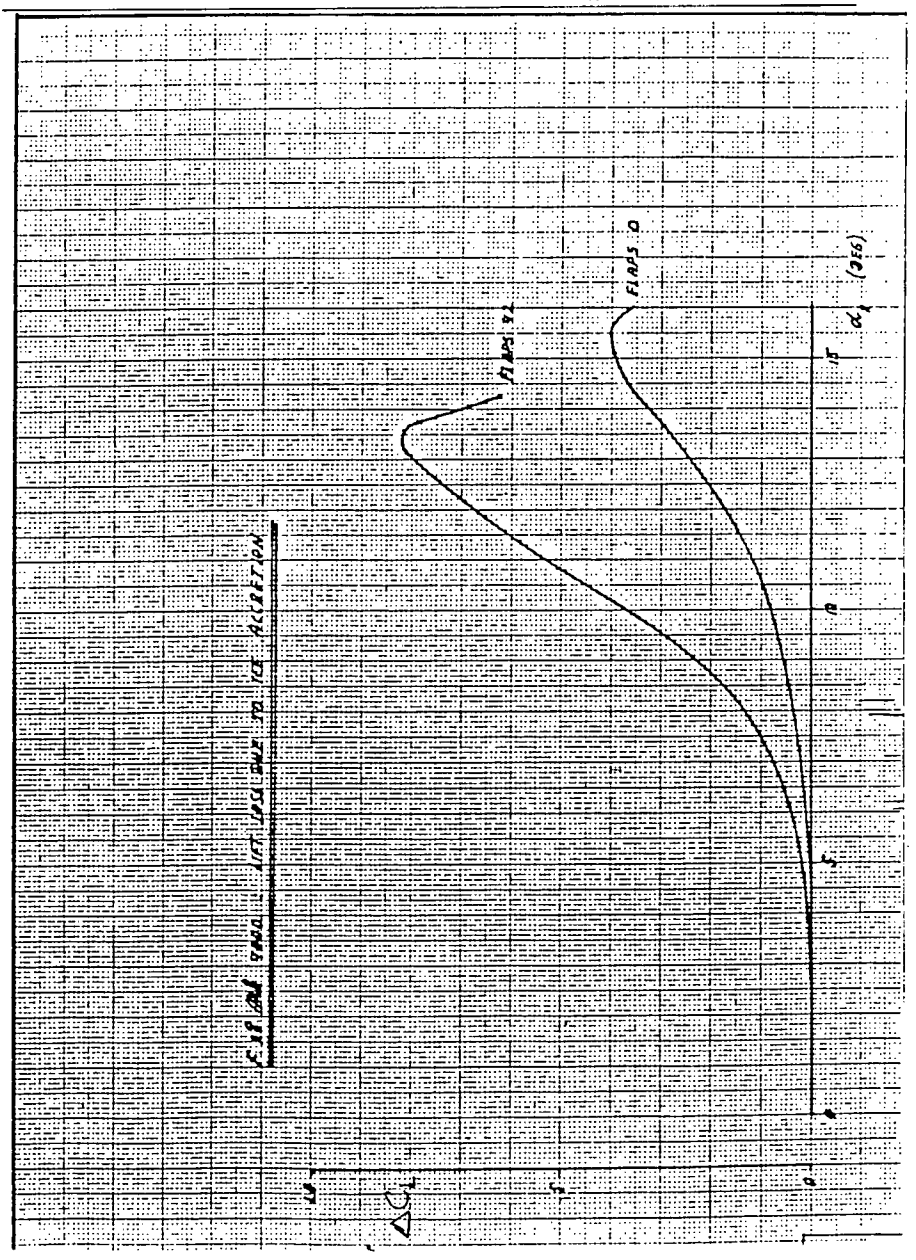
FLAPS 0
FLAPS 7.5
α_t (DEG)
ΔC_{L_t}

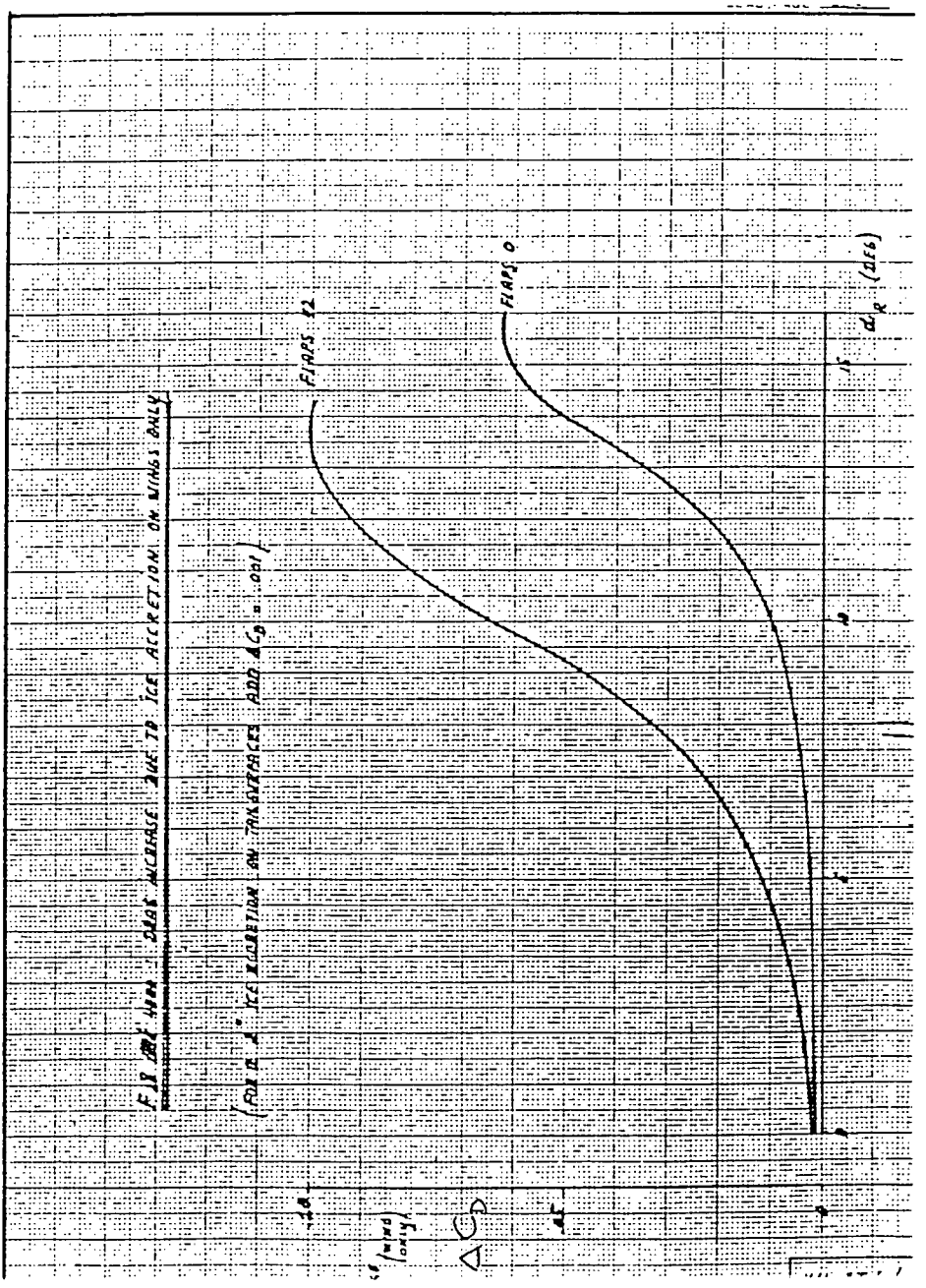
FLAPS 42
FLAPS 0
α_R (DEG)
ΔC_D
$\Delta\alpha$
FOR EACH 1° INCIDENCE ON SURFACES ADD ΔC_D = .001
FOR EACH 1° INCIDENCE ON SURFACES ADD ΔC_D = .001

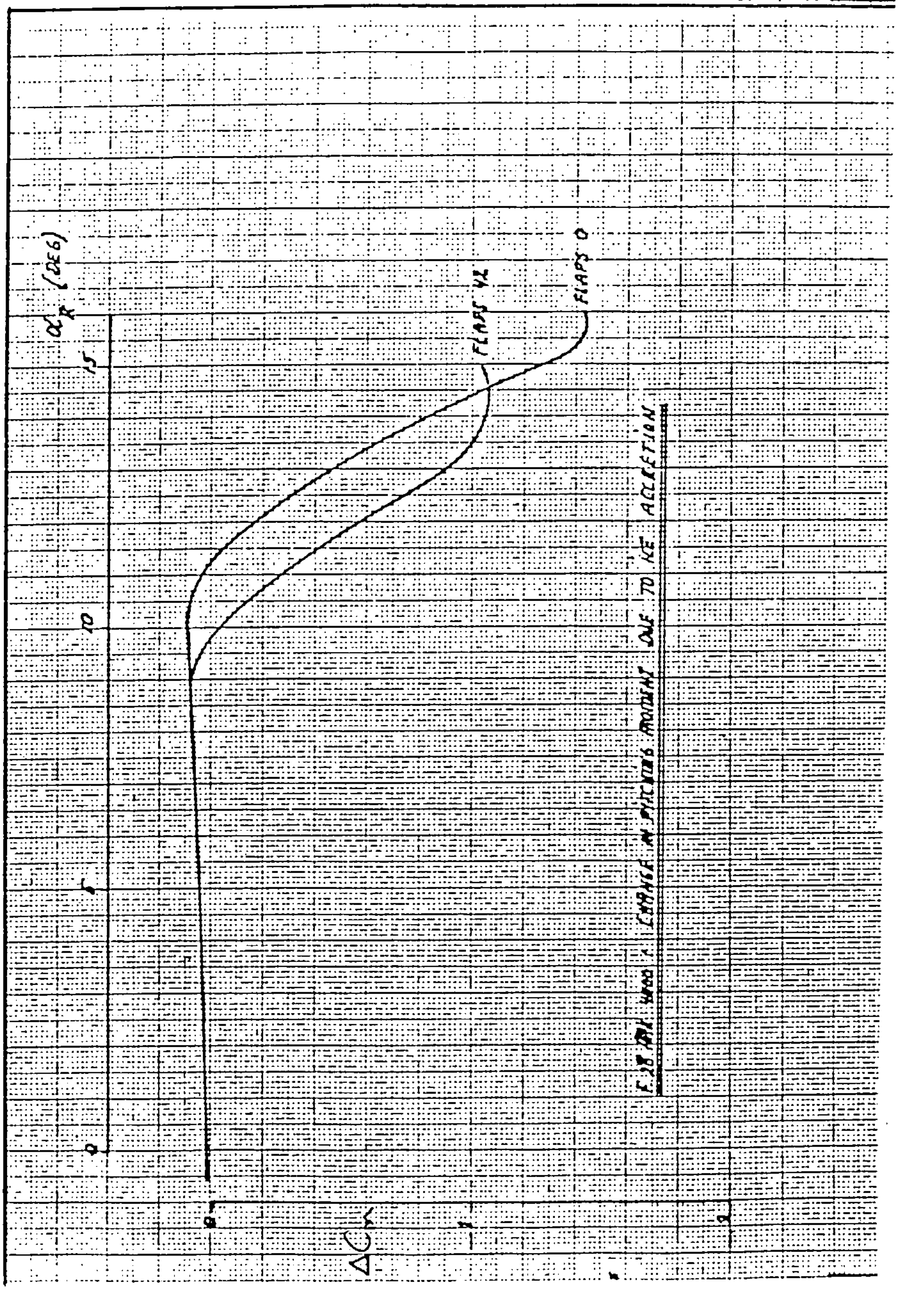
CHANGE IN PITCHING MOMENT DUE TO ICE ACCRETION
FLAPS 42
FLAPS 0
15
10
5
0

F-28 FLIGHT DYNAMICS Section 2 - Aerodynamics Figure 14d Page 42

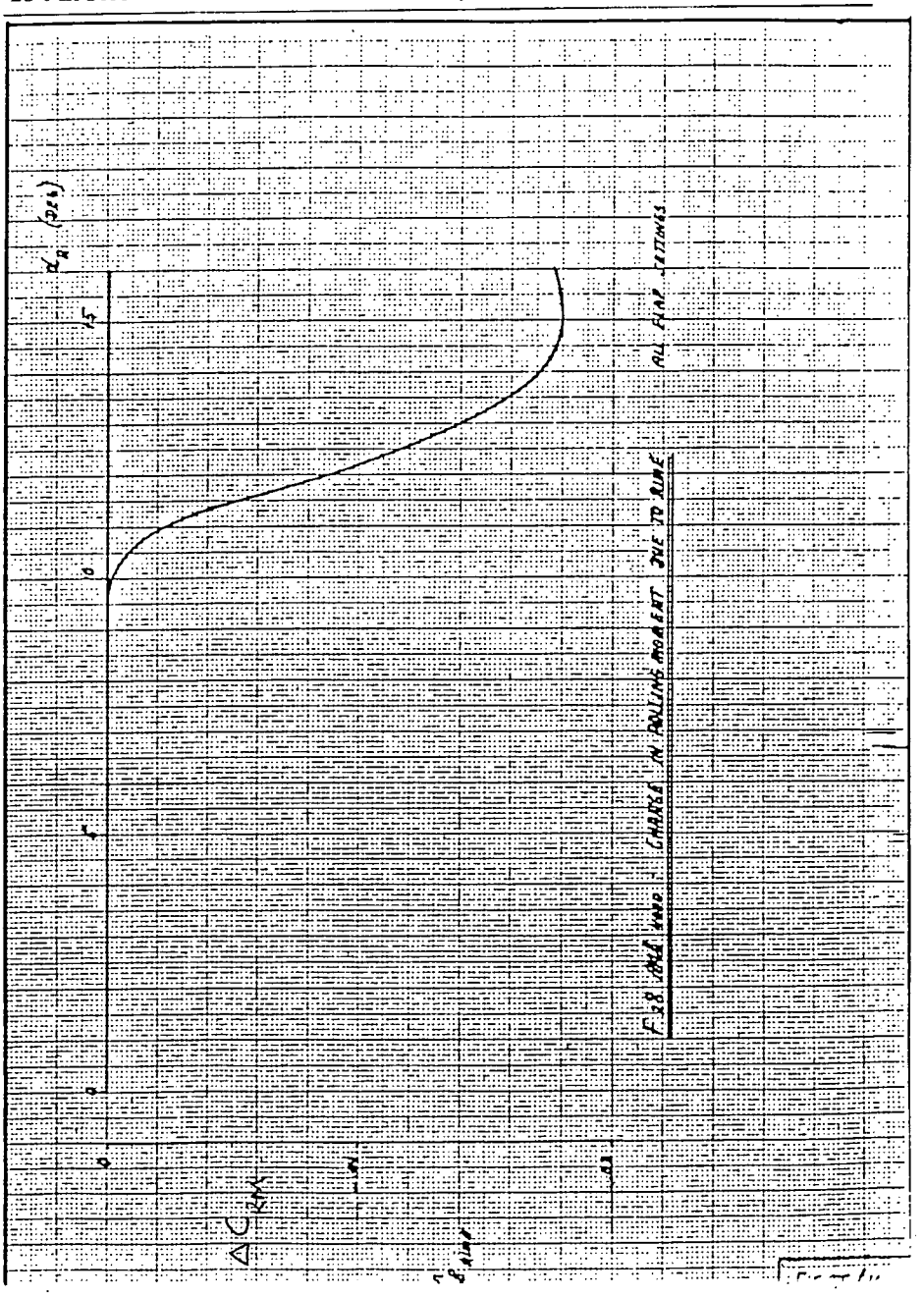

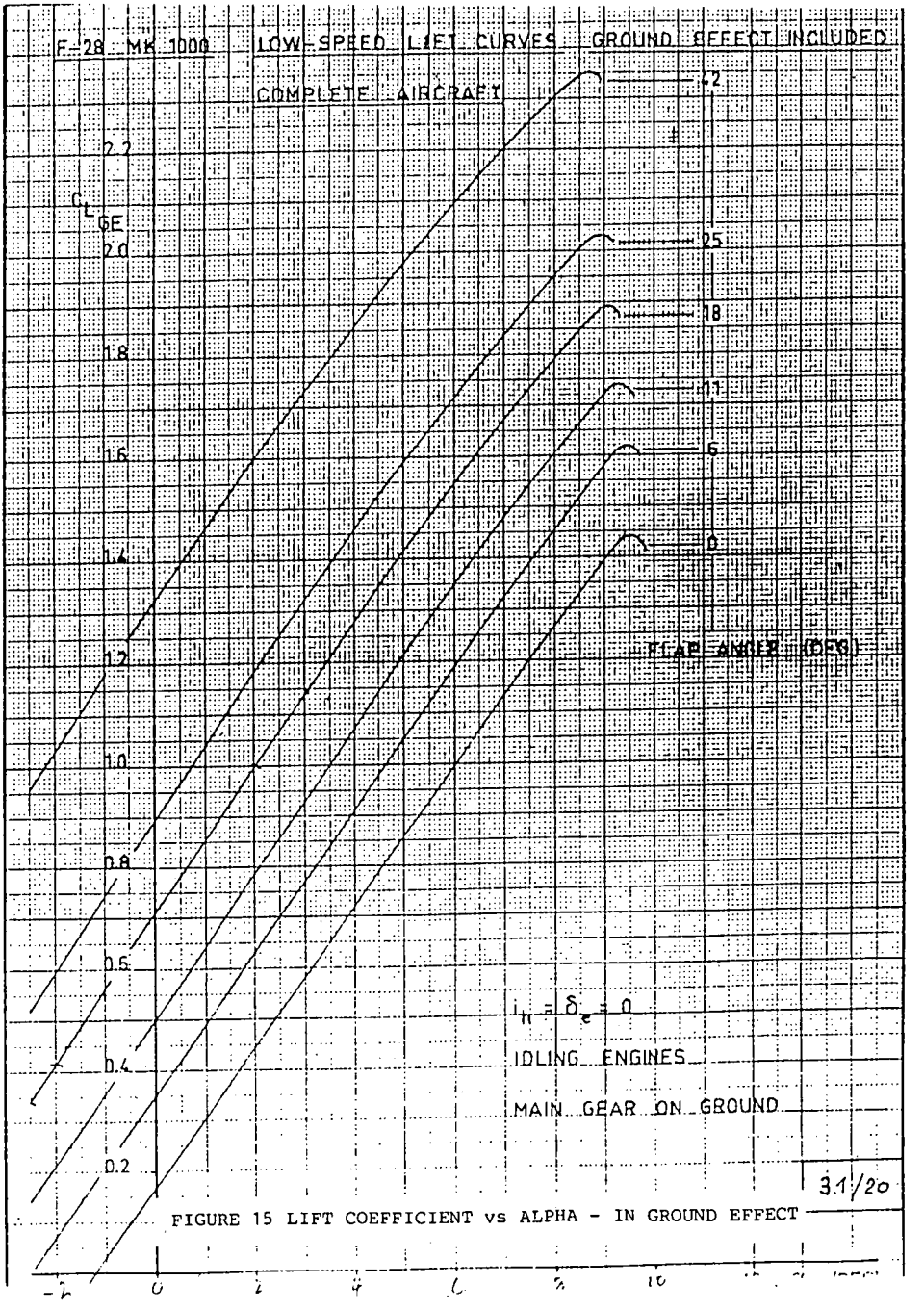

FIGURE 15 LIFT COEFFICIENT vs ALPHA - IN GROUND EFFECT

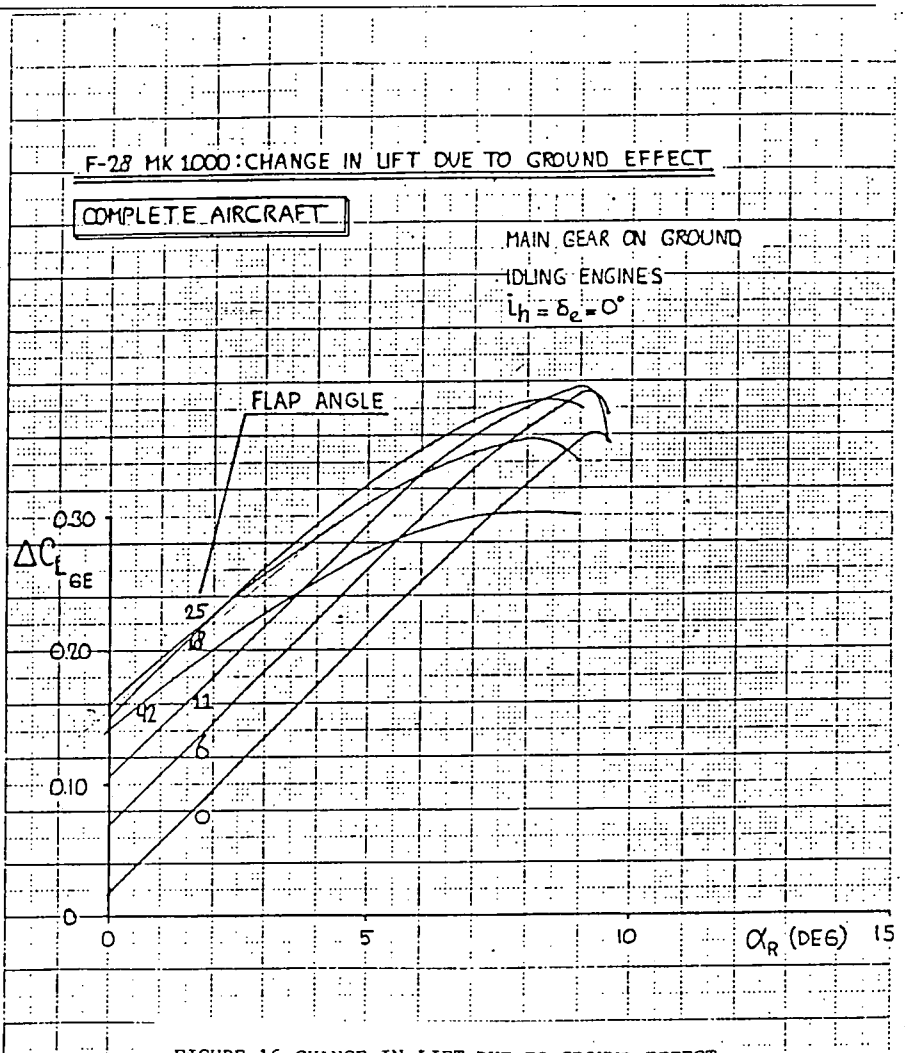

FIGURE 16 CHANGE IN LIFT DUE TO GROUND EFFECT

3.1/20A

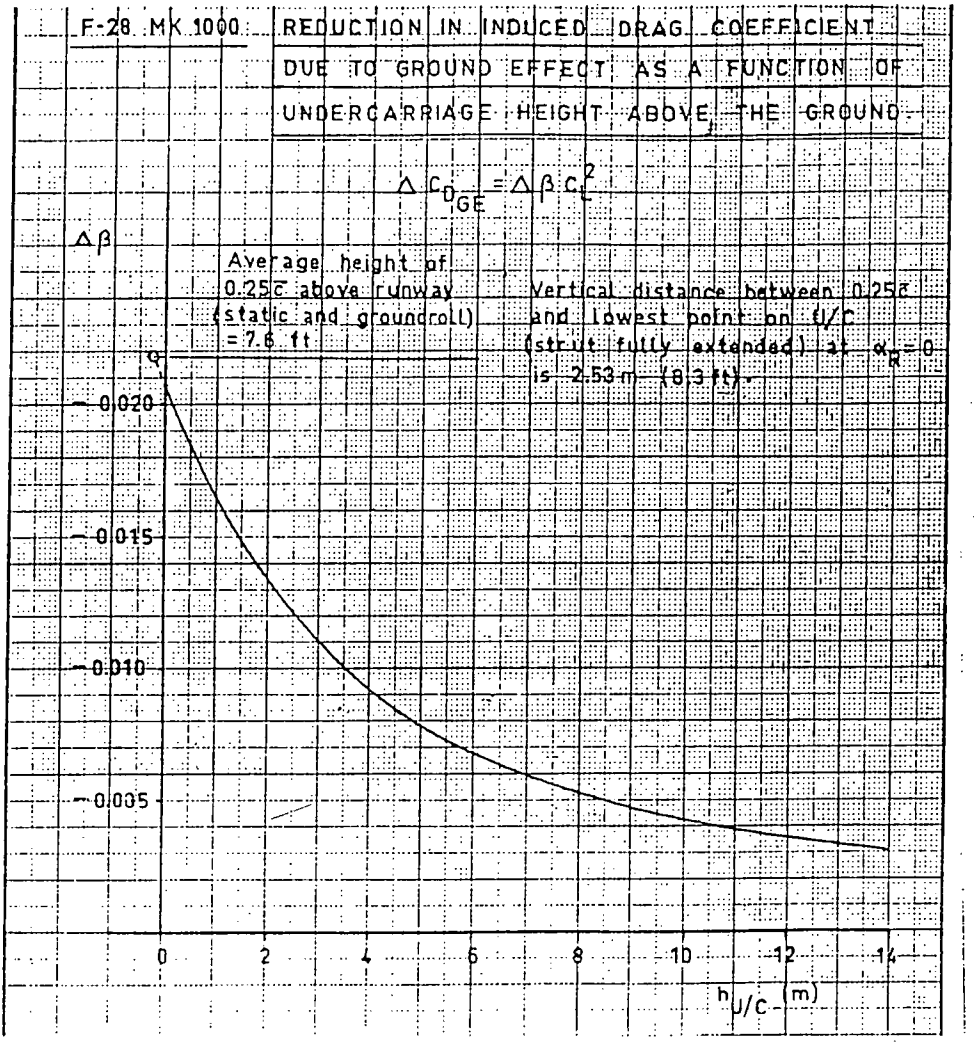

FIGURE 17 CHANGE IN INDUCED DRAG DUE TO GROUND EFFECT

APPENDIX A TO SECTION 2

TECHNICAL DETAILS OF THE FOKKER F-28 AIRCRAFT

FIGURE A-1

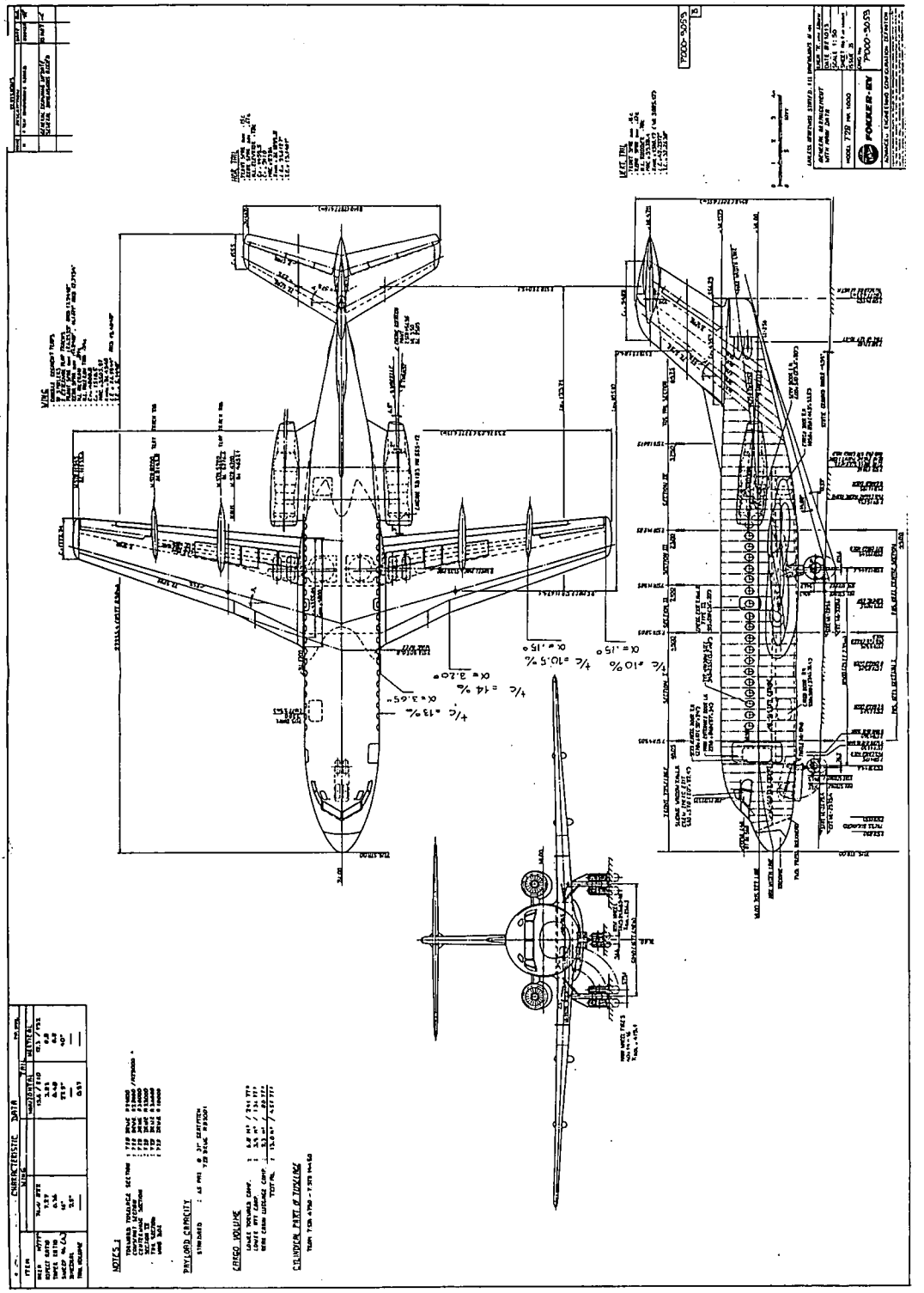

but a basic layout is available. In this, the cabin is divided into three sections: a conference room with six seats, a rest room with settee and divan, and a lounge with four seats. Toilet, galley, wardrobe, baggage space and seat for attendant in forward fuselage. Second toilet and baggage space at rear.

ACCOMMODATION (Mk 400 Combiplane): Principal feature of this version are a large cargo loading door forward of the wings on the port side, with the sill at truck-bed height, and a reinforced cargo floor with tiedown rings. Typical layouts include 40 passengers four abreast at 35·5 in (90 cm) seat pitch, plus 218 cu ft (6·17 m³) of cargo space; 28 passengers at same seat pitch in rear of cabin, plus 588 cu ft (16·65 m³) cargo space; or all-cargo version with 1,727 cu ft (48·9 m³) of cargo space. Alternative layouts for up to 48 passengers.

ACCOMMODATION (Mk 400M): Folding canvas seats, with safety harnesses, along cabin sides for up to 45 paratroops. Toilet and provision for medical supply box or pantry unit at rear. Ambulance version can accommodate 24 USAF-type stretchers, in eight tiers of three, with seats at front and rear for up to nine medical attendants or sitting casualties. All-cargo version fitted with skid strips, tiedown fittings, protection plates and hinged hatracks. Despatch door on each side of fuselage at rear for dropping supplies and personnel.

ACCOMMODATION (Mk 500): Main cabin has standard seating for 52 passengers four abreast at 35·25 in (89·5 cm) seat pitch; alternative layouts enable up to 56 passengers to be carried at 28·5 in (72 cm) pitch.

SYSTEMS: Pressurisation and air-conditioning system utilises two Rootes-type engine-driven blowers. Choke heating and air-to-air heat exchanger; optional bootstrap cooling system. Pressure differential 4·16 lb/sq in (0·29 kg/cm²) in Mks 400, 500 and 600; 5·5 lb/sq in (0·39 kg/cm²) in Mk 200. No hydraulic system. Pneumatic system, pressure 3,400 lb/sq in (239 kg/cm²), for landing gear retraction, nosewheel steering and brakes. Emergency pneumatic circuits for landing gear extension and brakes. Primary 28V electrical system supplied by two 375A 28V DC engine-driven generators. Secondary system supplied via two 115V 400Hz AC constant-frequency inverters. Variable-frequency AC power supply, from 120/208V 15kVA engine-driven alternators, for anti-icing and heating. Two 24V 40Ah nickel-cadmium batteries. 30·4 cu ft (1·12 m³) oxygen system for pilots.

ELECTRONICS AND EQUIPMENT: Standard provisions for VHF and HF transceivers, VHF navigation system (including glideslope), ADF, ILS, marker beacon, dual gyrosyn compass system and intercom system. Provision for weather radar, autopilot etc.

DIMENSIONS, EXTERNAL:

Wing span	95 ft 2 in (29·00 m)
Wing chord at root	11 ft 4 in (3·45 m)
Wing chord at tip	4 ft 7 in (1·40 m)
Wing aspect ratio	12
Length overall:	
except Mk 500	77 ft 3½ in (23·56 m)
Mk 500	82 ft 2½ in (25·06 m)
Fuselage: Max width	8 ft 10½ in (2·70 m)
Max height	9 ft 1½ in (2·79 m)
Height overall, standard landing gear:	
except Mk 500	27 ft 11 in (8·50 m)
Mk 500	28 ft 7½ in (8·71 m)
Height overall, rough-field landing gear:	
except Mk 500	28 ft 2 in (8·59 m)
Tailplane span	32 ft 0 in (9·75 m)
Wheel track (o/l shock struts)	23 ft 7½ in (7·20 m)
Wheelbase:	
except Mk 500	28 ft 8 in (8·74 m)
Mk 500	31 ft 11½ in (9·74 m)
Propeller diameter	11 ft 6 in (3·50 m)
Propeller ground clearance:	
standard landing gear:	
except Mk 500	3 ft 1 in (0·94 m)
Mk 500	3 ft 3 in (0·99 m)
rough-field landing gear:	
except Mk 500	3 ft 4½ in (1·02 m)
Passenger door (aft, port):	
Height	5 ft 5 in (1·65 m)
Width	2 ft 5 in (0·74 m)
Height to sill	4 ft 0 in (1·22 m)
Service/emergency door (aft, stbd):	
Height	3 ft 8 in (1·12 m)
Width	2 ft 5 in (0·74 m)
Height to sill	3 ft 3 in (0·99 m)
Standard cargo door (Mk 200 only):	
Height	3 ft 11 in (1·19 m)
Width	3 ft 6 in (1·04 m)
Height to sill	3 ft 3 in (0·99 m)
Large cargo door (Mks 400, 500 and 600):	
Height	6 ft 10 in (1·78 m)
Width	7 ft 7½ in (2·32 m)
Height to sill:	
except Mk 500	3 ft 3 in (0·99 m)
Mk 500	3 ft 4½ in (1·03 m)
Despatch doors (Mk 400M only, aft, port and stbd, each):	
Height	5 ft 5 in (1·65 m)
Width	3 ft 11 in (1·19 m)
Height to sill	4 ft 0 in (1·22 m)

DIMENSIONS, INTERNAL:

Cabin, excl flight deck:	
Length:	
except Mk 500	47 ft 5 in (14·46 m)
Mk 500	52 ft 4 in (15·95 m)
Max width	8 ft 4½ in (2·55 m)
Max height	6 ft 7½ in (2·02 m)
Volume:	
except Mk 500	2,130 cu ft (60·5 m³)
Mk 500	2,360 cu ft (66·8 m³)
Freight hold (fwd) max:	
Mk 200	169 cu ft (4·78 m³)
Mks 400, 500, 600	197 cu ft (5·58 m³)
Freight hold (aft) max:	
all versions	100 cu ft (2·83 m³)

AREAS:

Wings, gross	753·5 sq ft (70·0 m²)
Ailerons (total)	37·80 sq ft (3·51 m²)
Trailing-edge flaps (total)	136·20 sq ft (12·72 m²)
Vertical tail surfaces (total)	163 sq ft (14·20 m²)
Horizontal tail surfaces (total)	172 sq ft (16·00 m²)

WEIGHTS AND LOADINGS:

Manufacturer's weight, empty:	
Mk 200, 44 seats	22,436 lb (10,177 kg)
Mk 400, 40 seats	23,200 lb (10,564 kg)
Mk 400M	23,360 lb (10,596 kg)
Mk 500, 52-56 seats	23,578 lb (10,695 kg)
Mk 500M	24,325 lb (11,034 kg)
Mk 600, 44 seats	22,786 lb (10,330 kg)
Operating weight, empty:	
Mk 200, 44 seats	24,612 lb (11,164 kg)
Mk 400, 40 seats	24,875 lb (11,283 kg)
Mk 400M, all-cargo	23,947 lb (10,862 kg)
Mk 400M, medical evacuation	24,880 lb (11,288 kg)
Mk 400M, paratrooper	24,336 lb (11,039 kg)
Mk 500, 52-56 seats	25,015 lb (11,765 kg)
Mk 500M, all-cargo	24,912 lb (11,300 kg)
Mk 500M, medical evacuation	26,023 lb (11,804 kg)
Mk 500M, paratrooper	25,332 lb (11,491 kg)
Mk 600, 44 seats	24,062 lb (11,323 kg)
Max payload (weight limited):	
Mk 200, 44 seats	12,888 lb (5,846 kg)
Mk 400, 40 seats	12,625 lb (5,727 kg)
Mk 400M, all-cargo	13,553 lb (6,148 kg)
Mk 400M, medical evacuation	12,612 lb (5,721 kg)
Mk 400M, paratrooper	13,104 lb (5,971 kg)
Mk 500, 52-56 seats	13,585 lb (6,162 kg)
Mk 500M, all-cargo	14,588 lb (6,617 kg)
Mk 500M, medical evacuation	13,477 lb (6,113 kg)
Mk 500M, paratrooper	14,168 lb (6,427 kg)
Mk 600, 44 seats	12,538 lb (5,687 kg)
Max T-O weight:	
all versions	45,000 lb (20,410 kg)
Max landing weight:	
Mks 200, 400, 400M and 600	41,000 lb (18,600 kg)
Mks 500 and 500M	42,000 lb (19,050 kg)
Max zero-fuel weight:	
Mks 200, 400, 400M and 600	37,000 lb (17,010 kg)
Mks 500 and 500M	39,500 lb (17,900 kg)
Max wing loading:	
all versions	59·7 lb/sq ft (291·5 kg/m²)
Max power loading:	
all versions	10·5 lb/shp (4·76 kg/shp)

PERFORMANCE (at weights indicated):

Normal cruising speed at 20,000 ft (6,100 m) and AUW of 38,000 lb (17,237 kg):	
all versions	250 knots (288 mph; 460 km/h)
Rate of climb at S/L, AUW of 40,000 lb (18,143 kg):	
all civil versions	1,480 ft (451 m)/min
both military versions	1,620 ft (494 m)/min
Service ceiling at AUW of 38,000 lb (17,237 kg):	
all civil versions	29,500 ft (8,990 m)
both military versions	30,000 ft (9,145 m)
Service ceiling, one engine out, at AUW of 38,000 lb (17,237 kg):	
all civil versions	11,700 ft (3,565 m)
both military versions	13,300 ft (4,055 m)
Runway LCN at max T-O weight, standard landing gear	16
Required T-O field length (ICAO-PAMC) at AUW of 40,000 lb (18,143 kg), all civil versions:	
S/L, ISA	3,250 ft (991 m)
S/L, ISA +15°C	3,560 ft (1,085 m)
3,000 ft (914 m), ISA	3,980 ft (1,213 m)
Required T-O field length (military) at AUW of 40,000 lb (18,143 kg), both military versions:	
S/L, ISA	2,310 ft (704 m)
S/L, ISA +15°C	2,510 ft (765 m)
3,000 ft (914 m), ISA	2,750 ft (838 m)
Required landing field length (ICAO-PAMC) at AUW of 37,500 lb (17,010 kg), all civil versions:	
S/L	3,160 ft (963 m)
3,000 ft (914 m)	3,390 ft (1,033 m)
Required landing field length (military) at AUW of 37,500 lb (17,010 kg), both military versions:	
S/L	1,900 ft (579 m)
3,000 ft (914 m)	2,040 ft (622 m)
Range (ISA, zero wind conditions) with FAR 121.645 reserves for diversion, 30 min hold at 10,000 ft (3,050 m) and 10% flight fuel:	
Mks 200 and 600, 44 passengers	1,020 nm (1,197 miles; 1,926 km)
Mk 400, 40 passengers	1,025 nm (1,203 miles; 1,935 km)
Mk 500, 52 passengers	935 nm (1,082 miles; 1,741 km)
Military transport range (ISA, zero wind conditions) at max T-O weight, reserves for 30 min hold at S/L and 5% initial fuel:	
Mks 400M and 500M, all-cargo, max standard fuel	1,195 nm (1,376 miles; 2,213 km)
Mks 400M and 500M, all-cargo, max possible fuel	2,370 nm (2,727 miles; 4,390 km)
Military combat radius, conditions as above:	
Mks 400M and 500M, all-cargo, max standard fuel	625 nm (719 miles; 1,158 km)
Mks 400M and 500M, all-cargo, max possible fuel	1,230 nm (1,416 miles; 2,278 km)
Max endurance at 20,000 ft (6,100 m):	
Mk 400M, max standard fuel	7 hr 23 min
Mk 400M, max possible fuel	12 hr 47 min
Mk 500M, max standard fuel	7 hr 14 min
Mk 500M, max possible fuel	12 hr 26 min

OPERATIONAL NOISE CHARACTERISTICS (FAR Pt 36):

T-O noise level	89 EPNdB
Approach noise level	99 EPNdB
Sideline noise level	92·5 EPNdB

FOKKER-VFW F28 FELLOWSHIP

Announced in April 1962, the F28 Fellowship twin-turbofan short-haul transport was developed in collaboration with other European aircraft manufacturers and with the financial support of the Netherlands government. One half of the Dutch share of the development cost was supplied through the Netherlands Aircraft Development Board, the other half through a loan guaranteed by the government.

Under agreements signed in the Summer of 1964, production is undertaken by Fokker-VFW in association with MBB and VFW-Fokker in Germany and Short Bros and Harland in the UK.

Fokker-VFW is responsible for the front fuselage, to a point just aft of the flight deck, the centre fuselage and wing-root fairings. MBB builds the fuselage, from the wing trailing-edge to the rear pressure bulkhead, and the engine nacelles and support stubs. VFW-Fokker is responsible for the rear fuselage and tail unit, and for the cylindrical fuselage section between the wing leading-edge and flight deck. Shorts are responsible for the wings (including the slatted wings for the Mks 5000 and 6000), and other components, including the main-wheel and nosewheel doors.

First flight of the first prototype F28 (PH-JHG)

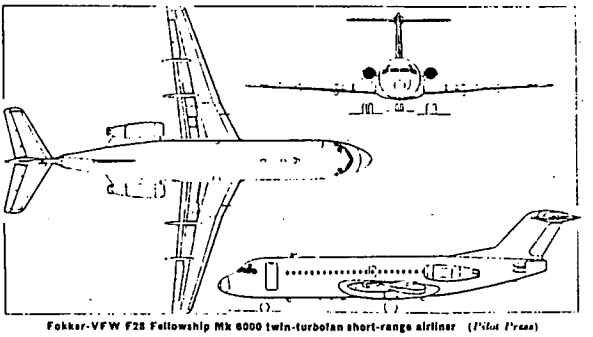

Fokker-VFW F28 Fellowship Mk 6000 twin-turbofan short-range airliner (*Pilot Press*)

Fokker-VFW F28 Fellowship Mk 2000 short-haul transport, in the insignia of Air Gabon

was made on 9 May 1967, and the second prototype, PH-WEV, flew on 3 August 1967. The third F28 (PH-MOL) flew for the first time on 20 October 1967 and was brought up to production standard in the early Summer of 1968.

The Dutch RLD granted a C of A to the F28 on 24 February 1969, and the first delivery (of the fourth aircraft, to LTU) was made on the same day. The aircraft received FAA Type Approval on 24 March 1969 and German certification on 30 March 1969. RLD certification for operation from unpaved runways was granted in mid-1972. The Mk 1000 was granted FAA-approved noise certification on 31 December 1971.

A total of 107 Fellowships (85 Mk 1000, 7 Mk 1000C, 10 Mk 2000 and 5 Mk 4000) had been ordered by 3 June 1975, as follows:

Mk 1000/1000C

Aerolineas Argentinas	3
AeroPeru	3
Air Gabon (1 Mk 1000VIP, 1 Mk 1000C)	2
Air Nauru	2
Ansett Transport Industries (Airlines of NSW and MacRobertson-Miller)	6
Argentine Air Force (Mk 1000C)	6
Argentine government	1
Australian Dept of Transport (Air)	3
Avinetion (Germany)	3
Braathens (Norway)	6
Colombian Air Force	1
Congo (Brazzaville)	1
Eastex (USA)	1
Fairchild Industries	1
Garuda Indonesian Airways	18
Germanair	4
Iberia	3
Itavia (Italy)	3
Ivory Coast (1 Mk 1000, 1 Mk 1000C)	2
Linjeflyg (Sweden)	3
LTU (Germany)	4
Malaysian government	2
Martinair-Holland	1
Netherlands government	1
Nigeria Airways	2
Nigerian government	1
Polita/Pertamina	2
Peruvian government	1
THY (Turkey)	5
Togo government	1
Touraine Air Transport	1
Transair (Canada)	2

Mk 2000

Air Gabon	2
Ghana Airways	2
Nigeria Airways	6

Mk 4000

Undisclosed	5

Six versions have been announced, as follows:

Mk 1000. Initial version, in production and service, with seating for up to 65 passengers. First F28 commercial service was flown by Braathens on 28 March 1969. Available optionally, for all-cargo or mixed passenger/cargo operations, with large freight door at front on port side, aft of passenger door, in which form it is designated **Mk 1000C**.

Mk 2000. Similar to Mk 1000 except for lengthened fuselage, permitting an increase in accommodation for up to 79 passengers in all-tourist layout. F28 first prototype modified to Mk 2000 standard and flown for first time on 28 April 1971. Dutch certification awarded on 30 August 1972. In production and service.

Mk 3000. See Addenda.

Mk 4000. High-density version, announced in early 1975, to seat up to 85 passengers at 29 in (74 cm) pitch. Airframe basically that of Mk 6000, except for omission of leading-edge slats; uprated Spey Mk 555-15H is retained as power plant. Intended for use over stage lengths of about 800 nm (1,025 miles; 1,850 km), using a T-O field length of 5,740 ft (1,750 m). Two additional overwing emergency exits (making a total of four). Design criteria, due to be finalised by April 1975, include a max T-O weight of 70,990 lb (32,200 kg), max landing weight of 63,035 lb (29,000 kg) and max zero-fuel weight of 57,540 lb (26,100 kg).

Mk 5000. Similar to Mk 1000 except for slatted, long-span wings and improved Spey engines. Available with large cargo door.

Mk 6000. Similar to Mk 2000 except for slatted, long-span wings and improved Spey engines. Prototype, modified from F28 first prototype (previously used for Mk 2000 certification flying) and fitted with modified wings from the second prototype, made its first flight on 27 September 1973. Certification expected by mid-1976.

The following details apply generally to all versions, except where a specific model is indicated:

Type: Twin-turbofan short-range airliner.

Wings: Cantilever low/mid-wing monoplane. Wing section NACA 0000-X 40Y series with camber varying along span. Thickness/chord ratio up to 14% on inner wing, 10% at tip. Dihedral 2° 30'. Sweepback at quarter-chord 16°. Single-cell two-spar light alloy torsion-box structure, comprising centre-section, integral with fuselage, and two outer wings. Fail-safe construction. Lower skin made of three planks. Taper-rolled top skin. Forged ribs in centre-section, built-up ribs in outer panels. Double-skin leading-edge with ducts for hot-air de-icing. Irreversible hydraulically-operated ailerons. Emergency manual operation of ailerons, through tabs. Hydraulically-operated Fowler double-slotted flaps over 70% of each half-span with electrical emergency extension. Five-section hydraulically-operated lift dumpers in front of flaps on each wing. Trim tab in each aileron. Mks 5000 and 6000 have extended-span wings with full-span hydraulically-operated leading-edge slats.

Fuselage: Circular-section semi-monocoque light alloy fail-safe structure, made up of skin panels with Redux-bonded Z-stringers. Bonded doubler plates at door and window cut-outs. Quickly-detachable sandwich (metal/end grain balsa) floor panels. Hydraulically-operated petal airbrakes form aft end of fuselage.

Tail Unit: Cantilever light alloy structure, with hydraulically-actuated variable-incidence T tailplane. Electrical emergency actuation of tailplane. Hydraulically-boosted elevators. Hydraulically-operated rudder with duplicated actuators and emergency manual operation. Honeycomb sandwich skin panels used extensively, in conjunction with multiple spars. Double-skin leading-edges for hot-air de-icing.

Landing Gear: Retractable tricycle type of Dowty-Rotol manufacture, with twin wheels on each unit. Hydraulic retraction, nose-wheels forward, main units inward into fuselage. Oleo-pneumatic shock-absorbers. Goodyear wheels, tyres and electronically-controlled braking system. Steerable nosewheel. Main-wheel tyres size 39 × 13, 16-ply rating, pressure 100 lb/sq in (7·0 kg/cm²) on Mk 1000, 102 lb/sq in (7·1 kg/cm²) on Mk 2000, 110 lb/sq in (7·7 kg/cm²) on Mks 5000 and 6000. Nosewheel tyres size 24·5 × 8·5, 10-ply rating, pressure 85 lb/sq in (5·98 kg/cm²) on Mk 1000, 78 lb/sq in (5·5 kg/cm²) on Mk 2000, 80 lb/sq in (5·6 kg/cm²) on Mk 5000 and 75 lb/sq in (5·3 kg/cm²) on Mk 6000. Low-pressure tyres optional on all units.

Power Plant (Mks 1000 and 2000): Two Rolls-Royce RB.183-2 Spey Mk 555-15 turbofan engines with blade-cooling (each 9,850 lb; 4,468 kg st), mounted in pod on each side of rear fuselage. No water injection or thrust reversers. Thermal anti-icing for air intakes. For Mks 5000 and 6000, a Mk 555-15H version of the Spey engine is under development. This will retain the existing nominal thrust rating of the Mk 555-15, but at ambient temperatures up to 28°C, and will be fitted with a five-chute silencing nozzle. Integral fuel tank in each outer wing panel with total usable capacity of 2,143 Imp gallons (9,740 litres) in Mks 1000/2000; 2,130 Imp gallons (9,682 litres) in Mks 5000/6000. Optional seven bladder-type tank units in wing centre-section with total usable capacity of 720 Imp gallons (3,300 litres). Single refuelling point under starboard wing, near root.

Accommodation: Crew of two side by side on flight deck, with jump-seat for third crew member. Electrically-heated windscreen. Pantry/baggage space immediately aft of flight deck on starboard side, followed by entrance lobby with hydraulically-operated airstair door on port side, service and emergency door on starboard side, and seat for stewardess. On Mks 1000 and 5000, an optional upward-opening cargo door, to permit all-cargo or all-passenger operation, can be added aft of the passenger airstair door. Additional emergency door on each side of main cabin, over wing. Main cabin layout of Mks 1000/5000 can be varied to accommodate 55, 60 or 65 passengers five abreast as 27, 32/33 or 31 in (94, 81/84 or 79 cm) seat pitch respectively. In Mks 2000/6000, layout can be varied to accommodate 79 passengers at 31 in (79 cm) seat pitch. Aft of cabin are a wardrobe (port), baggage compartment (port) and toilet compartment (starboard). Underfloor cargo compartments fore and aft of wing, with single door on starboard side of forward hold, with one door on rear hold of each version.

Systems: AiResearch air-conditioning system, using engine bleed air. Max pressure differential 7·45 lb/sq in (0·52 kg/cm²). Two independent hydraulic systems, pressure 3,000 lb/sq in (210 kg/cm²). Primary system for flight controls, landing gear, nosewheel steering and brakes, secondary system for duplication of certain essential flight controls. Flying control hydraulic components supplied by Jarry Hydraulics. All-AC electrical system utilises two 20kVA Westinghouse engine-driven generators to supply three-phase constant-frequency 115/200V 400Hz power. One 20Ah battery for starting APU and for emergency power. AiResearch GTCP 36-4A APU, mounted aft of rear pressure bulkhead, for engine starting, ground air-conditioning and ground electrical power, and to drive a third AC generator for standby use on essential services in flight.

Electronics and Equipment: Standard equipment includes VHF transceivers, VHF navigation system (with glideslope), DME, marker beacon, weather radar, ADF, ATC transponder, dual compass system, interphone and public address systems, Smiths SEPD autopilot, Collins FD 108 flight director, flight guidance caution system, flight data recorder and voice recorder. Thermal bleed air system for wing leading-edges (slats on Mks 5000/6000), tailplane leading-edge and engine air intakes. Stick pusher system on Mks 5000/6000. Optional equipment to customer's requirements, including equipment for operation in Cat. 2 weather minima.

Dimensions, external:

Wing span:	
1000, 2000	77 ft 4½ in (23·58 m)
5000, 6000	82 ft 3 in (25·07 m)
Wing chord at root:	
all versions	15 ft 9 in (4·80 m)
Wing chord at tip:	
1000, 2000	5 ft 9½ in (1·77 m)
Wing aspect ratio:	
1000, 2000	7·27
Length overall:	
1000, 5000	89 ft 10½ in (27·40 m)
2000, 6000	97 ft 1½ in (29·61 m)
Length of fuselage:	
1000, 5000	80 ft 6½ in (24·55 m)
2000, 6000	87 ft 9½ in (26·76 m)

AUSTRALIA/NEW ZEALAND: AIRCRAFT—FOKKER-VFW/AEROSPACE

Fuselage: Max width 10 ft 10 in (3·30 m)
Height overall 27 ft 0¾ in (8·47 m)
Tailplane span 28 ft 4¾ in (8·64 m)
Wheel track (c/l of shock struts)
16 ft 6¾ in (5·04 m)
Wheelbase:
1000, 5000 29 ft 2¼ in (8·90 m)
2000, 6000 33 ft 11¼ in (10·35 m)
Passenger door (fwd, port):
Height 6 ft 4 in (1·93 m)
Width 2 ft 10 in (0·86 m)
Service/emergency door (fwd, stbd):
Height 4 ft 3 in (1·27 m)
Width 2 ft 0 in (0·61 m)
Emergency exits (centre, each):
Height 3 ft 0 in (0·91 m)
Width 1 ft 8 in (0·51 m)
Freight hold doors (each):
Height (fwd, each) 2 ft 11½ in (0·90 m)
Height (aft) 2 ft 7½ in (0·80 m)
Width (fwd, each) 3 ft 1½ in (0·95 m)
Width (aft) 2 ft 11 in (0·89 m)
Height to sill (fwd, each) 4 ft 10 in (1·47 m)
Height to sill (aft) 5 ft 2½ in (1·59 m)
Baggage door (rear, port, optional):
Height 1 ft 11½ in (0·60 m)
Width 1 ft 8 in (0·51 m)
Optional cargo door (fwd, port):
Height 6 ft 1½ in (1·87 m)
Width 8 ft 2 in (2·49 m)
Height to sill 7 ft 4½ in (2·24 m)

DIMENSIONS, INTERNAL:
Cabin, excl flight deck:
Length:
1000, 5000 43 ft 0 in (13·10 m)
2000, 6000 50 ft 3 in (15·31 m)
Max length of seating area:
1000, 5000 35 ft 2¾ in (10·74 m)
2000, 6000 42 ft 6¾ in (12·95 m)
Max width 10 ft 2 in (3·10 m)
Max height 6 ft 7½ in (2·02 m)
Floor area:
1000, 5000 413·3 sq ft (38·4 m²)
2000, 6000 482·2 sq ft (44·8 m²)
Volume:
1000, 5000 2,525 cu ft (71·5 m³)
2000, 6000 2,931 cu ft (83·0 m³)
Freight hold (underfloor, fwd):
1000, 5000 245 cu ft (6·90 m³)
2000, 6000 308 cu ft (8·70 m³)
Freight hold (underfloor, rear):
1000, 5000 135 cu ft (3·80 m³)
2000, 6000 169 cu ft (4·80 m³)
Baggage hold (aft of cabin), max
80 cu ft (2·265 m³)

AREAS:
Wings, gross:
1000, 2000 822 sq ft (76·40 m²)
5000, 6000 850 sq ft (78·97 m²)
Ailerons (total) 24·74 sq ft (2·67 m²)
Trailing-edge flaps (total) 150·7 sq ft (14·00 m²)
Fuselage airbrakes (total) 38·97 sq ft (3·62 m²)
Fin (incl dorsal fin) 132·4 sq ft (12·30 m²)
Rudder 24·76 sq ft (2·30 m²)
Tailplane 209·9 sq ft (19·50 m²)
Elevators (total) 41·33 sq ft (3·84 m²)

WEIGHTS AND LOADINGS:
Manufacturer's weight empty:
1000, 65 seats 31,954 lb (14,492 kg)
1000C 31,954 lb (14,492 kg)
2000, 79 seats 32,929 lb (14,936 kg)
5000, 65 seats 33,504 lb (15,196 kg)
6000, 79 seats 34,477 lb (15,638 kg)
Operating weight empty:
1000, 65 seats 35,464 lb (16,084 kg)
1000C 35,853 lb (16,261 kg)
2000, 79 seats 36,795 lb (16,690 kg)
5000, 65 seats 37,014 lb (16,790 kg)
6000, 79 seats 38,345 lb (17,393 kg)
Max weight-limited payload:
1000 19,036 lb (8,636 kg)
1000C 18,647 lb (8,457 kg)
2000 17,705 lb (8,030 kg)
5000 17,486 lb (7,930 kg)
6000 17,655 lb (8,007 kg)

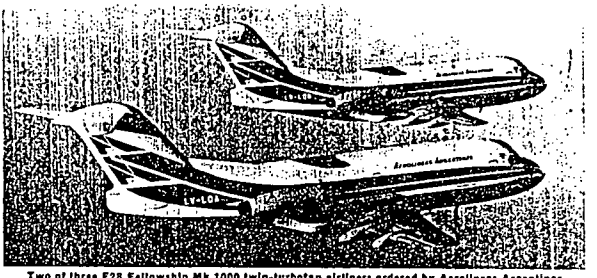

Two of three F28 Fellowship Mk 1000 twin-turbofan airliners ordered by Aerolineas Argentinas in early 1975

Max T-O weight:
1000, 2000 65,000 lb (29,485 kg)
5000, 6000 70,800 lb (32,115 kg)
Max zero-fuel weight:
1000, 2000, 5000 54,500 lb (24,720 kg)
6000 56,000 lb (25,400 kg)
Max landing weight:
1000, 2000 59,000 lb (26,760 kg)
5000, 6000 64,000 lb (29,030 kg)
Max wing loading:
1000, 2000 79·1 lb/sq ft (386 kg/m²)
5000, 6000 83·3 lb/sq ft (406 kg/m²)
Max cabin floor loading:
all passenger versions 76 lb/sq ft (380 kg/m²)
1000, 5000, with large cargo door
125 lb/sq ft (610 kg/m²)
Max power loading:
1000, 2000 3·3 lb/lb at (3·3 kg/kg at)
5000, 6000 3·6 lb/lb at (3·6 kg/kg at)

PERFORMANCE (ISA, except where indicated):
Max never-exceed speed (all versions)
390 knots (449 mph; 723 km/h) EAS
or Mach 0·83
Max permissible operating speed (all versions)
330 knots (380 mph; 611 km/h) EAS
or Mach 0·75
Max cruising speed at 23,000 ft (7,000 m) (all versions) 426 knots (523 mph; 843 km/h) TAS
Econ cruising speed at 30,000 ft (9,150 m), AUW of 59,000 lb (26,760 kg):
1000, 2000
362 knots (416 mph; 670 km/h) TAS
5000, 6000
366 knots (421 mph; 678 km/h) TAS
Threshold speed at max landing weight:
1000, 2000
110 knots (127 mph; 220 km/h) EAS
5000, 6000
110 knots (127 mph; 204 km/h) EAS
Max cruising altitude:
all versions 35,000 ft (10,675 m)
Min ground turning radius:
1000, 5000 31 ft 6 in (9·60 m)
2000, 6000 35 ft 9 in (10·90 m)
Runway LCN at max T-O weight (hard runway):
1000, standard tyres 20·5
1000, low-pressure tyres 22
2000, standard tyres 27
2000, low-pressure tyres 22·5
5000, standard tyres 31
5000, low-pressure tyres 27
6000, standard tyres 30
6000, low-pressure tyres 26
Runway LCN at max T-O weight (flexible runway):
1000, standard tyres 21
2000, standard tyres 21·5
5000, standard tyres 25
5000, low-pressure tyres 21
6000, standard tyres 24
6000, low-pressure tyres 20
FAR T-O field length at max T-O weight (1000, 2000):
S/L 5,490 ft (1,673 m)
S/L, ISA + 10°C 5,820 ft (1,774 m)
S/L, ISA + 15°C 6,160 ft (1,878 m)
2,000 ft (610 m) 5,970 ft (1,820 m)
3,000 ft (915 m) 6,320 ft (1,926 m)
FAR T-O field length at max T-O weight (5000, 6000):
S/L 5,860 ft (1,786 m)
S/L, ISA + 10°C 6,040 ft (1,843 m)
S/L, ISA + 15°C 6,168 ft (1,880 m)
2,000 ft (610 m) 6,120 ft (1,865 m)
3,000 ft (915 m) 6,530 ft (1,990 m)
FAR landing field length at max landing weight (1000, 2000):
S/L 3,510 ft (1,070 m)
5,000 ft (1,525 m) 4,010 ft (1,222 m)
FAR landing field length at max landing weight (5000, 6000):
S/L 3,120 ft (951 m)
5,000 ft (1,525 m) 3,527 ft (1,075 m)
Range, high-speed schedule, FAR 121.654 reserves:
1000, 65 passengers
1,020 nm (1,174 miles; 1,889 km)
2000, 79 passengers
630 nm (725 miles; 1,167 km)
*5000, 65 passengers
1,210 nm (1,392 miles; 2,240 km)
6000, 79 passengers
900 nm (1,036 miles; 1,667 km)
Range, long-range schedule, FAR 121.654 reserves:
1000, 65 passengers
1,130 nm (1,300 miles; 2,093 km)
2000, 79 passengers
700 nm (806 miles; 1,296 km)
*5000, 65 passengers
1,400 nm (1,611 miles; 2,593 km)
6000, 79 passengers
1,030 nm (1,185 miles; 1,908 km)

With wing centre-section tanks

OPERATIONAL NOISE CHARACTERISTICS (FAR Pt 36):
T-O noise level:
1000, 2000 90 EPNdB
5000, 6000 (estimated) 88 EPNdB
Approach noise level:
1000 101·2 EPNdB
2000 101·8 EPNdB
5000, 6000 (estimated) 97·5 EPNdB
Sideline noise level:
1000, 2000 99·5 EPNdB
5000, 6000 (estimated) 97 EPNdB

Fuselage: Max width	10 ft 10 in (3·30 m)
Height overall	27 ft 9½ in (8·47 m)
Tailplane span	28 ft 4½ in (8·64 m)
Wheel track (c/l of shock struts)	16 ft 6½ in (5·04 m)
Wheelbase:	
1000, 5000	29 ft 2½ in (8·90 m)
2000, 6000	33 ft 11½ in (10·35 m)
Passenger door (fwd, port):	
Height	6 ft 4 in (1·93 m)
Width	2 ft 10 in (0·86 m)
Service/emergency door (fwd, stbd):	
Height	4 ft 2 in (1·27 m)
Width	2 ft 0 in (0·61 m)
Emergency exits (centre, each):	
Height	3 ft 0 in (0·91 m)
Width	1 ft 8 in (0·51 m)
Freight hold doors (each):	
Height (fwd, each)	2 ft 11½ in (0·90 m)
Height (aft)	2 ft 7½ in (0·80 m)
Width (fwd, each)	3 ft 1½ in (0·95 m)
Width (aft)	2 ft 11 in (0·89 m)
Height to sill (fwd, each)	4 ft 10 in (1·47 m)
Height to sill (aft)	5 ft 2½ in (1·59 m)
Baggage door (rear, port, optional):	
Height	1 ft 11½ in (0·60 m)
Width	1 ft 8 in (0·51 m)
Optional cargo door (fwd, port):	
Height	6 ft 1½ in (1·87 m)
Width	8 ft 2 in (2·49 m)
Height to sill	7 ft 4½ in (2·24 m)
DIMENSIONS, INTERNAL:	
Cabin, excl flight deck:	
Length:	
1000, 5000	43 ft 0 in (13·10 m)
2000, 6000	50 ft 3 in (15·31 m)
Max length of seating area:	
1000, 5000	35 ft 2½ in (10·74 m)
2000, 6000	42 ft 6½ in (12·95 m)
Max width	10 ft 2 in (3·10 m)
Max height	6 ft 7½ in (2·02 m)
Floor area:	
1000, 5000	413·3 sq ft (38·4 m²)
2000, 6000	482·2 sq ft (44·8 m²)
Volume:	
1000, 5000	2,525 cu ft (71·5 m³)
2000, 6000	2,931 cu ft (83·0 m³)
Freight hold (underfloor, fwd):	
1000, 5000	245 cu ft (6·90 m³)
2000, 6000	308 cu ft (8·70 m³)
Freight hold (underfloor, rear):	
1000, 5000	135 cu ft (3·80 m³)
2000, 6000	169 cu ft (4·80 m³)
Baggage hold (aft of cabin), max	80 cu ft (2·265 m³)
AREAS:	
Wings, gross:	
1000, 2000	822 sq ft (76·40 m²)
5000, 6000	850 sq ft (78·97 m²)
Ailerons (total)	28·74 sq ft (2·67 m²)
Trailing-edge flaps (total)	150·7 sq ft (14·00 m²)
Fuselage airbrakes (total)	38·07 sq ft (3·62 m²)
Fin (incl dorsal fin)	132·4 sq ft (12·30 m²)
Rudder	24·76 sq ft (2·30 m²)
Tailplane	209·9 sq ft (19·50 m²)
Elevators (total)	41·33 sq ft (3·84 m²)
WEIGHTS AND LOADINGS:	
Manufacturer's weight empty:	
1000, 65 seats	31,954 lb (14,492 kg)
1000C	31,954 lb (14,492 kg)
2000, 79 seats	32,020 lb (14,938 kg)
5000, 65 seats	33,504 lb (15,198 kg)
6000, 79 seats	34,477 lb (15,638 kg)
Operating weight empty:	
1000, 65 seats	35,464 lb (16,084 kg)
1000C	35,853 lb (16,263 kg)
2000, 79 seats	36,795 lb (16,690 kg)
5000, 65 seats	37,014 lb (16,790 kg)
6000, 79 seats	38,345 lb (17,393 kg)
Max weight-limited payload:	
1000	19,036 lb (8,636 kg)
1000C	18,647 lb (8,457 kg)
2000	17,705 lb (8,030 kg)
5000	17,486 lb (7,930 kg)
6000	17,055 lb (8,007 kg)
Max T-O weight:	
1000, 2000	65,000 lb (29,485 kg)
5000, 6000	70,800 lb (32,115 kg)
Max zero-fuel weight:	
1000, 2000, 5000	54,500 lb (24,720 kg)
6000	56,000 lb (25,400 kg)
Max landing weight:	
1000, 2000	59,000 lb (26,760 kg)
5000, 6000	64,000 lb (29,030 kg)
Max wing loading:	
1000, 2000	79·1 lb/sq ft (386 kg/m²)
5000, 6000	83·3 lb/sq ft (406 kg/m²)
Max cabin floor loading:	
all passenger versions	75 lb/sq ft (366 kg/m²)
1000, 5000, with large cargo door	125 lb/sq ft (610 kg/m²)
Max power loading:	
1000, 2000	3·3 lb/lb at (3·3 kg/kg at)
5000, 6000	3·6 lb/lb at (3·6 kg/kg at)
PERFORMANCE (ISA, except where indicated):	
Max never-exceed speed (all versions)	390 knots (449 mph; 723 km/h) EAS or Mach 0·83
Max permissible operating speed (all versions)	330 knots (380 mph; 611 km/h) EAS or Mach 0·75
Max cruising speed at 23,000 ft (7,000 m) (all versions)	455 knots (523 mph; 843 km/h) TAS
Econ cruising speed at 30,000 ft (9,150 m), AUW of 59,000 lb (26,760 kg):	
1000, 2000	362 knots (416 mph; 670 km/h) TAS
5000, 6000	366 knots (421 mph; 678 km/h) TAS
Threshold speed at max landing weight:	
1000, 2000	119 knots (137 mph; 220 km/h) EAS
5000, 6000	110 knots (127 mph; 204 km/h) EAS
Max cruising altitude:	
all versions	35,000 ft (10,675 m)
Min ground turning radius:	
1000, 5000	31 ft 6 in (9·60 m)
2000, 6000	35 ft 9 in (10·90 m)
Runway LCN at max T-O weight (hard runway):	
1000, standard tyres	20·5
1000, low-pressure tyres	22
2000, standard tyres	27
2000, low-pressure tyres	22·5
5000, standard tyres	31
5000, low-pressure tyres	27
6000, standard tyres	30
6000, low-pressure tyres	28
Runway LCN at max T-O weight (flexible runway):	
1000, standard tyres	21
2000, standard tyres	21·5
5000, standard tyres	25
5000, low-pressure tyres	21
6000, standard tyres	24
6000, low-pressure tyres	20
FAR T-O field length at max T-O weight (1000, 2000):	
S/L	5,490 ft (1,673 m)
S/L, ISA + 10°C	5,820 ft (1,774 m)
S/L, ISA + 15°C	6,100 ft (1,878 m)
2,000 ft (610 m)	5,970 ft (1,820 m)
3,000 ft (915 m)	6,320 ft (1,926 m)
FAR T-O field length at max T-O weight (5000, 6000):	
S/L	5,860 ft (1,786 m)
S/L, ISA + 10°C	6,046 ft (1,843 m)
S/L, ISA + 15°C	6,168 ft (1,880 m)
2,000 ft (610 m)	6,129 ft (1,865 m)
3,000 ft (915 m)	6,530 ft (1,990 m)
FAR landing field length at max landing weight (1000, 2000):	
S/L	3,540 ft (1,079 m)
5,000 ft (1,525 m)	4,010 ft (1,222 m)
FAR landing field length at max landing weight (5000, 6000):	
S/L	3,120 ft (951 m)
5,000 ft (1,525 m)	3,527 ft (1,075 m)

Range, high-speed schedule, FAR 121.654 reserves:

1000, 65 passengers
1,020 nm (1,174 miles; 1,889 km)

2000, 70 passengers
630 nm (725 miles; 1,167 km)

*5000, 65 passengers
1,210 nm (1,392 miles; 2,240 km)

6000, 70 passengers
900 nm (1,036 miles; 1,667 km)

Range, long-range schedule, FAR 121.654 reserves:

1000, 65 passengers
1,130 nm (1,300 miles; 2,093 km)

2000, 70 passengers
700 nm (806 miles; 1,296 km)

*5000, 65 passengers
1,400 nm (1,611 miles; 2,593 km)

6000, 70 passengers
1,030 nm (1,185 miles; 1,908 km)

**With wing centre-section tanks*

OPERATIONAL NOISE CHARACTERISTICS (FAR Pt 36):

T-O noise level:	
1000, 2000	90 EPNdB
5000, 6000 (estimated)	88 EPNdB
Approach noise level:	
1000	101·2 EPNdB
2000	101·8 EPNdB
5000, 6000 (estimated)	97·5 EPNdB
Sideline noise level:	
1000, 2000	99·5 EPNdB
5000, 6000 (estimated)	97 EPNdB

APPENDIX B TO SECTION 2

ILLUSTRATIONS OF STALL TYPES AND
VORTEX FLOW ABOUT A WING

TYPE I - TRAILING EDGE STALL
GRADUAL FLOW BREAKDOWN - HIGH $C_{L_{MAX}}$

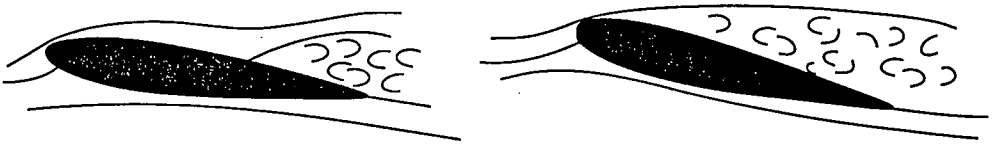

TYPE II - LEADING EDGE STALL
ABRUPT FLOW BREAKDOWN - HIGH $C_{L_{MAX}}$

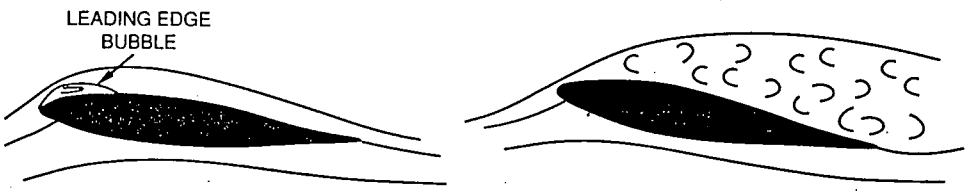

TYPE III - THIN AIRFOIL STALL
GRADUAL FLOW BREAKDOWN - LOW $C_{L_{MAX}}$

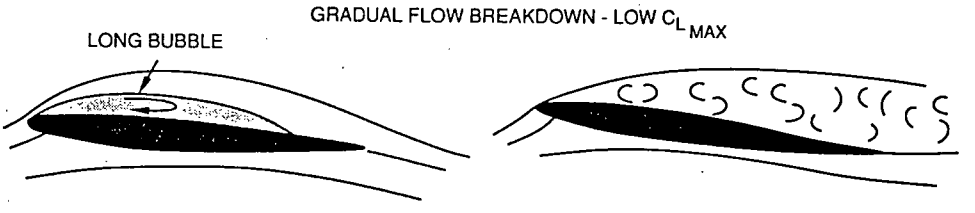

STALLING CHARACTERISTICS OF AIRFOILS

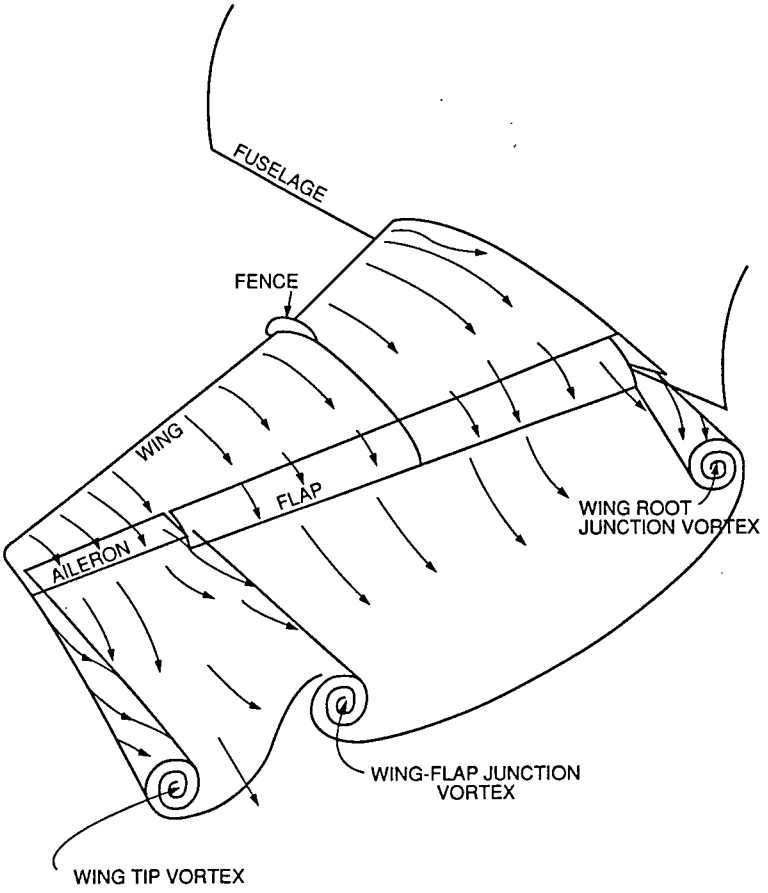

NORMAL FLOW AND WAKE FROM CLEAN WING

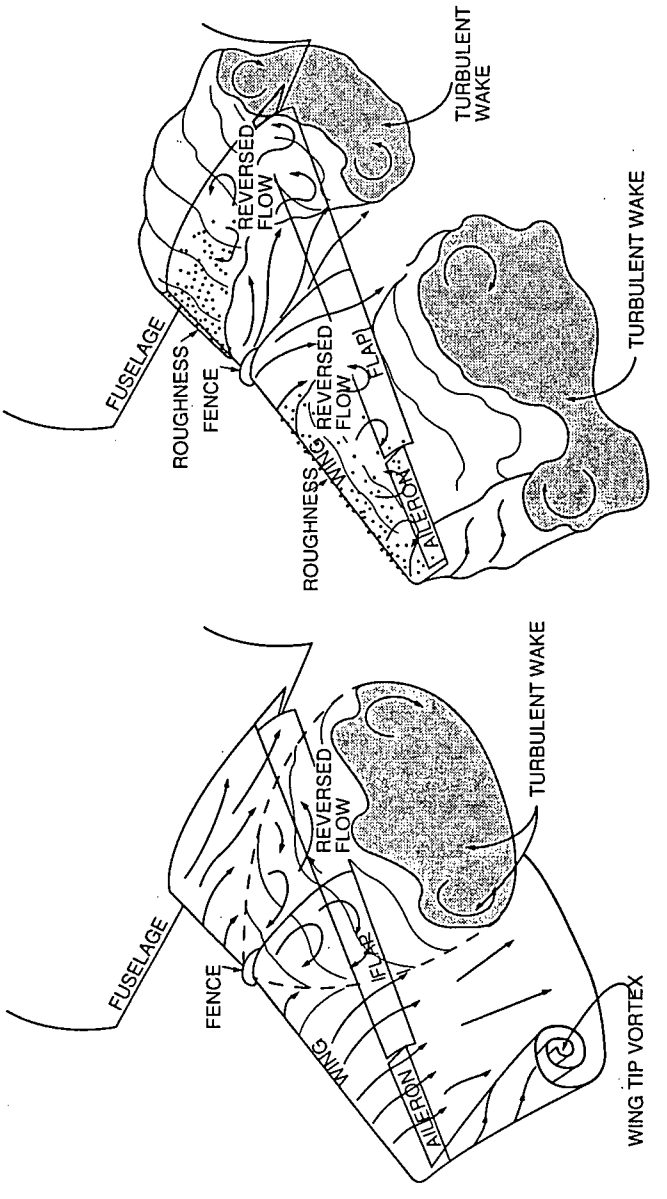

REGIONS OF SEPARATED FLOW FROM OUTER WING PANELS AND WING ROOT; CONTAMINATED WING

STALL AND TURBULENT WAKE FROM CLEAN WING

SKETCH OF TYPICAL VORTEX AND TURBULENT WAKE FROM A PARTIALLY-STALLED WING.

F-28 FLIGHT DYNAMICS
SECTION 3
REAL-TIME SIMULATION STUDIES AND ANALYSES

INTRODUCTION

As noted in the introductory section, the destruction of the FDR tape in this accident meant that there were no numerical data on which to base any analysis of the aircraft's trajectory at any point during the attempted take-off: the only guidance available to the investigators was embodied in various witness reports. This meant that simulation, either analytical or real-time, man-in-the-loop, was the only tool available to assist the performance steering group in studying the circumstances of the Dryden accident. Both forms of simulation were used: a visit by the group to the manufacturer's facility in Amsterdam, Netherlands, yielded the opportunity to use the company's engineering dynamic simulator, while extensive mathematical modelling (analytical simulation) was conducted to check and validate the observations made at Fokker Aircraft. This section describes and comments on the results of the dynamic simulations.

DYNAMIC SIMULATION IN THE FOKKER ENGINEERING SIMULATOR

At the time that these dynamic simulations were conducted in the Fokker engineering simulator[4], it was configured as a Fokker F100 aircraft, a somewhat larger derivative of the F-28 with appreciable aerodynamic differences. This aircraft is a new Fokker aircraft and the F28 is no longer produced. Since there was insufficient time to reprogram the engineering simulator with F28 data, it was decided to use the simulator in its existing form, approximating the F28 aircraft by selecting thrust/weight values so that the performance of the machine would be similar to that of the F28. The simulator is a single seat development simulator equipped with a full set of electronic flight instruments at the captain's station, full engine instruments and standard flight controls. It was also equipped with a visual system which provided a night runway scene.

The mathematical model of the F100 used in the engineering simulator included icing performance characteristics for a variety of levels of wing ice. Also, the ground model included the capability to introduce various levels of slush on the runway to provide rolling resistance contamination for the simulation. It was decided to fly the dynamic simulations using a variety of different wing and runway contaminant levels. The data from these simulations were saved and plotted to present pictorially and numerically the flight profiles and changes in the aircraft performance which would be experienced.

[4] An engineering simulation is one of great technical detail often used by aircraft designers as a development and research tool.

SIMULATOR APPROXIMATIONS FOR F28-1000 REPRESENTATION

Scaling the Fokker 100 to an F28 MK1000

The objective of the dynamic simulation was to obtain flight profiles which would have been achieved by an F28 MK1000 for various sets of conditions. To accomplish this task, it was necessary to choose a number of parameters carefully.

A weight was selected for the F100 so that the stall speeds and other reference speeds (V_1, V_R and V_2) were the same as those of a F-28 at 63,500 lb weight. This would provide for the same rotation and V_2 speeds and allow for take off roll comparisons to be made for dry and contaminated runways with the thrust level appropriately selected. Also, use of the same speeds resulted in achieving roughly the same wing Reynold's number (a non dimensional ratio of dynamic to viscous forces used in aerodynamics) at rotation. This would ensure that the aerodynamic characteristics of the wing would simulate as closely as possible to those of the F28 in the same conditions.

With the weight so selected, it was necessary to select a thrust level less than full takeoff thrust for the F100 so that the thrust to weight (T/W) ratio was equivalent to that of the accident F28. The T/W ratios were matched for zero velocity. Fokker engineers indicated that thrust decay with speed of the F100 engine was similar to that of the F-28 engine. Thus, the acceleration of the dynamic model should have been similar to the F28.

The aerodynamic drag profiles of the aircraft were similar enough that it was felt that the data the dynamic simulation would provide would be representative since:

- Aerodynamic drag did not become a significant factor until roughly 80 knots during the takeoff roll.
- The exact characteristics of the icing contaminant being modelled were unknown but adjustment to the contaminant level would compensate for minor differences in the drag profiles.

An obvious concern was the use of the F100 wing in icing studies where wing profile was critical to the results. The Fokker F-100 wing has the same wing box section as the F-28 wing, however, the aerofoil section forward of the front spar has been redesigned. The wing planform has been changed and the wing tips extended and redesigned. The trailing edge flaps have a different camber to change the wing load distribution.

Although differences in wing section characteristics may have some effects as regards this study, the magnitude and nature of the effects due to severe ice/frost contaminant does not seem to be strongly dependent on the wing section in this class of jet transport aircraft. (See Section 1 - Aerodynamics)

The centre of gravity position of the F100 was set at 30% MAC to give the F100 the same rotation response to control as the F28 at 22%, the setting for the Dryden takeoff.

The F28 involved in the Dryden accident took off at a weight of approximately 63,500 lb plus the accumulated weight of the snow/ice. The aircraft had a static takeoff thrust level of 19,700 lb. total, assuming that the engines were functioning normally. The T/W ratio equalled 0.30 at this full takeoff thrust. The F100 in the simulation had a weight of 87,000 lb and a thrust level of 26,100 lb was selected so that the T/W ratio also equalled 0.30. The F100 weight was selected so that the stall speeds for clean wings were the same in both cases, 107 kt. In both cases, flap settings of 18 degrees were used.

Baseline Conditions

The baseline conditions for the dynamic simulation were established with clean wings and a dry runway. Takeoffs were accomplished in these conditions and the rotation point checked against witness reports of the accident to validate, roughly, the modelling of the F28.

The baseline simulation results correlated well, in general terms, with the F28 characteristics. In addition, these baseline runs gave the simulation pilot time to develop a feel for the simulator so that consistent rotation and handling techniques could be applied to all takeoffs.

Slush Modelling

The slush model depth was varied to determine the level of slush contaminant required to extend the takeoff roll to the distance reported by the witnesses.

Slush depth was varied from 0 to 0.45 inches in small steps. The additional takeoff distance was noted in each case and a slush depth of 0.15 inches selected as a baseline value for the simulation. This slush depth resulted in an increase in takeoff distance of approximately 500 feet, that is, of the same order as the excess take-off run reported by witnesses to the Dryden accident. It should be noted, however, that there is an additional component of extended takeoff roll which results from the icing contaminant on the wings requiring rotation to a higher pitch attitude prior to liftoff. This factor was considered later in the simulation.

Wing Contaminant Modelling

The wing contaminant was modeled by using the Fokker rough ice/snow simulation for the entire wing. The contaminant factor could be varied between 0 and 1.0. It should be carefully noted, however, that this factor is <u>not</u> equivalent to contaminant depth although it is so labelled on the plots provided by Fokker. The reason is that wing contaminants with different characteristics will result in very different performance of the wing at the same depth. In other words, a very thin layer of a very rough contaminant can result in a far greater performance loss than a thick layer of very smooth contaminant which follows the

wing contour. It is sufficiently important a point that despite repetition it must be restated that *the FORM and POSITION of a wing contaminant is much more important than its thickness in considering wing performance.*

Hence, a better description of the contaminant factor would be to say that at levels above approximately 0.8, the aircraft would not fly off the runway at the speeds and in the conditions of the test. As a result, we worked with a variety of contaminant levels in the range of 0.5 to 0.80 which resulted in flight profiles which matched, in general terms, the accident profile.

The runs which most closely matched the profile described by witnesses at Dryden were achieved with a slush depth of 0.15 inches and a contaminant level of about 0.8.

Fokker's description of the wing ice simulation is quoted from page 3 of Warrink[7].

> *Ice on the wing is simulated as a change in lift-, drag- and pitching moment coefficient. The magnitude of it has been determined in the wind tunnel, in which one inch thick horn shaped ice on the leading edge was simulated. From tests with different ice shapes and from literature it is known that these effects are also valid for rime ice or frozen slush in the leading edge region. Through calculations in which static equilibrium conditions are determined the effect of 1 inch ice (in ground-effect) on lift, flight path angle and elevator deflection has been assessed. See figures 1, 2 and 3. In the simulation the effect of ice on the wing could be varied linearly between 0 and 1.0.*

Engine Failure On Take-off

A few take offs were flown during which an engine was failed just after rotation. Regardless of the contaminant level on the aircraft, directional control was not a problem. However, the contaminant level at which the aircraft was still able to liftoff and climb was significantly reduced. Successful takeoffs were accomplished at a contaminant factor of less than 0.5, and that level provided for minimal performance. It should be noted that the relationship between contaminant *level* and contaminant *thickness* is highly nonlinear, so that this should not be interpreted as meaning that the aircraft is able to carry half the contaminant load with an engine failure.

However, it was clear that the reduced thrust at rotation severely reduced the available performance margin and thus limited the aircraft's capability to carry any contaminant through a successful takeoff.

DYNAMIC SIMULATION HANDLING TECHNIQUES

Overview

A fundamental assumption made during the simulation exercise was that the pilots of the accident aircraft would have believed that their aircraft was flyable and would, therefore, have employed normal handling techniques. Therefore, for 'Dryden' simulations no special procedures or techniques were allowed which would have provided a better flight profile due to the simulator pilots' a priori knowledge of the external conditions being applied. Ad hoc experiments with off nominal techniques left no doubt that handling technique greatly affects the resulting flight profile in the presence of contamination. This observation was later confirmed by the off-line numerical modelling.

Handling technique in the context of this exercise includes the following:

- Selection of rotation speed. A pilot who applied a speed increment above V_r prior to rotation would have a higher probability of a successful takeoff. The converse is also true.

- Use of a lower rotation rate. A pilot who used a slower rotation rate would also have a higher probability of a successful takeoff.

- Use of a partial rotation. A pilot who rotated the aircraft to the usual liftoff attitude and held it there rather than rotating further would also have a higher probability of a successful takeoff.

It is important to note that the above comments should not be interpreted as recommendations for aircraft handling in adverse conditions. The reason is that there are many other trade-off factors which are balanced out in any takeoff which these techniques may degrade. The only parameter being examined in this case is the specific question of whether, for the selected conditions at the planned speeds, this aircraft would fly.

The dynamic simulations were all flown by Mr. Wagner, a current B767 first officer with Air Canada, to preserve consistency in the handling of the simulation. The simulator flying was monitored by Mr. Morgan, an engineering test pilot with National Aeronautical Establishment. Techniques for flight control handling during different phases of the simulation were reviewed by the two pilots during the exercise to attempt to ensure that reasonable procedures were used at all times.

Flying Techniques and Methods

Each takeoff run was started from the threshold of the runway at zero velocity with the thrust already at planned takeoff power. The brakes were released and the takeoff roll commenced. No wind was simulated because in the Dryden accident, the wind was effectively calm.

The aircraft was accelerated to rotation speed with a very slight push force on the control wheel to ensure positive nosewheel steering. As rotation speed was reached, the rotation was initiated by use of nominal wheel pull force to achieve a rotation rate of approximately 3 degrees per second. The rotation attitude was limited to 18 degrees, somewhat higher than that for the F28, but appropriate for the Fokker 100 aircraft.

After the aircraft became airborne, the aircraft was accelerated to the reference V_2 speed plus a speed increment, depending on the configuration and conditions for the test run. The run was terminated at an altitude of about 400 feet above airport altitude or when the aircraft impacted with the ground during unsuccessful takeoff runs. Some takeoffs were also terminated after extended flight just above the terrain in ground effect where a successful climb-out could not be achieved.

All the data from each run were recorded by the simulation computer.

Flying Techniques During Contaminated Runway Takeoffs

For the contaminated runway takeoffs, normal control wheel inputs were used except for a few runs where the nose was raised about 2 to 3 degrees at about 80 knots to get the nosewheel out of the slush. This is a procedure specified in the F28 manual and was flown to determine what effect use of the technique could have had on the takeoff in this case.

The data from the runs were analyzed and it was found that raising the nosewheel to reduce slush drag had a measurable, but rather small effect, on takeoff distance. The difference was on the order of 100 feet.

Flying Techniques During Contaminated Wing Takeoffs

For contaminated wing takeoffs, normal control wheel rotation forces were used, even though the rotation rate that resulted was somewhat slower than with the clean wing model. This is because the contaminant had the effect of
increasing the nose down pitching moment of the wing therefore there was less excess nose up moment from the elevator to cause rotation.

As the contaminant levels were increased, numerous takeoff runs were flown where the stick shaker[5] actuated immediately on or just after liftoff. This was due to the significantly greater angles of attack achieved in these cases. It was judged that normal pilot technique would be to attempt to reduce the angle of attack to stop the stick shaker and nose down control wheel inputs were made accordingly. However, an attempt was made to maintain

[5] A 'stick shaker' is a warning device which vibrates the pilot's control column if the wing reaches a pre-determined angle of attack. Under normal operations this device warns against impending stall, and its onset is generally used to indicate the prudent limit of useable lift.

an aircraft attitude right at the edge of stick shaker activation. This is because it is believed that most pilots, in view of current training with respect to wind shear escape manoeuvres and ground school training, would expect to achieve close to maximum available lift at the point of stick shaker activation.

It should be noted that in cases of significant wing contamination, the wing can be well beyond the stalling angle of attack by the time the stick shaker activates. In essence, the stick shaker is responding to the normally expected maximum angle of attack of the clean wing. The stall warning system is not actually measuring stall and flow separation from the wing. Rather, it infers the onset of stall from the known performance of the wing and is programmed to activate at a fixed geometric angle of attack based on that knowledge.

Thus, the pilot flew many contaminated airfoil simulations in or near stick shaker. The simulation pilot worked hard to try to keep the aircraft at the edge of stick shaker and that is the reason that there is noticeable pitch oscillation on the recordings from those runs.

Flying Techniques During Engine Out Takeoffs

Normal pitch handling of the aircraft was used for the engine out takeoffs. In these cases, an engine was failed just at Vr and appropriate rudder inputs made by the pilot to ensure that the aircraft continued to track straight. Small roll inputs were required to correct any incipient rolling tendency in the aircraft due to any remaining yaw from the engine failure. The climb-out characteristics of the aircraft were conventional with the engine failure, except that, as described, only a limited wing contaminant load could be carried in these cases.

Summary of Dynamic Simulation Experience

The Dynamic Simulation data is presented in Fokker Report VS-28-25, Order Number 22192. This report summarizes the work done in the Fokker simulator between June 7th and June 8th, 1989.

The effect of varying runway slush depth was primarily reflected in increased takeoff run. There were some additional effects seen related to the ability of the aircraft to accelerate after rotation with the wing significantly contaminated. However, the slush effect was limited in its effect, in general terms, to increasing the takeoff run.

The effect of the wing contamination was to degrade the performance of the wing, the degree of degradation being a nonlinear function of the contaminant level.

A few principal effects were noted in this simulation.

1. As the wing contaminant level increased from zero, the aircraft's performance immediately reflected the fact by a reduction in climb performance.

2. At moderate levels of contaminant, the aircraft experienced stick shaker shortly after unstick and the profile after that point was related to the simulation pilot attempting to keep the aircraft right at the edge of stick shaker, 13 degrees angle of attack. It should be pointed out that for the contaminated wing, that angle of attack was already post stall in most of those cases. Climbing out of ground effect became impossible in many instances.

3. At critical levels of wing contaminant between 0.75 and 0.825, the aircraft was able to unstick and sometimes fly. However, as the aircraft climbed out of ground effect, the performance loss resulted in the aircraft descending, touching down again or crashing off the end of the runway.

4. In summary, as the contaminant level increased, the liftoff pitch attitude and airspeed (not rotation airspeed) had to be increased to provide adequate lift to unstick. Also, since increasing levels of contaminant decreased the stalling angle of attack, liftoff occurred closer and then beyond the true stalling angle of attack. Eventually, liftoff was occurring post stall (contaminated wing) or the aircraft stalled shortly after liftoff as it climbed out of ground effect. Successful flight with the wing contaminated at levels between 0.7 and 0.825 was effectively impossible using normal techniques. The profiles resulting from flight at these contaminant levels were, in general terms, close to the profile which is representative of the Dryden accident. (See figures 17 to 19 in the Fokker Report)

5. In cases where an engine was failed, the aircraft was not flyable with even moderate levels of contaminant. The drag increase due to the contaminant is so great that the thrust of only one powerplant is inadequate to carry even these moderate ice levels. The reason is that the high angles of attack required to generate adequate lift with the contaminated wing produces much higher drag levels. Post stall drag also is extremely high. The only way to get the aircraft to fly with the contaminant is to have enough thrust to accelerate to a high enough speed. However, the thrust level with one engine is inadequate to provide that acceleration.

F-28 FLIGHT DYNAMICS
SECTION 4

OFF-LINE MODELLING
INTRODUCTION

Subsequent to a visit to the manufacturer of the aircraft and man-in-the-loop ground based simulations carried out there (Section 2), off line modelling of the F-28 during take off was performed to examine both the normal take-off performance and the effects of runway and flying surface contamination. The purpose of the numerical simulations was to confirm observations made at the Fokker Establishment using a modified engineering simulation of the Fokker 100, a similar but not identical vehicle. This report outlines the methods used, approximations and extrapolations made and provides appropriate samples of the model output. Two models were developed simultaneously by Wagner in Montreal and Morgan in Ottawa. Their outputs were periodically checked one against the other and where differences were found the source was isolated and either corrected or, if conceptual or algorithmic, modified after consultation.

A secondary, but important, purpose of this section is to provide accountability for the theoretical engineering used in modelling the F-28 take-off. To that extent, the language used is, at times, quite technical and there is an extensive use of descriptive mathematics. For this, the author apologises to the lay reader, but it was felt to be imperative that the work which led to the conclusions presented here should be available for scrutiny by his peers.

DATA SOURCES

Three primary and two secondary data sources were used in building the off-line simulation. Aerodynamic and performance data were taken from the F-28 simulation data base provided by Fokker Aircraft[8] and from an internal Fokker wind tunnel study of the F-28 lift and drag characteristics when the flying surfaces were contaminated with artificial roughness. For cognitive pilot modelling through the rotation and immediately post lift-off, flight data were extracted from time histories of 21 previous take-offs flown in the actual aircraft involved in the Dryden accident (C-FONF), which were provided by the Engineering Branch of the CASB. Runway contamination was modelled using information published by NASA[9] and the Royal Aeronautical Establishment (UK)[10].

SITUATION OVERVIEW

Fokker F-28 C-FONF crashed into a treed area some 750 or so meters from the end of the runway at Dryden immediately after a take-off attempt. The aircraft struck trees at a height about one meter above the runway height at the lift-off end and subsequently cut a swath through the trees for a further 240 meters before coming to rest. The flight data recorder (FDR) suffered fire damage to the extent that no data were recoverable and eye witness reports are the only available source of information regarding the trajectory of the aircraft during the take-off run and prior to the crash. There was a general trend in the witness reports suggesting that the aircraft's wings were at least partially contaminated with slush or ice during the take-off attempt and there is additional information suggesting that the runway was to some extent or other contaminated with slush or wet snow at the time

of the accident. The general tenor of the witness reports, together with the absence of ground markingsground markings between the runway end and the first point of impact suggests a sequence of events approximately thus:

> The aircraft, in an 18 degree flap configuration, commenced its take-off run from a normal position on the runway, achieved rotation speed somewhat further down than was normal and commenced a rotation. During the initial rotation the machine either became briefly airborne, or simply extended the oleos, and then settled back onto the runway, reducing its body angle somewhat. A second rotation very close to the end of the runway resulted in the aircraft becoming airborne but maintaining a very low altitude until striking the trees. Subsequent technical investigation has shown that at some time during the take-off attempt the wing flaps were extended from 18 to 25 degrees and that at the time of impact the undercarriage was in transit (neither fully down nor fully up).

The above general concept has, for modelling purposes been termed the 'Dryden Scenario'.

SCOPE OF MODELLING

Since it is clear that the aircraft did not gain significant altitude, the modelling task was greatly simplified. The change of flap setting was accounted for after the first rotation, while the change on overall drag coefficient due to in-transit undercarriage was so small that it was ignored. The take-off was treated as a three phase task, ground run, rotation and post lift-off, these being defined as follows:

> a: **Ground Run.** This was taken to be the phase from the start of the take-off, with the aircraft stationary at the end of the runway to the point at which the pilot commenced rotation into the pre-planned take-off attitude. Pilot intervention at this stage is not significant: with aircraft of this class it usually consists of maintaining a continuous forward pressure on the control column to ensure good nosewheel contact with the runway and hence good directional control by use of nosewheel steering.
>
> b: **Rotation.** This phase covers the time from the end of the ground run during which the aircraft is rotated in pitch with the object of permitting the wing to generate sufficient lift to raise the aircraft from the surface so that it becomes completely airborne. While the technique may vary somewhat between aircraft types, it is usual to rotate to a pre-set attitude and at a given rate, the aircraft generally becoming airborne as or shortly after the target attitude is achieved. Here pilot technique becomes of significance if the best performance of the wing is to be realised. The pitch rate used and the precision with which the target attitude is achieved can both influence the realisation of the optimum performance of the wing.

c: **Post Lift-Off.** This phase is here taken to mean the time between the aircraft becoming completely airborne from rotation to its either climbing out of ground-effect or settling back to the surface as the case may be. In developing the numerical model it became apparent that pilot technique was a vital ingredient during this phase of flight.

The aircraft has been continuously modelled through these three phases, however the rudimentary pilot cognitive model changes in reaction to the phase condition.

PILOT MODELLING AND AIRCRAFT DYNAMICS

Early experience during model development indicated that the results of the simulations were likely to be critically dependent on pilot technique, which supported observations made during the dynamic simulations. It was also thought desirable to explore alternate pilot control strategies in the case of badly contaminated flying surfaces. To these ends a rudimentary pilot cognitive model was built. That is, no attempt was made to model pilot compensatory or physiological characteristics, but provision was made for a variety of pilot behaviours, each resulting in a commanded pitch rate for the aircraft. The output from this section of the simulation was fed to a simple first order low-pass filter with a break point set at 1.5 radians/sec, roughly representative of the expected pitching response of an aircraft of this class at typical take-off speeds.

Pilot behaviour was modelled during two of the take-off phases, the rotation and the immediate post lift-off regime, as described below.

ROTATION

For the rotation, four representative behaviours were considered, these being:

a. **Normal.** A study of the time histories of 21 take-offs provided by the CASB indicated that the 'normal' or customary take-off rotation consisted of a fairly rapid rotation to about 10 degrees of pitch attitude, followed a short time later (about 1.5 seconds or so) by a further rotation to between 13 and 15 degrees of pitch. The latter increment in pitch attitude appears to be 'open loop' in nature as on a significant number of the take-offs recorded it was accompanied by a slight transient reduction in airspeed. This procedure was taken as the initial model. The take-off data available showed a mean pitch rate during the first stage of rotation of 3.81 deg/sec with a standard deviation of 0.76 deg/sec, the maximum value noted was 5.1 deg/sec and the minimum 2.9. The mean value was used in the model as a commanded pitch rate limit.

b. **Slow Rotation.** The structure of the rotation manoeuvre here is exactly the same as that described in paragraph a., with the exception that the limit on commanded pitch rate was set to 1.9 deg/sec, a half of the nominal value.

c. **Over-rotation.** This strategy was based on a consideration of typical pilot response when the aircraft unexpectedly fails to become airborne after the normal rotation to 10 degrees of pitch attitude. After a slight delay (1.5 seconds) the aircraft is further rotated in pitch to 12.0 degrees. Under normal circumstances, that is with an uncontaminated aircraft such a failure to fly at the normal attitude might be experienced if, say, the weight of the vehicle had been underestimated or an error had developed in the airspeed measuring system. In this case an increment in attitude *could* cause sufficient lift to be developed to achieve lift-off. In the case of the uncontaminated F28 the wing would still be operating below the maximum C_L and the drag penalty for the additional rotation would be small.

d. **The 'Dryden' Scenario.** Eye witness reports generally agree that the aircraft at Dryden was rotated twice, though whether or not it became temporarily airborne after the first rotation is uncertain. A significant number of the passenger witnesses remarked on a final power surge shortly before the machine became airborne close to the end of the runway. A basic scenario which answers to the preponderance of the witness reports was described on pages 1 and 2. For modelling purposes this was treated as a dynamic sequence with the aircraft being pitched nose down after the initial rotation either at a fixed rate or to an arbitrary attitude. The further flap extension to 25 degrees was modelled assuming that the crew selected the extension after having failed to become fully airborne at the first rotation: the extension was modelled at 1 degree per second with a linear interpolation of both lift and drag between the 18 degree and 25 degree conditions. While this set of motions meets the described aircraft motions and is, to an experienced pilot, a plausible set of pilot actions under these circumstances, *it can not be too strongly emphasised that this is conjecture, based, in the absence of factual knowledge, on an informed but judgemental interpretation of witness descriptions.*

POST LIFT-OFF

Following lift-off, three piloting options are provided, these being:

a. **Increment Pitch Attitude.** This mode was derived from a study of the time-histories of take-offs previously performed in the actual crash aircraft which suggest that an increase in pitch attitude immediately after lift-off is usual. Whether or not this is an habitual procedure or whether the pilot is at that time attempting to track airspeed is uncertain. For the majority of samples the airspeed is stagnant during this manoeuvre, but there were several cases where an airspeed loss was noted during the secondary rotation. The increment in pitch attitude by 3 degrees is again based on a survey of the data mentioned above. This procedure follows closely the approved procedure contained in the Fokker flight manual for the F-28.

b. **Constant Airspeed.** This is akin to a frequently used procedure for aircraft of this class, wherein the pilot, during initial climb, attempts to maintain the speed at which he broke ground plus a certain increment, the 10 knots used in the model being typical.

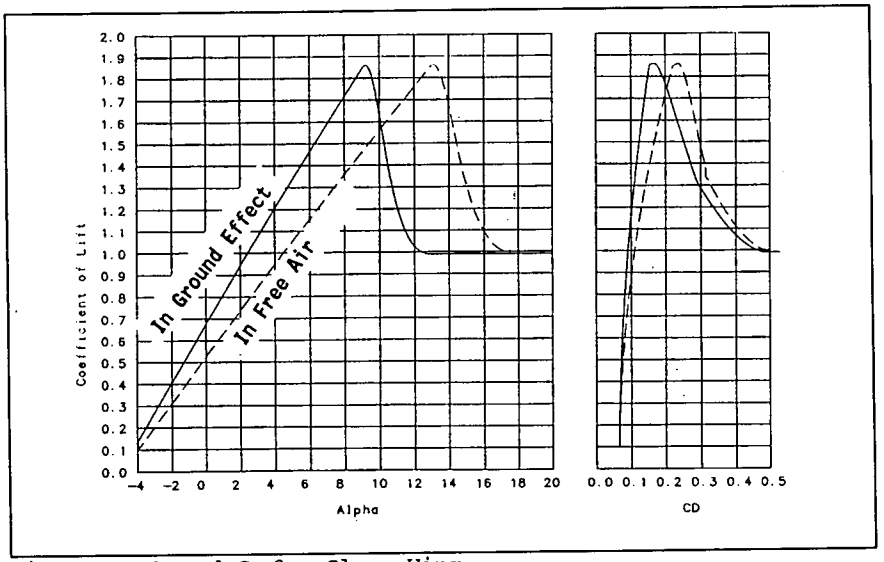

Figure 2: C_L and C_D for Clean Wing

c. **Constant Angle of Attack.** While not in the normal piloting repertoire, since the required information is not generally available in the cockpit, this probably represents the most efficient way of establishing an initial climb. It was included for performance limit comparisons only and is not intended to represent real pilot behaviour.

AERODYNAMIC MODELLING

Since, by its very nature, this investigation had to concentrate on stall and post-stall behaviour of the aircraft, great care was taken to achieve good modelling of the aircraft's characteristics in this region. Additionally it was necessary to model ground effect with some precision and to derive an intelligent estimate of the effects on both lift and drag of a wing contaminant. The model was developed using data from both Reference 1 and the Fokker wind-tunnel experiments. The procedure used in determining the clean wing characteristics in and out of ground effect was first to use curve fitting techniques to obtain the C_L/α curve for the 18 flap wing out of ground effect (OGE) and then to enter this curve using not the reference angle of attack, but an effective angle of attack based on the aircraft's height and a ground effect interpolation curve provided in Reference 1. The curve for angles lower than 13 degrees was taken directly from Reference 1, while the extended range was derived by interpolation from the wind tunnel data, maintaining the

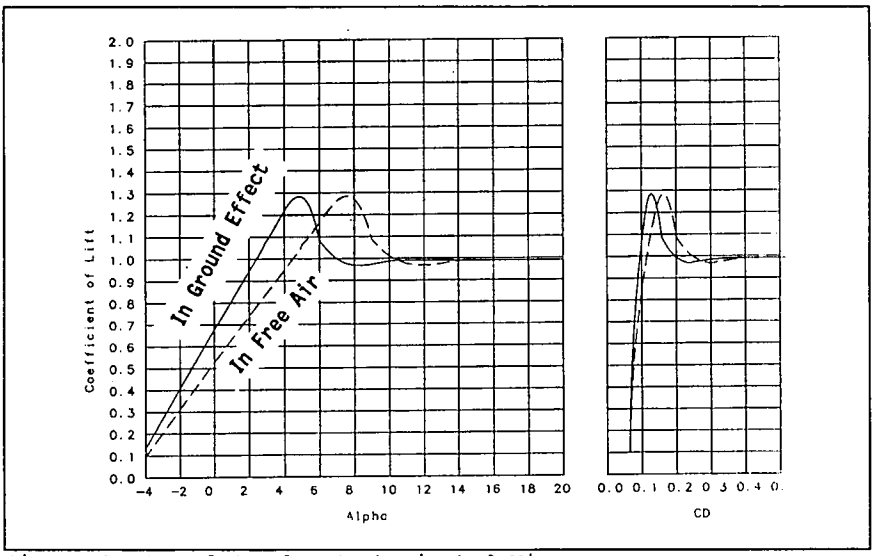

Figure 3: C_L and C_D for Contaminated Wing

form of the curve while reducing its magnitude to that anticipated for the 18 flap case. The resulting curves for the uncontaminated wing are shown in Figure 1. In modelling flap extensions to 25 a simple increment, again based on the data in Reference 1 was used.

The contaminated wing curve was derived from three sources, the clean wing curve for very low angles of attack, a plot of lift loss due to rime ice as given in Reference 1 and the wind tunnel data, using the same techniques as described above. The final curves used are at Figure 2. While this may appear to be a rather sparse data set on which to model a regime critical to the study, it has the merit of being fact based and applying specifically to the F-28 wing. Additionally, there is ample theoretical support for the form of the curves used and even their magnitude, particularly following Jones and Williams[11] and Cebeci[12]. Additional information derived from both wind tunnel and flight test was obtained from Zierten and Hill[13], although the research reported here referred to aircraft with leading edge high lift devices, the general trend and the specific references to stick shaker activation were of use.

Drag

An initial examination of the available F28 data indicated that drag would be critical to these simulations. Provided the wing is producing a reasonable value of C_L even when contaminated, then if the aircraft accelerates to a sufficiently high speed it will fly. If, however, the drag becomes so great that there is insufficient engine thrust to accelerate the aircraft after rotation, then such an event becomes impossible. For the take-off to be

successful it is also necessary for the aircraft to accelerate when airborne to compensate for the reduction in C_L at a given angle of attack as the machine climbs out of ground effect. Drag curve estimates were again derived from a combination of data from the Fokker data base and the company's wind tunnel data. The effects of wing contamination came from the same sources. Figures 1 and 2 also show the drag polar plots used in the simulation and their relationship to C_L and α.

Degree of Wing Contamination

Since it is impossible to determine the exact form of the wing contamination present during the Dryden accident, it is taken that the wing is either contaminated beyond the critical condition or not. The evidence for this type of binary approach to critical contamination is strong. It was implied by Jones[14] 53 years ago and is amply supported by Abbott and Von Doenhoff[15] and Hoerner[16]. However, to permit gradations of contamination, it may be considered that part of the wing was contaminated and part was not. There is some witness support for this approach. This being accepted, the contamination coefficient used in the simulations simply interpolates the lifting capability of the wing on a proportional basis between the clean and contaminated conditions. This approach leads to a C_L/α curve with two distinct peaks for intermediate contamination conditions, which may or may not occur in reality but does indicate a reduced performance capability commensurate with that described by Wolters[17] and the previously cited works of Cebici and Zierten and Hill: this is considered to provide an adequate and realistic representation of performance degradation due to wing contamination.

Engine Failure

The Wagner model accounts for possible engine failure during the take off attempt, this is done for the sake of completeness, *not because there is any suspicion that the power plants behaved abnormally during this accident.* While there is a general agreement in the witness reports that there was a power increase shortly before the final lift off, very few suggest that a power reduction occurred during the take off. The professional pilot who was seated adjacent to the engine intakes did not report any power reduction. Engine failure was modelled by reducing the thrust instantly to approximately half of nominal, while adding the drag term corresponding to the ram drag of the failed engine and the required deflection of the rudder to maintain directional control.

MODEL RUN MATRIX

Once the modelling had been completed and validated (Section 5), a matrix of cases to be run was determined empirically. For all cases, the baseline configuration was a weight of 63,500 lb, full rated thrust, 18 degrees of flap and a V_r of 122.5 kt. The nominal rotation was an initial pitch rate of 3 deg/sec towards a target attitude of 10 degrees followed by a further rotation at 1 deg/sec to 13 degrees of pitch attitude after unstick, ie, following the preferred Fokker procedure. Thereafter, three parameters were varied as being of prime interest in this study, the depth of slush, the proportion of wing contamination and the selection of V_r. These runs were completed using both the nominal rotation

technique described above and the 'Dryden Scenario' described at length earlier. Nominal (3 deg/sec) and a reduced (2 deg/sec) rotation rates were used for the initial rotation. The full set of conditions tested was:

a. Slush Depth. 0,0.1,0.2,0.3 and 0.4 inches.

b. Contaminant Ratio. 0 and 50 to 100 % in steps of 1%. When this resolution produced ambiguous results boundaries were defined by making special runs at finer resolution

c. Rotate Speeds. 117.5, 122.5 (nominal) and 127.5 kt.

d. Rotation Rates. 3 and 2 degrees/second.

PRESENTATION OF RESULTS

Initial plots, Figures 4 to 6 are presented to clarify some of the effects of flying surface and runway contamination described earlier. Figure 4 shows the effect of runway slush and wing contamination on the take-off distances to both rotation and lift-off. It can be seen that while the presence of slush changes the distance required to reach V_r significantly, wing contamination has very little effect, almost all the traces for distance to rotation overlay each other. This is definitely not so for the distance to lift off. As the level of wing contamination increases, the distance penalty to unstick increases quite rapidly due to the marked increase in drag produced by the contaminated wing at high angles of attack. This characteristic represents a situation in which the full extent of performance loss may not be apparent until the aircraft is rotated; prior to this the reduction in acceleration is little more than could be attributed to a slush layer. Figure 5 is presented to indicate the reasons for this effect. It shows that as contamination level increases, even in the absence of slush, the distance the aircraft has to travel between V_r and the unstick point increases only slowly until a dramatic 'knee' is reached (numerically at just over 0.6 contamination ratio). This is coincident with the aircraft being at or beyond C_{Lmax} for the contaminated wing at its rotation angle of 10 degrees and having to generate the necessary lift by increasing speed rather than C_L. The low acceleration rates available once the drag rise caused by wing contamination has been encountered mean that excessive distance has to be consumed for this to occur. A secondary effect can be seen in the same figure by examining the trace of Theta (body angle). At first moderate increases for Theta at lift off are enough to compensate for the loss of C_L due to contamination, but a point is reached, at about 0.58 contamination ratio, when the rate of increase in theta steepens noticeably. This is related to the reduced lifting capability of the wing as indicated earlier in Figure 2.

The next two plots in this section represent the crux of this investigation. They show that it is possible to define two boundary conditions in terms of combinations of slush depth and contamination factor which can both lead to catastrophic results of attempted take-offs. A *boundary condition* here means a continuous relationship between level of

contamination and runway slush depth which represents the dividing line between a successful take-off or not, as illustrated in Figure 3. In both Figures 6 and 7, several boundaries are shown for varying conditions of V_r and rotation rate, these should be individually interpreted according to Figure 3.

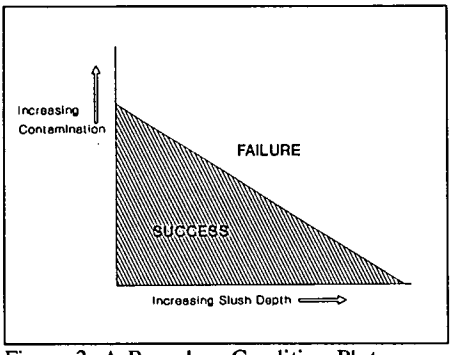

Figure 3: A Boundary Condition Plot

Figure 6 indicates a boundaries for a condition in which the aircraft will simply fail, in the distance available, to leave the ground and will run off the end of the runway. It also shows that any reduction in the rotation speed will have an adverse effect on the available performance. At somewhat lesser levels of both factors, another boundary was found to exist, defining a condition wherein the aircraft would at first leave the runway, but fail to climb out of ground effect and settle back to the surface (Figure 7). This boundary existed for all conditions of rotation speed and rotation rate tested, and is annotated to indicate the effects of varying the various aircraft handling parameters on the placement of the boundary. When this condition was met it was possible, by making subtle changes in the assumed pilot control strategy after the initial lift off (eg, rate of pitch, response to stick shaker) to cause the model to fly for considerable distances at very low altitudes, but it was not possible to make it fly except by assuming extremes in pilot behaviour.

The final sets of Figures provided with this section are intended to illustrate the effects and observations made earlier in the text. Figure 8, a,b and c shows the overall effects of increasing contamination factor in a gross way. The rotation speed here was 122.5 kt and slush depth 0.25 in. At 65% contamination the aircraft flies away normally, at 68% the machine sinks following the initial lift off, due both to the loss of lift with height and the pilot's reaction to stick shaker, but then climb away. Note that the scale of the height trace is such that at 6500 feet (500 feet beyond the end of the runway) the aircraft is still only at 10 feet. In 7c, contamination now being set at 69% the aircraft returns to the runway and subsequently runs off the end. The series in Figure 9 a,b and c shows that fine graduation of the contaminant level creates subtle differences in the aircraft responses. This set of plots refers to a much shallower slush layer (0.1 in) and an incremented rotation speed of 127.5 kt. Figure 9a indicates that at 82.3% contamination the aircraft flies away despite two bursts of stick shaker, while by the time contamination is at 82.4% the machine never exceeds about 5 ft, eventually returning to the surface some 1100 feet beyond the end of the runway. When there is 0.1% additional contamination the result is a short hop and an over-run. Finally, Figure 10 a and b demonstrate the remarkable sensitivity to assumed pilot behaviour noted earlier. The only difference in these two runs is that the angle to

which the aircraft is un-rotated following the initial hop is two degrees lower in 9b than 9a, the latter strategy resulting in a second lift-off and climb out and this at a very high level of contamination.

The implication of the results presented here, especially the two sets of boundary conditions, is that there exist a combination of values of slush depth and wing contamination which can cause aircraft trajectories of the type described by witnesses to the Dryden accident.

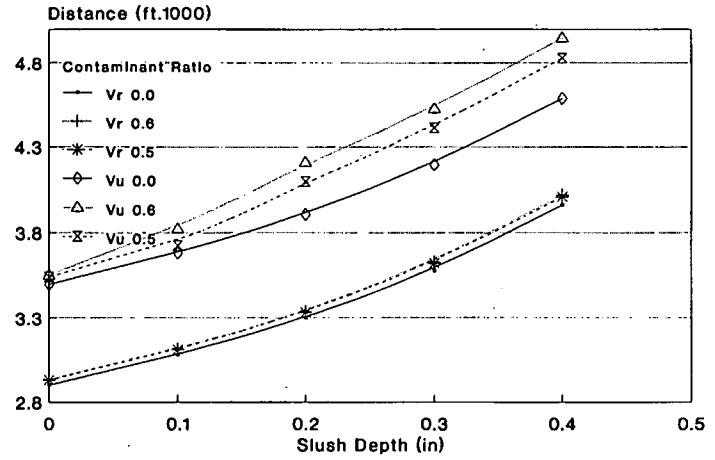

Figure 4 Effect of Contamination and Slush on the Distance Required to Reach V_r and V_u

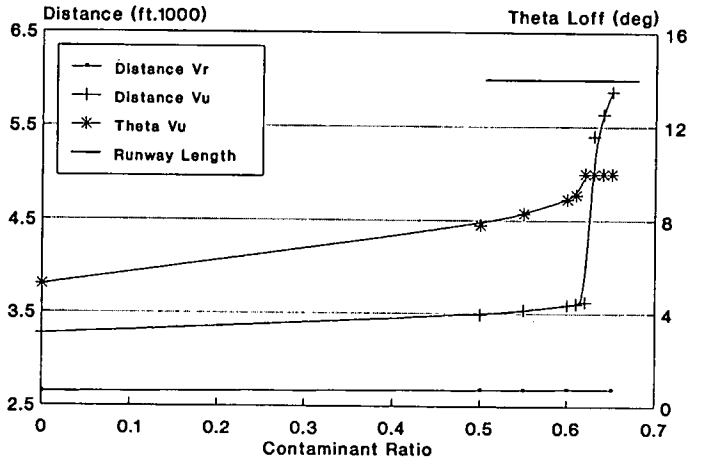

Figure 5 Effect of Wing Contamination on Distance Required To Reach V_r and V_u Illustrating the 'Knee' Effect at Limiting Body Angle

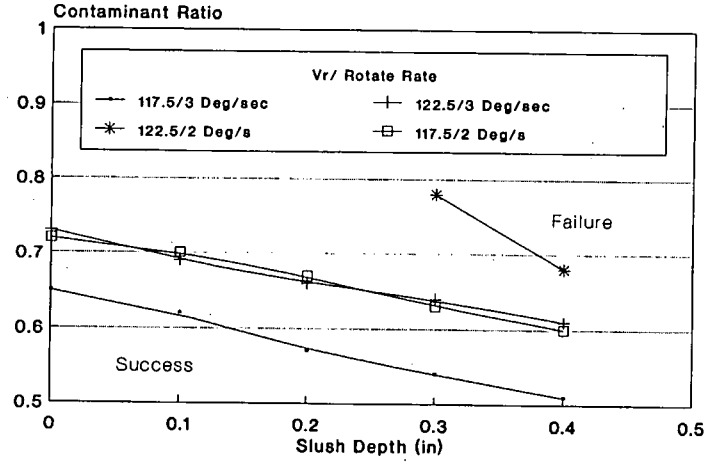

Figure 6 Various Boundary Plots at Different Values of V_r and Rotation Rate for Overrun Case

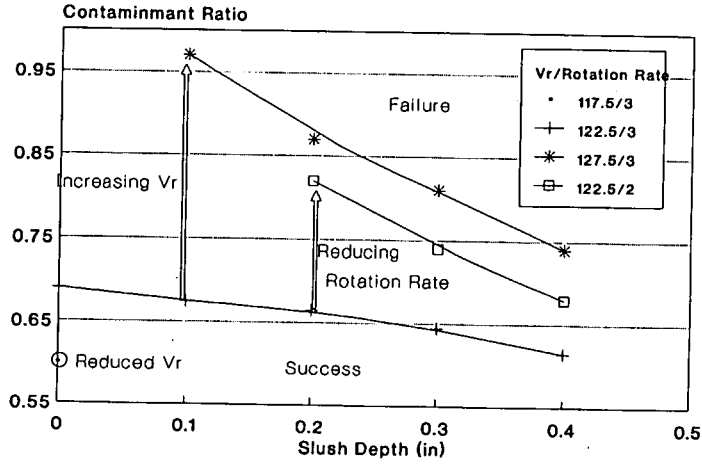

Figure 7 Various Boundary Plots for the 'Bounce' Case

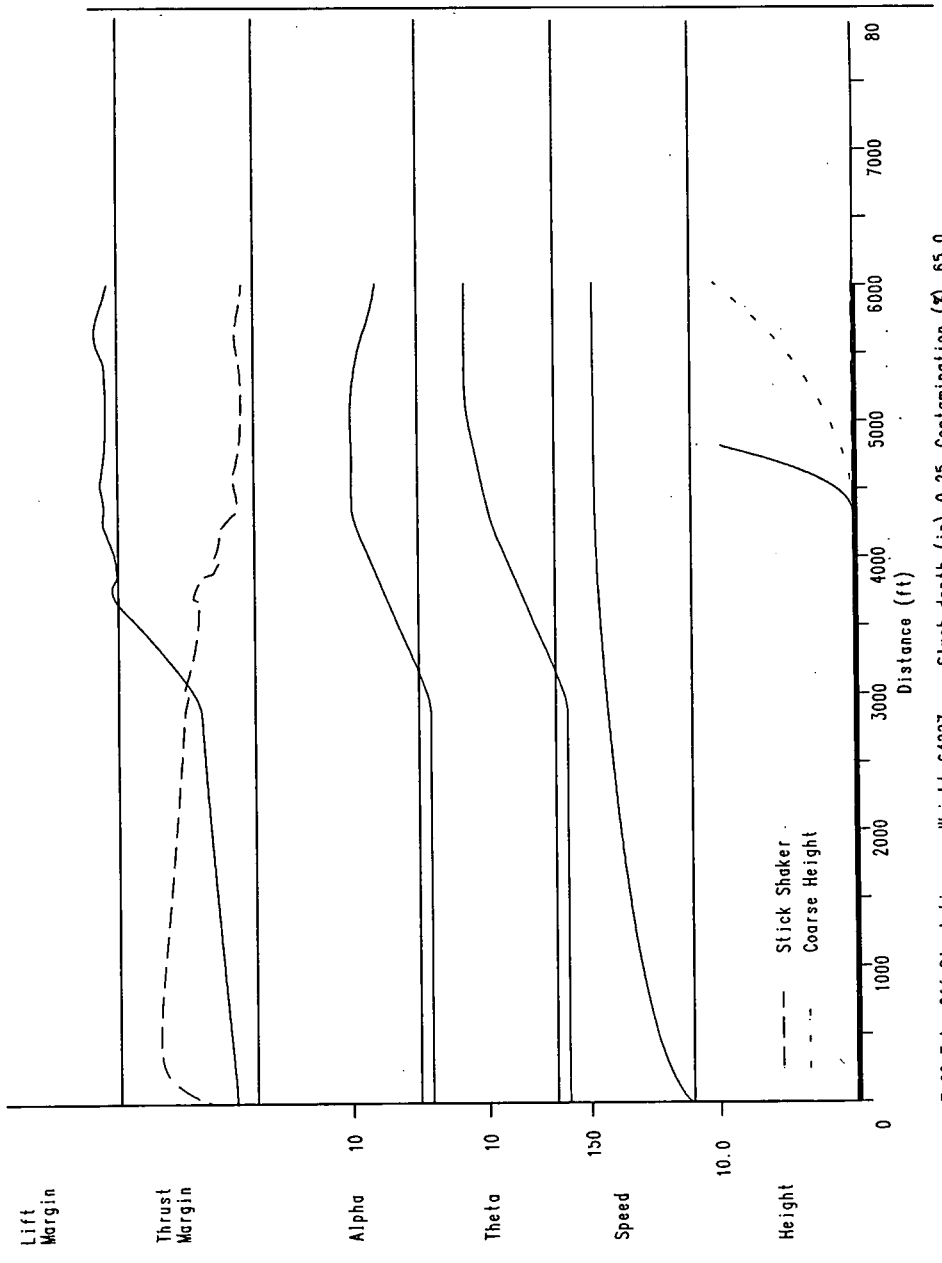

Figure 8a Successful Take-Off

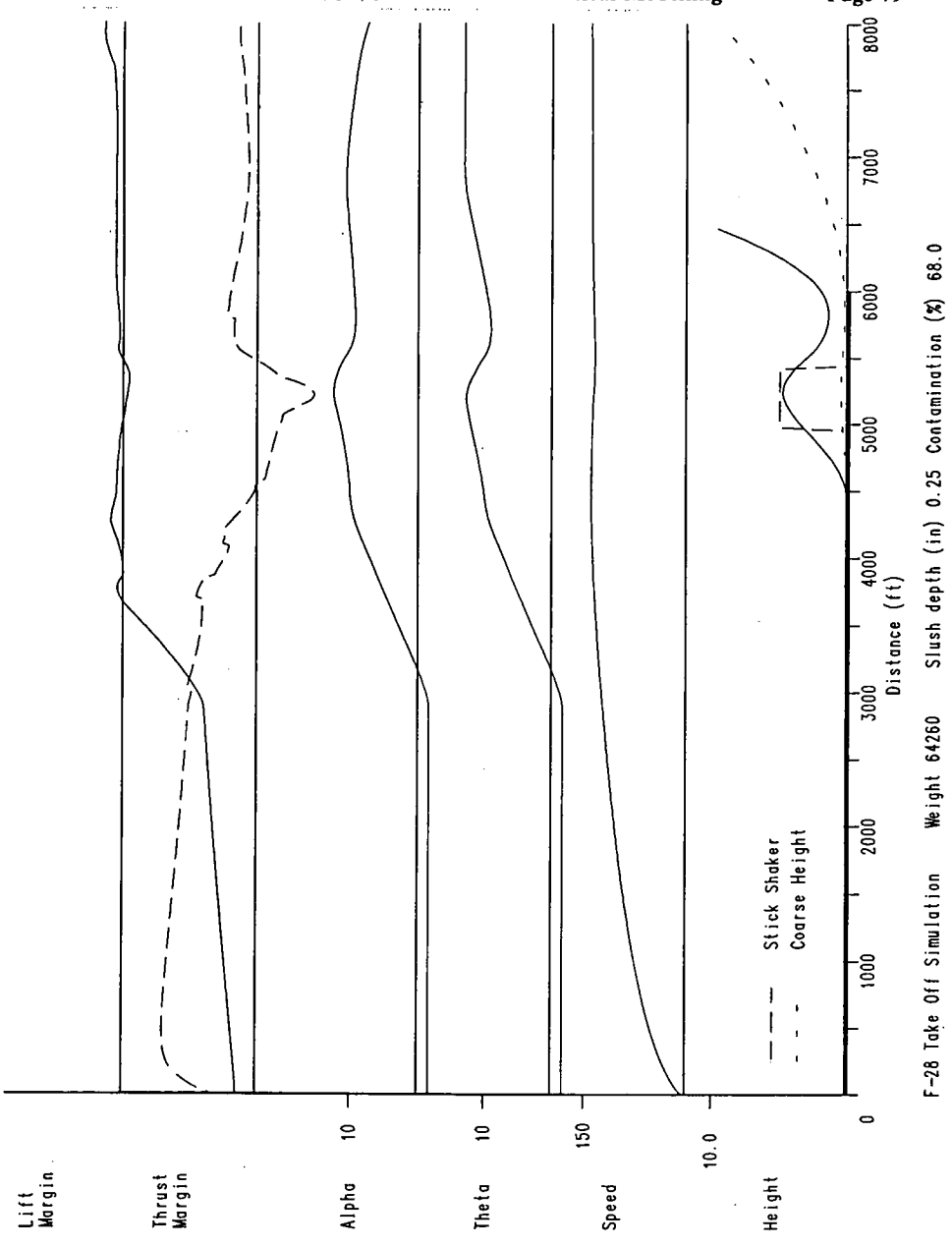

Figure 8b Marginal Take-Off

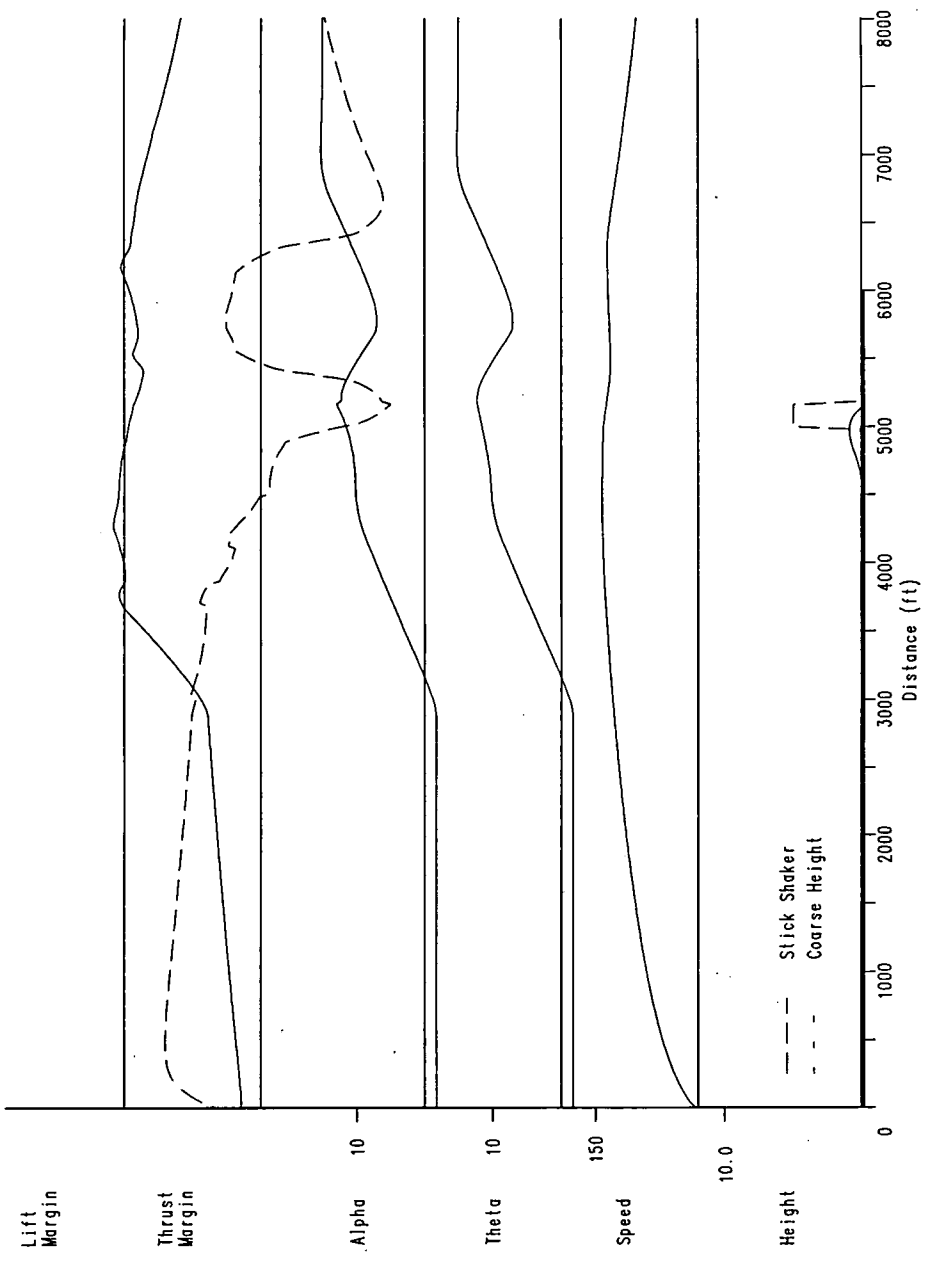

Figure 8c Unsuccessful Take-Off

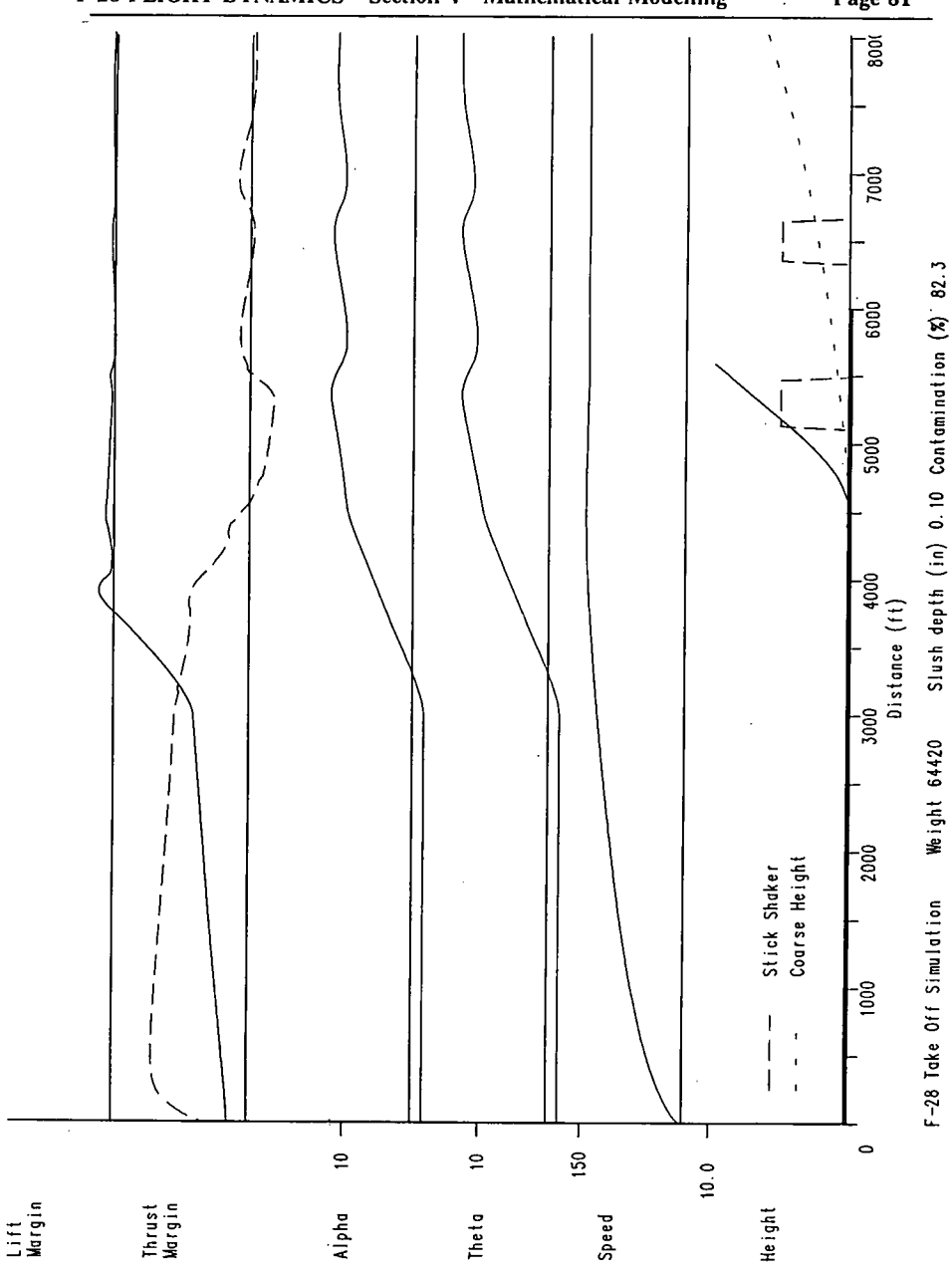

Figure 9a Successful Take-Off at 82.3% Contamination

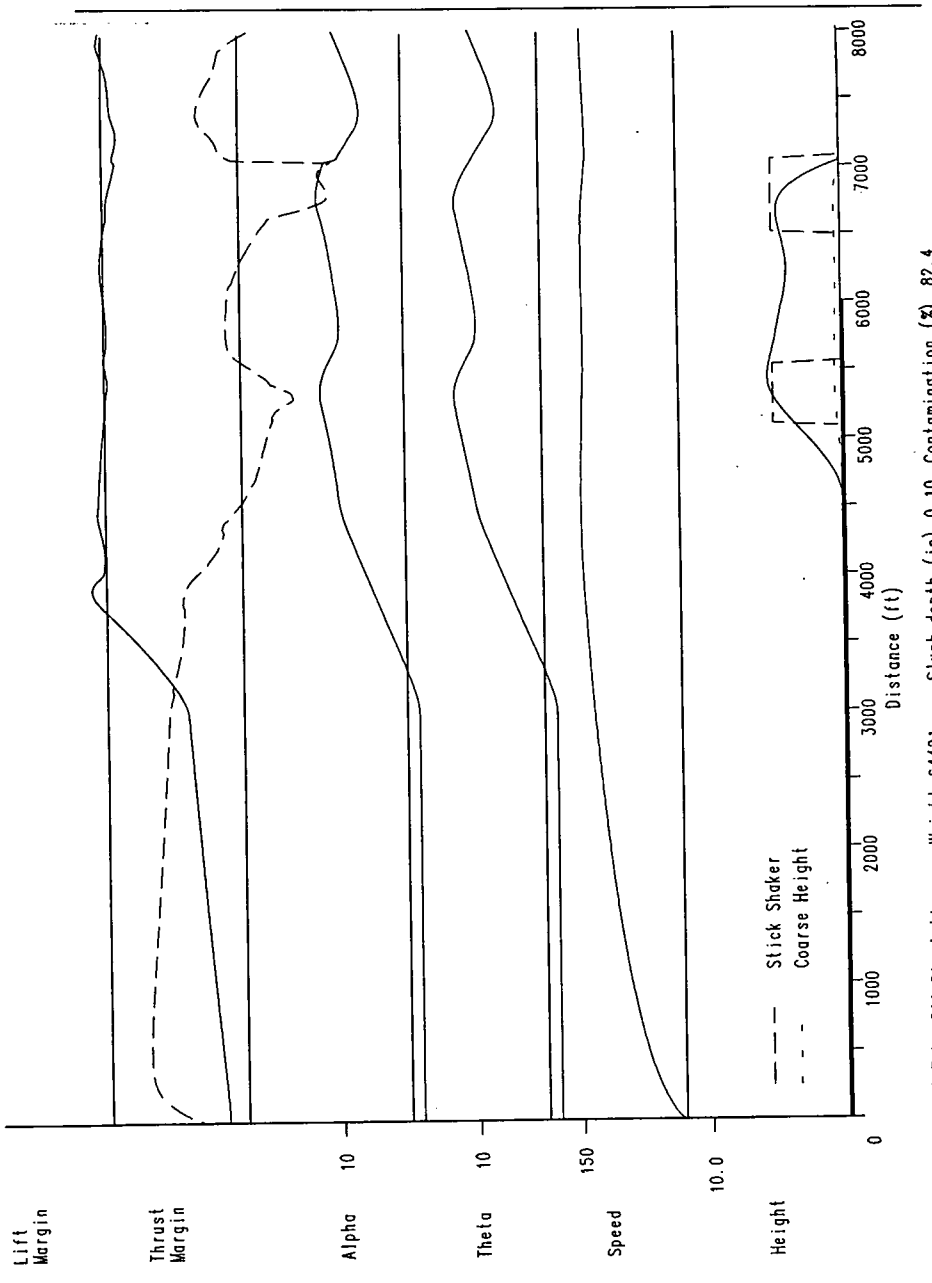

Figure 9b Unsuccessful Take-Off at 82.4 % Contamination, Identical Technique The Aircraft Flew over 2400 feet before Crash

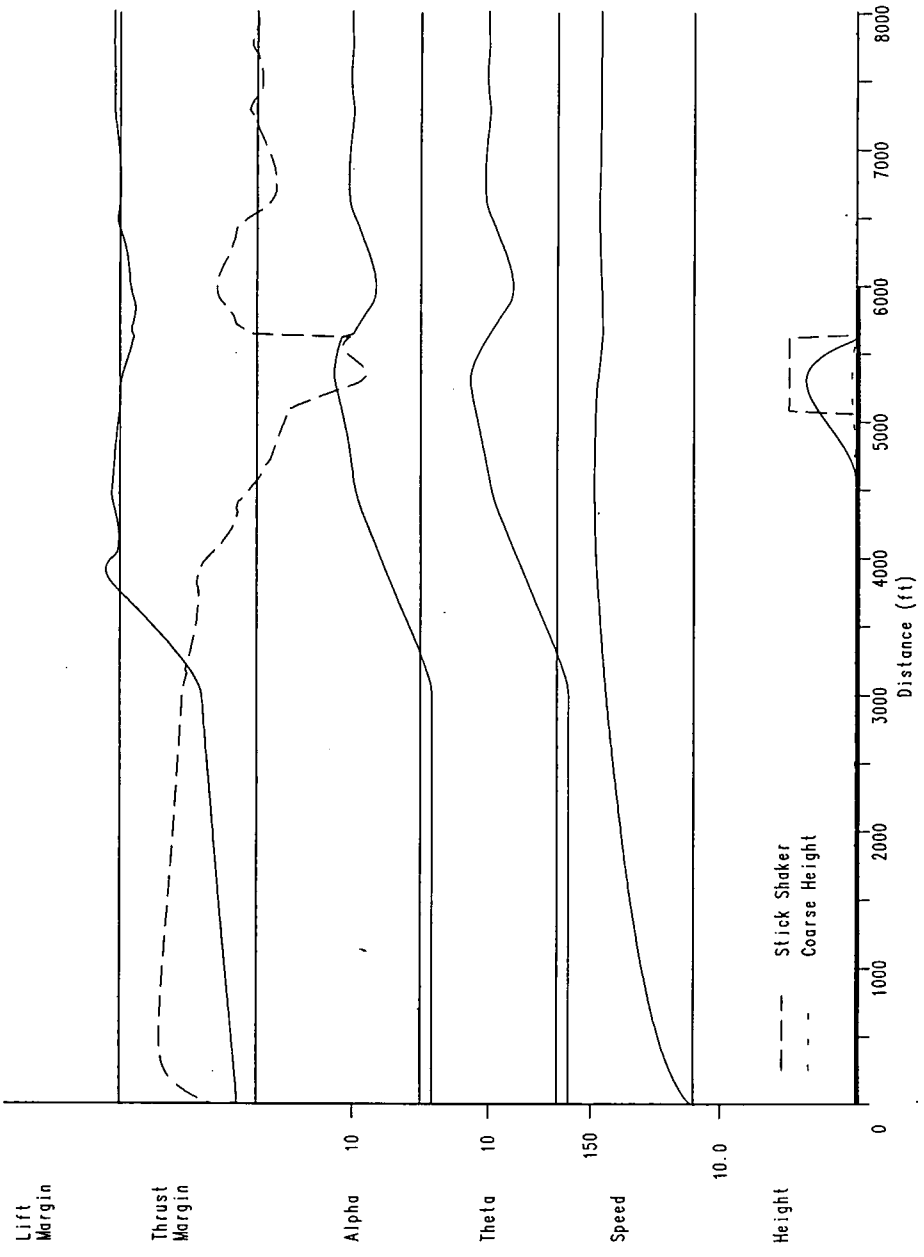

Figure 9c At 82.5% Contamination the Take-Off Becomes a Short Hop and Runway Overrun

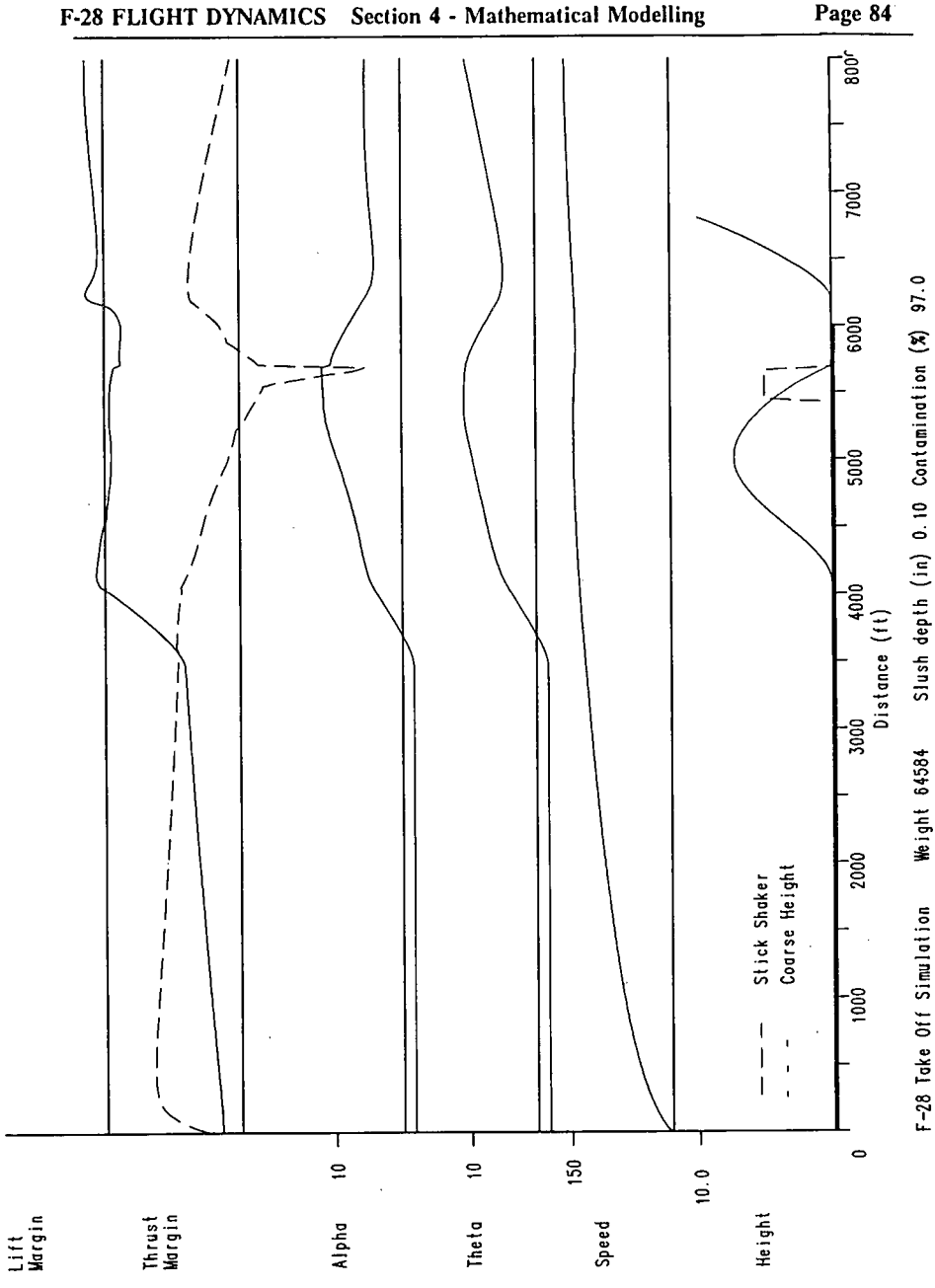

Figure 10a Second Lift-Off Following Hop

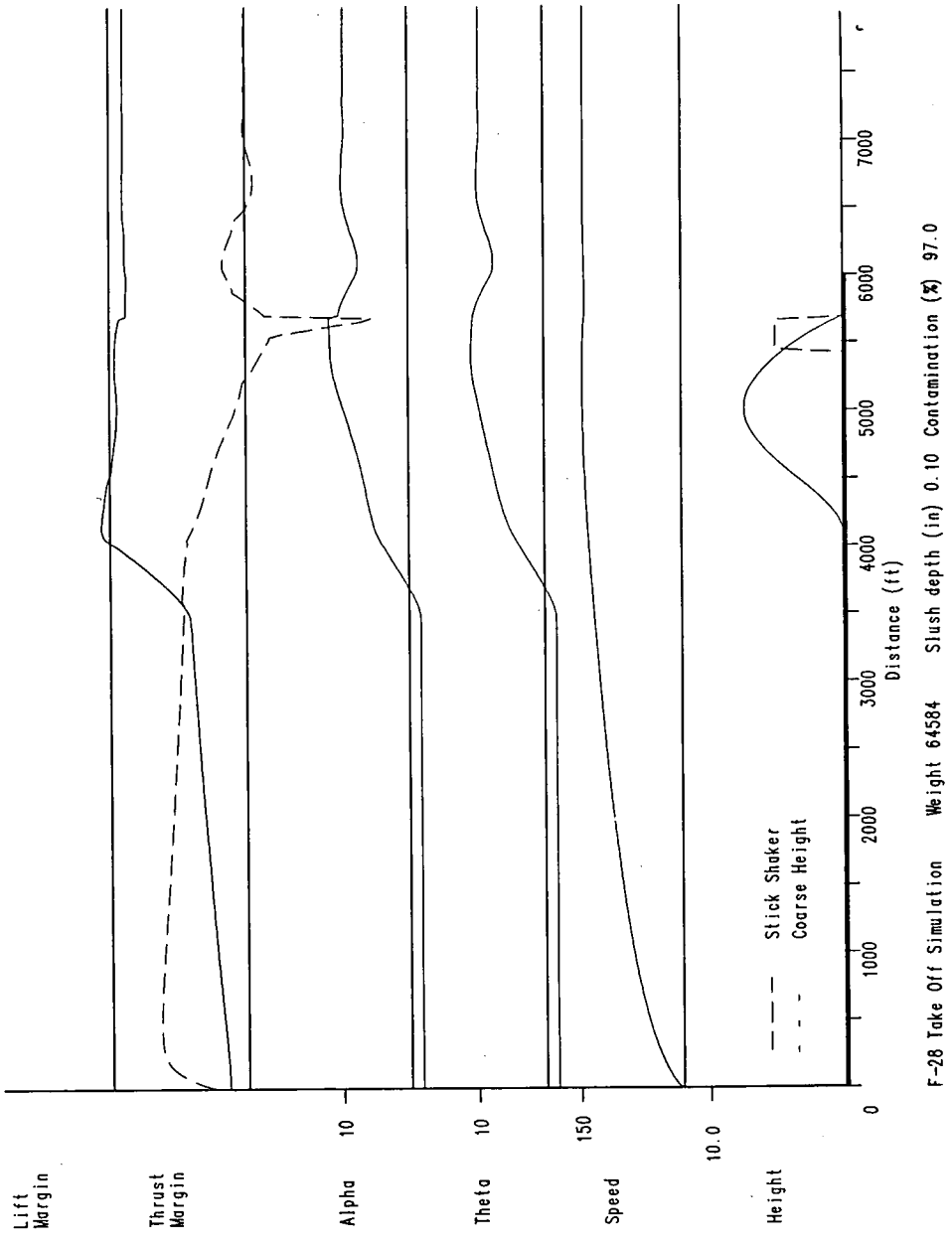

Figure 10b Slight Change in Technique Causes Overrun

APPENDIX A TO SECTION 4
NUMERICAL MODEL STATEMENTS

SYMBOL TABLE

C_L	Coefficient of Lift, complete aircraft, flap 18
C_{Lc}	As above for fully contaminated wing
C_{Lw}	Effective C_L sample wing with contaminant
C_D	Coefficient of drag uncontaminated wing
δC_D	Increment in C_D due to wing contamination
C_{Dw}	Effective C_D for sample wing with contaminant
c	Wing contamination factor (0 to 1.0)
d	Depth of runway contaminant (in)
D	Drag (lb force)
e	The Naperian constant
h	height (feet)
K_{ge}	Ground effect interpolation parameter
L	Lift (lb force)
m	mass (lb)
q_a	dynamic pressure of atmosphere ($\frac{1}{2}\rho V^2$ psf)
q_s	dynamic pressure of slush (psf)
q	body pitch rate (deg/sec)
s	the Laplace operator
t	time
t_0	reference time
T	Engine thrust (lb force)
u	velocity along body axis X
V	total velocity (ft/sec)
V_r	Planned rotation speed
W	Weight (lb force)
δW	Weight increase due to contaminant
w	velocity along body axis Z
w	width of wheel tyre
α	angle of attack (referenced to fuselage) degrees
λ	flight path angle (degrees)
δ	static depression of tires
ϵ	error
Θ	pitch attitude (degrees)
ρ	Air density

Subscripts

a	aerodynamic
b	body
c	commanded
e	effective

n	iteration cycle
max	maximum value
main	pertaining to mainwheel
nose	pertaining to nosewheel
ref	reference value at moment of lift-off
s	slush
T	true
tot	total
0	reference value (in context)

ADJUST WEIGHT FOR CONTAMINANT

(This assumes an even coating of contaminant of specific gravity 0.85 covering the contaminated proportion of all horizontal surfaces to a depth of 0.3 in. Contaminant on the fuselage is not considered.)

$$\delta W = 1117c$$

$$W = W + \delta W$$

AERODYNAMIC COEFFICIENTS

Obtain C_L and C_D for pertaining conditions

Note: C_L and C_D are computed by curve fitting from data provided in the Fokker simulation data base for the 18 degrees of flap Out of Ground Effect (OGE) case. The curves for In Ground Effect are computed by calculating an α_e (alpha effective) based on the displacement of C_{Lmax} in and out of ground effect and noting that C_{L0} for the F28 is at -5.3 degrees, α_e is a function of the ground effect interpolation parameter thus:

$$K_{ge} = e^{-0.11h} \quad \text{(Approximation of Fokker parameter)}$$

$$\alpha_e = (\alpha + 5.3)(1 + 0.27K_{ge}) - 5.3 \quad | \ \alpha_e \leq 19.9 \text{ (arbitrary limit)}$$

Compute C_L

1.1 $\alpha_e < 13.0$

$$C_L = 0.52508 + 0.10672\alpha_e - 0.0003387\alpha_e^2$$

1.2 $13.0 \leq \alpha_e < 15.0$

$$C_L = -235.18 + 50.024\alpha_e - 3.4957\alpha_e^2 + 0.08097\alpha_e^3$$

1.3 $\alpha_e \geq 15.0$

$$C_L = 60.6598 - 9.7969\alpha_e + 0.53588\alpha_e^2 - 0.0097648\alpha_e^3$$

1.4 $\alpha_e > 17.5$

$$C_L = 0.99$$

For the fully contaminated wing, a parameter C_{Lc} is computed thus:

2.1 $\alpha_e < 5.0$

$$C_{Lc} = C_L$$

2.2 $5.0 \leq \alpha_e < 9.0$

$$C_{Lc} = 3.8156 - 1.5516\alpha_e + 0.27697\alpha_e^2$$

2.3 $9.0 \leq \alpha_e < 15.0$

$$C_{Lc} = 5.5399 - 1.0486\alpha_e + 0.079142\alpha_e^2 - 0.0019817\alpha_e^3$$

2.4 $\alpha_e \geq 15.0$

$$CLc = 0.99$$

Combining these two coefficients:

$$C_{Lw} = C_L - c(C_L - C_{Lc})$$

To evaluated C_{Dw} the procedure to compute C_D is:

3.1 $\alpha_e \leq 13.0$

$$C_D = 0.0405 + 0.0235 + (0.04760 - 0.2K_{ge})C_{Lw}^2$$

3.2 $13.0 < \alpha_e \leq 14.9$

$$C_D = 0.46097 - 0.072393\alpha_e + 0.0042269\alpha_e^2$$

3.3 $\alpha_e > 14.9$

$$C_D = -3.5630 + 0.42198\alpha_e - 0.01086\alpha_e^2$$

For the contaminated wing a value for δC_D is computed by table look-up and linear interpolation and the value

$$C_{Dw} = C_D + c\delta C_D$$

is evaluated

FLUID DYNAMIC FORCES

$L = C_{Lw} q_a S$

$D_a = C_{Dw} q_a S$

$D_W = 0.2(L - W)$

if $h > 0.0$ $D_W = 0.0$

Compute Slush Drag

$D_S = C_{DS} q_s df(w)$

$f(w) = 2w\sqrt{[(\delta + d)/w - ((\delta + d)/w)^2]}$

$\delta nose = 2.1(W - L)/W$

$\delta_{main} = 2.4(W - L)/W$

$D_{Stot} = 4D_{Smain} + 2D_{Snose}$

if $\Theta > \Theta_0 + 1$

$D_{Stot} = 4D_{Smain}$

Total drag

$D_{tot} = D_a + D_W + D_S$

Engine Thrust

$T = 19592. - 17.75(V_T/1.69)$

PILOT MODELLING

GROUND RUN

$q_b = q_c = 0.0$

$\Theta_0 = -2.0$

ROTATION (Commences when $V_T > V_r$)

Normal

$\Theta_c = 10.0$

$\epsilon_\Theta = \Theta_c - \Theta$

$q_c = \epsilon_\Theta \mid 3.81 \geq q_c$

Slow

$q_c = \epsilon_\Theta \mid 1.9 \geq q_c$

Overrotate

if $(\Theta \geq 10.0).(q_c = 0.0)$ $t_0 = t$

rotate as normal

if $(t - t_0) \geq 1.5$ $\Theta_c = 12.0$

POST UNSTICK

if $(h_n > 0.0).(h_{n-1} = 0.0)$

$\alpha_{ref} = \alpha$

$V_{ref} = V_T$

Constant alpha

$\epsilon_\Theta = \alpha_{ref} - \alpha$

$q_c = \epsilon_\Theta$

Normal (increment Theta)

$\Theta_c = 13.0$

$q_c = \Theta_c - \Theta$

Constant Speed

$\epsilon_\Theta = V_T - V_{ref}$

$$q_c = 0.5\epsilon_\theta$$

RESPONSE TO STICK SHAKER

The stick shaker response assumes a 0.8 second delay in reaction to onset (assuming 0.5 second recognition time and 0.3 seconds neuromuscular delay) but only 0.4 seconds delay to termination, assuming a 0.1 second recognition delay for an alerted pilot.

if $\alpha \geq$ 11.4 ssk TRUE

if (ssk_n = TRUE).(ssk_{n-9} = TRUE) q_c = -2.0

if (ssk_{n-5} = FALSE) $q_c = q_c$

ALL CASES (The aircraft is not permitted to decelerate without pilot intervention)

if ($V_{i(n)} < V_{i(n-1)}$)·($q_c > 0.0$) q_c = -0.5

ROTATIONAL EQUATIONS

$$\frac{q_b}{q_c} = \frac{1.5}{(s + 1.5)}$$

$$\theta = \int q_b dt + \theta_0$$

$$\lambda = \mathrm{Tan}^{-1}(\dot{h}/\dot{x})$$

$$\alpha = \theta - \lambda$$

KINEMATIC EQUATIONS IN BODY AXES

$$m = W/32.18$$

$$\dot{u} = (T + L\sin(\alpha) - D\cos(\alpha) - W\sin(\theta))/m - qw$$

$$\dot{w} = (L\cos(\alpha) + D\sin(\alpha) - W\cos(\theta))/m + qu$$

$$u = \int \dot{u} dt$$

$$w = \int \dot{w} dt$$

$$V_T = \sqrt{(u^2 + w^2)}$$

$$\dot{x} = u\cos(\theta) + w\sin(\theta)$$

$$d = \int \dot{x} dt$$

$$\dot{z} = w\cos(\theta) - u\sin(\theta)$$

$$\ddot{h} = -\dot{z}$$

$$h = \int \ddot{h}dt$$

Note: in all cases

$\int xdt$ is approximated as $\Sigma(x_{(n-1)} + x_{(n)})/2\ \delta t$

where $\delta t = 0.1$ secs

F-28 FLIGHT DYNAMICS
SECTION 5

FOKKER F-28 MODELLING VALIDATION

INTRODUCTION

As a part of the investigation into the accident involving Fokker F-28 C-FONF at Dryden airport, an off-line computer model was constructed to investigate the effects of aircraft and runway contaminants on the take-off performance of this aircraft. The model was based on a simulation data base provided by the manufacturer. At the same time, actual Flight Data Recorder (FDR) records were available covering some 21 take-offs of this specific aircraft during the month of February 1989 (the accident occurred in March).

Since the FDR was destroyed in the crash and there are, therefore no numerical data available concerning the aircraft's trajectory prior to impact, it was felt to be of prime importance that the model used in the investigation be validated as rigorously as possible. To this end, the existing FDR records were analysed and compared with the model outputs for the same sets of conditions. Generally there was very close agreement once one minor adjustment to the model had been made; this will be described in detail in a following section.

FLIGHT DATA RECORDER DATA

To use the existing FDR data to validate the simulation, it was first necessary to confirm the internal consistency of the FDR records and then to develop a sense of their quality or accuracy. Four of the FDR parameters were of prime interest in determining the runway performance of the aircraft, these being:

Indicated Airspeed (IAS) [kt]
Thrust [%]
Pitch Attitude (Θ)[deg]
Longitudinal Acceleration (A_x) ['g' units]

For each take-off, the aircraft weight, airport elevation, ambient temperature and prevailing wind were known.

The Relationships

The relationships among the above parameters can be quite complex if the aircraft is permitted to enjoy all of its degrees of freedom so to simplify the analytical processes only the take-off ground roll up to, but not including rotation, was used in this exercise. This effectively constrains the aircraft in the pitch, roll and yaw rotational freedoms and permits simpler linear

comparisons to be used in testing for mutual consistency. In this condition, the relationships may be expressed thus:

$$\ddot{x} = (A_x - \mathrm{Sin}(\Theta))g \quad (1)$$

$$V = \int \ddot{x}\, dt \quad (2)$$

$$V_i = V\sqrt{\sigma} + V_w \quad (3)$$

$$V = (V_i - V_w)/\sqrt{\sigma} \quad (4)$$

$$\ddot{x} = T_{net}/\mathrm{Weight} \quad (5)$$

$$T_{net} = \mathrm{Thrust} - \mathrm{Drag} \quad (6)$$

Where $\ddot{x}$ is the acceleration along the runway, 'g' the acceleration due to gravity, V_i the equivalent airspeed (closely related to, but not identical with IAS), V is true inertial speed relative to the earth, V_w the component of wind along the aircraft's longitudinal axis, positive for a headwind, σ the relative density of the atmosphere and T_{net} the net thrust. These equations offer sufficient redundancy to permit a recursive approach towards validation to be effective. It is accepted that Equation (1) is an approximation, and should read, in its full form

$$\ddot{x}/g = (A_x - \mathrm{Sin}(\Theta))\cdot\mathrm{Cos}(\Theta) - (A_z + \mathrm{Cos}(\Theta)\mathrm{Cos}(\Phi))\cdot\mathrm{Sin}(\Theta)$$

(where A_z is the body axis vertical acceleration and Φ the angle of bank) the restricted range of Θ while on the runway (from -2 to .5 degrees) makes the second term so small, and $\mathrm{Cos}(\Theta)$ so close to unity that the approximation is justified in the interests of simplicity.

Interpreting FDR Records

The most difficult of the FDR parameters with which to deal was the one named Thrust, which was expressed as a percentage, but for which we had no a priori relationship to the thrust being developed by the engines. Since during normal take-offs the thrust was applied slowly (up to 10 seconds at times) it was critical not only to understand the relationship between the recorded parameter and actual thrust, but also to make the model capable of accepting the same schedules of thrust application as the aircraft for each take-off. It was also noted that the Thrust parameter reached different maximum values for each take-off.

To obtain a relationship between the Thrust parameter and actual thrust, an assumption was made that each take-off was performed using normal take-off thrust, ie, 19,500 lb force. The FDR print-outs were examined for maximum values of acceleration

(using Eqn (1) to compute $\ddot{x}$) the value of V_i at this point was estimated by the use of Equations (2) and (3) and the total aircraft drag estimated from

$$\text{Drag} = C_d qS + (\text{Weight} - \text{Lift})\mu$$

Where C_d, the coefficient of drag, was derived from the Fokker data base, (q) was the dynamic pressure at V_i, (S) the reference wing area and μ the assumed coefficient of rolling friction for the aircraft. This permitted the use of Equations (5) and (6) to estimate a value for thrust at that point. The value of V_i was also used to calculate the thrust decrement due to speed (approximately 17 lb per knot) which was applied to the model thrust output at the same point. Since the point of maximum acceleration was always met at very low speeds, such that the aerodynamic drag was always low (of the order of 150 lb, compared to normal engine thrust of 19500 lb), the sensitivity of this procedure to errors in the aerodynamic model is very weak. Differences between the values for thrust developed from the FDR data and the model could therefore be assumed to be dominated by other factors, off-nominal engine performance in the aircraft, erroneous estimations of μ, discrepancies in the recorded values of A_x or Θ or an incorrect initial assumption that full rated power was being used. In fact, agreement was generally quite close, and a minor adjustment to μ from .02 to .022[6] was sufficient to produce agreement within reasonable scatter.

Having gained some measure of confidence in the FDR recordings by this method, the same technique was now used to compute actual thrust from the start of throttle advance to maximum Thrust parameter value for a selection of take-offs chosen from the full set. The selection criterion was that a time-history of airspeed (once the IAS sensor had become fully functional) should show as little wind effect as possible, thereby reducing errors in the application of Equations (3) and (4) due to indeterminate variations in V_w. The resulting data showed a remarkably good linear correlation between thrust and the Thrust parameter, regression analysis yielding the relationship:

$$T = T_{max}(-.55464 + 1.56045T_{irel})$$

Where T_{max} is the full rated thrust and T_{irel} is the ratio between the value of the recorded Thrust parameter and its maximum value for that specific take-off. This value for thrust (T) was used for the remaining validations.

Speed Profile Comparisons

Since the whole object of the modelling exercise was to examine the effects of contamination on both the take-off run and post lift-off behaviour of the F-28, it was felt that the final stage of validation of the model should be a full comparison of the speed

[6] The literature on rolling friction was very sparse, giving such generalities as "μ can vary from .02 on a runway or deck to .05 on a well kept grass field", so this adjustment is by no means excessive.

profiles between the FDR data and the model. However, prior to this a final check on the modelling was made by comparing model indicated airspeed with that of the FDR for a variety of weights and ambient wind conditions. Two short segment plots, Figures 1 and 2, show the FDR IAS, and integrations of the corrected FDR longitudinal acceleration and the model output of IAS. It can be seen from these that a very close match has been achieved, and it should be noted that the model on which this is based did not vary in any way from the data provided by the manufacturer, while model thrust was based on the standard engine model. The extremely close agreement noted provides adequate confidence to complete the final comparisons.

Figures 3,4,5 and 6 show the full airspeed correlations between FDR IAS, FDR accelerations integrated and model output. It can be seen that the airspeed trace displays considerable non-linearity below 100 kt, but that in all cases there is a terminal confluence of all three parameters. Figure 6 is of considerable interest. This take-off case was reported to have taken place in zero wind, yet the curves did not overlay but, as can be seen from Figures 6,10 and 15, both the speed, thrust and acceleration traces diverged as time increased. This indicated an error in some function of speed rather than in the thrust estimation. The assumption of a rolling take off for this case produced curves which overlay very closely as can be seen in Figures 6 (diamond symbol),11 and 15(Filled square symbol). The rolling take-off assumption is analytically attractive since it has exactly the desired effect of removing the speed dependent divergence between FDR and model, since it serves simply to displace the inertial velocity to time curve without changing its form, while it changes the slope of the V^2 to time relationship, as illustrated in Figure 16.

Acceleration and Thrust Comparisons

Figures 12 to 15 for acceleration and 7 to 11 for thrust estimates also show agreements which are probably as close as can be reasonably hoped for using data of this kind.

SUMMARY

The plots provided with this document are sufficient to indicate that very close agreement between the recorded performance of C-FONF and the math model has been achieved. This being so, the author has very high confidence that the model outputs will fairly and accurately represent the basic behaviour of the subject aircraft in its normal state.

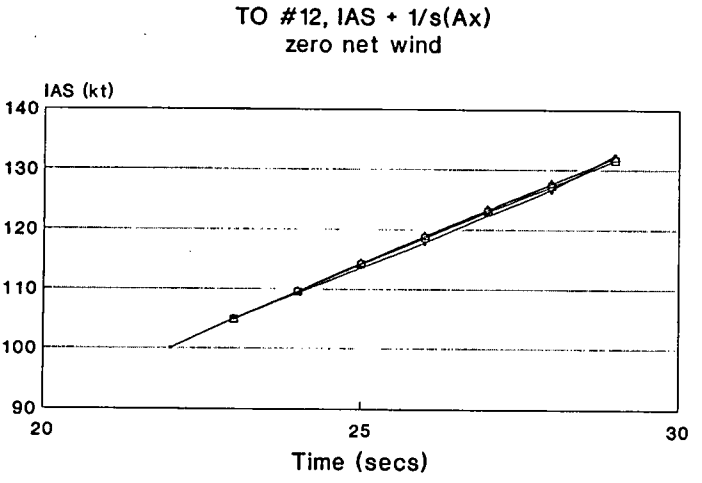

Figure 1 Airspeed, FDR Ax and Model Correlation

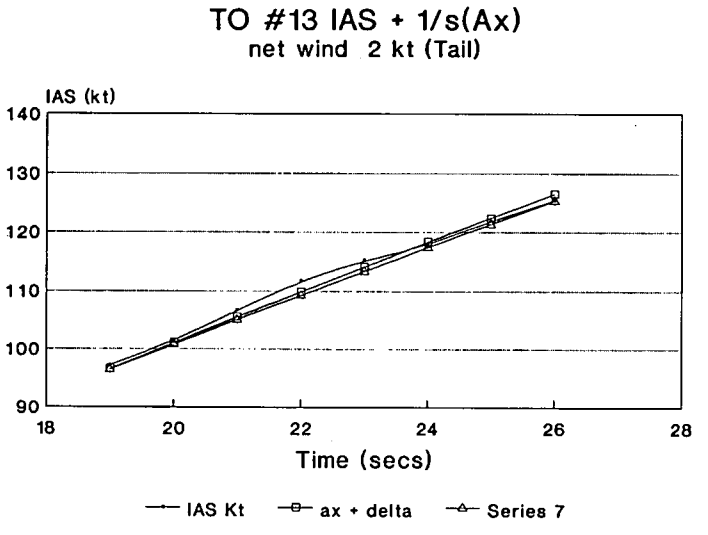

Figure 2 Airspeed, FDR Ax and Model Correlation

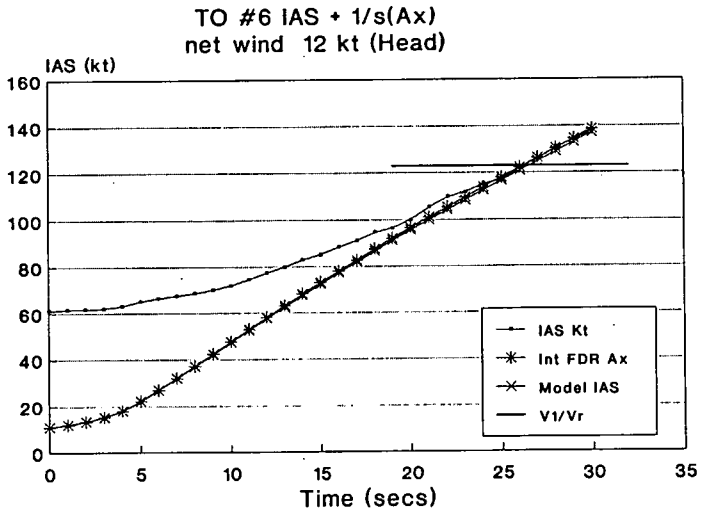

Figure 3 FDR and Model Comparison, Speeds

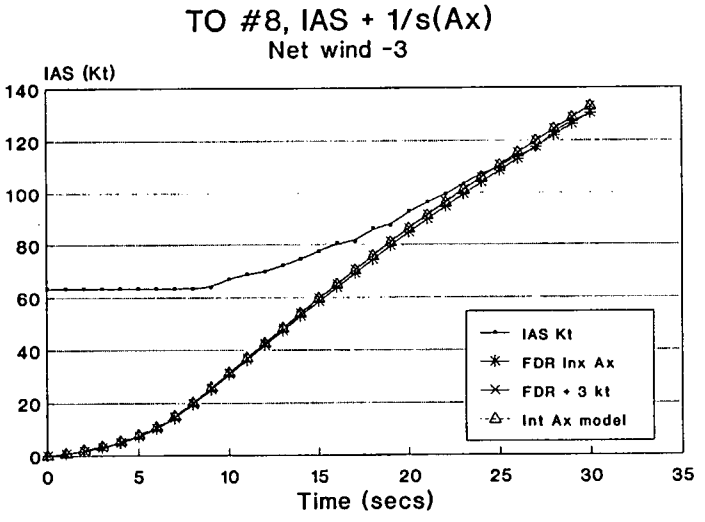

Figure 4 FDR and Model Comparisons, Speeds

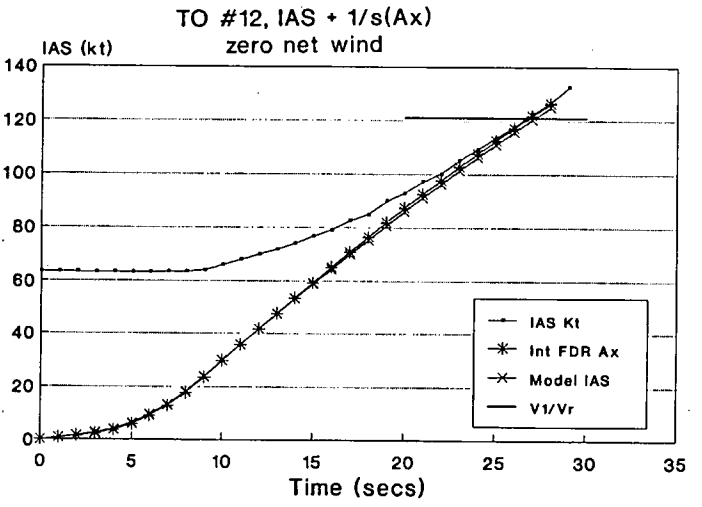

Figure 5 FDR and Model Comparisons, Speeds

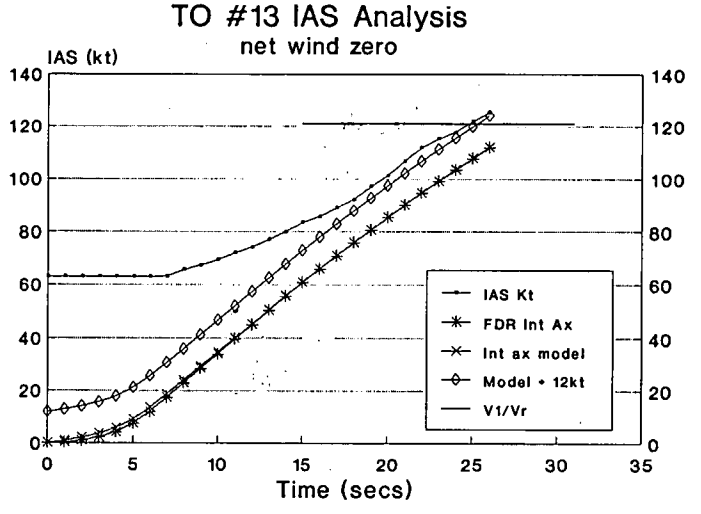

Figure 6 FDR and Model Comparisons, Speeds

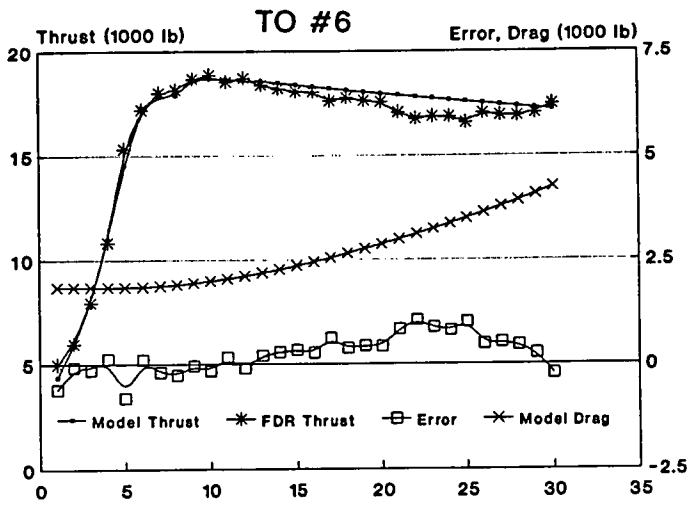

Figure 7 FDR and Model Comparisons, Thrust

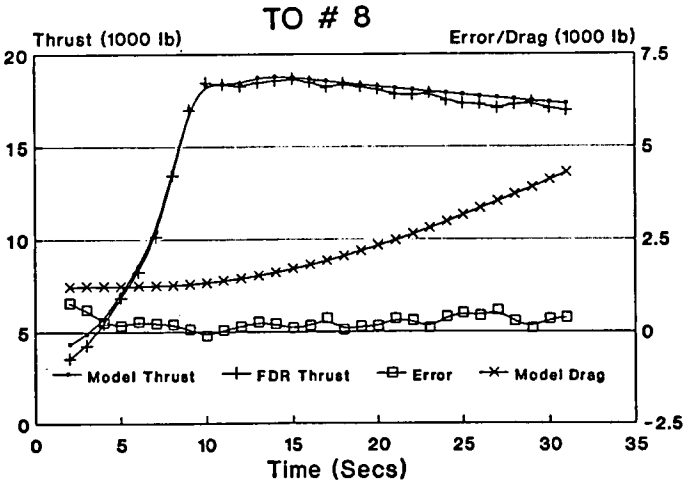

Figure 8 FDR and Model Comparisons, Thrust

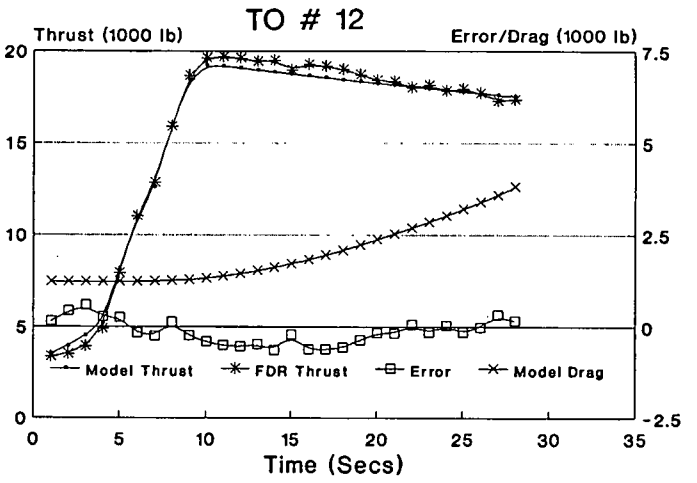

Figure 9 FDR and Model Comparisons, Thrust

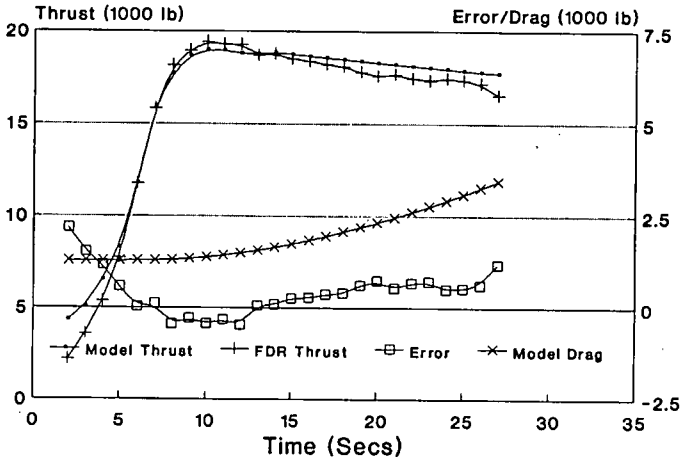

Figure 10 FDR and Model Thrusts, TO #13, Standing Start

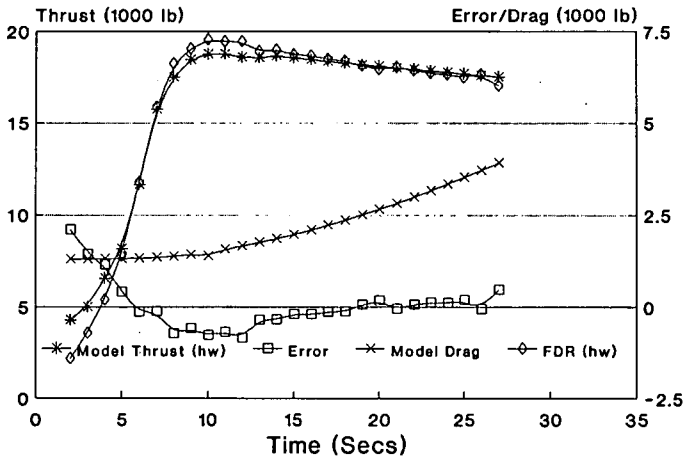

Figure 11 FDR and Model Thrusts, TO #13, Rolling Start

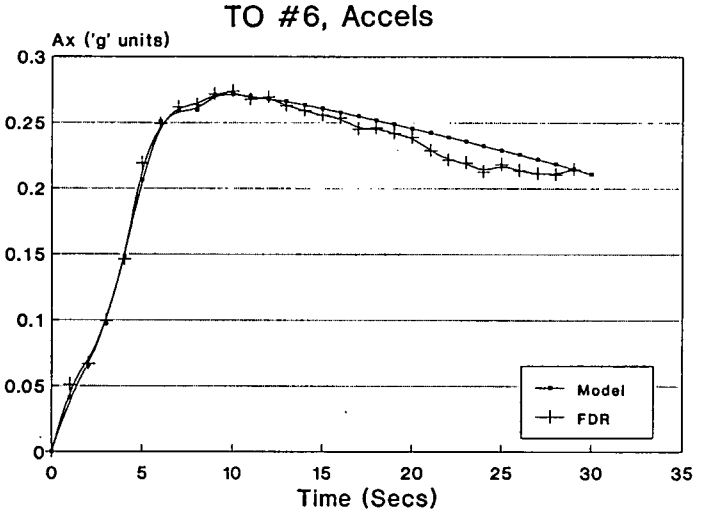

Figure 12 FDR and Model Comparisons, Acceleration

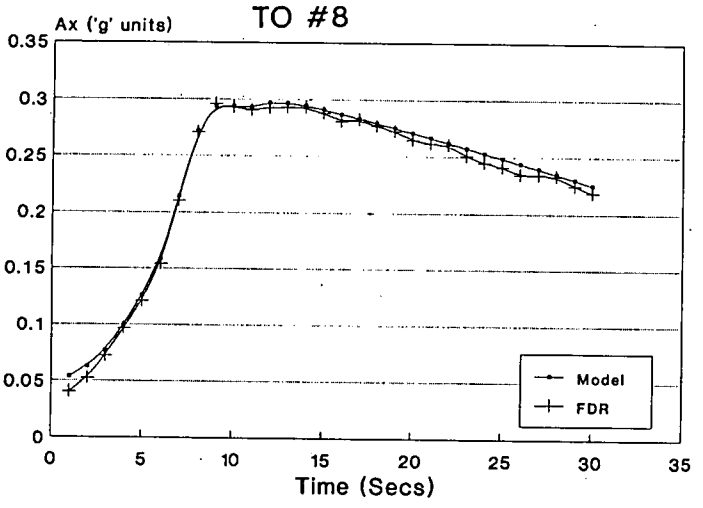

Figure 13 FDR and Model Comparisons, Acceleration

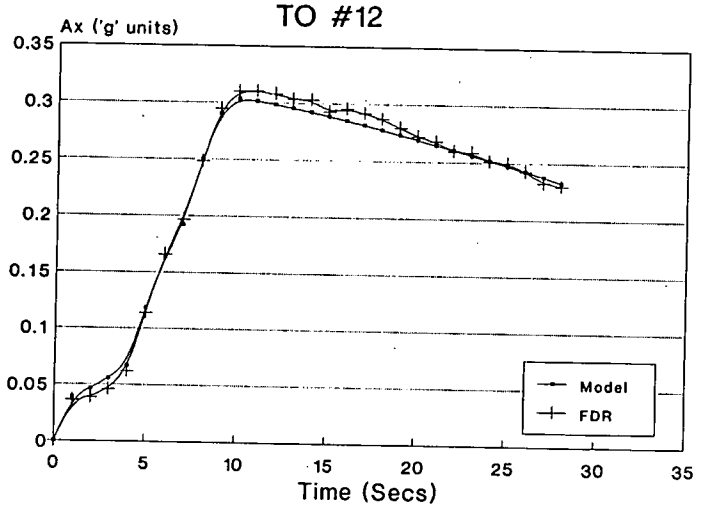

Figure 14 FDR and Model Comparisons, Acceleration

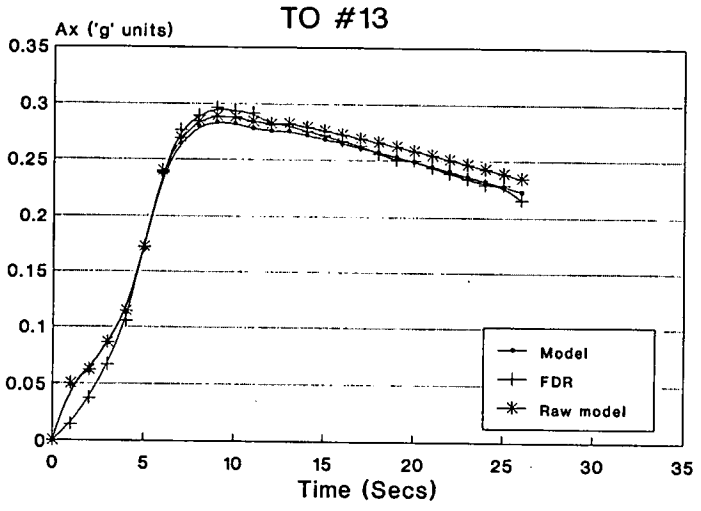

Figure 15 FDR and Model Comparisons, Acceleration Showing Raw Model and Model with Assumed Rolling Start

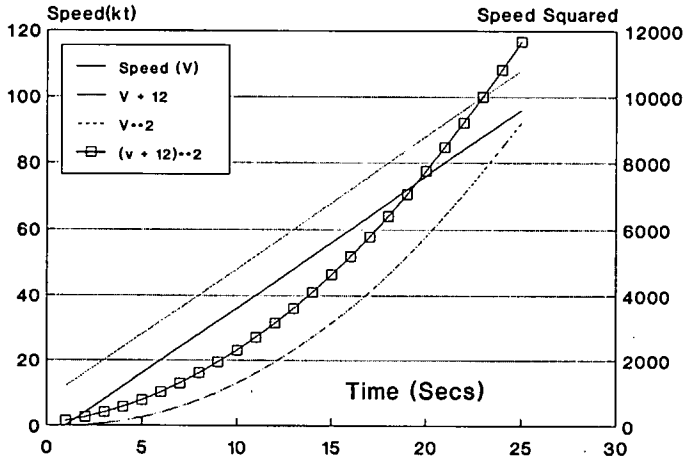

Figure 16 Effects of Rolling Take-off

F-28 FLIGHT DYNAMICS
SECTION 6

DISCUSSION AND CONCLUSIONS

DYNAMIC SIMULATIONS

The dynamic simulations demonstrated that the increased takeoff roll and short airborne segment could have been the result of the conditions tested in these simulations.

An increase in takeoff run on the order of 500 to 700 feet will result from slush accumulation on the takeoff runway on the order of 0.15 inches for the F28-1000 aircraft in those conditions, combined with the additional time to rotate the aircraft to the higher required liftoff attitude.

The airborne segment is more difficult to clearly define because there is a lack of a clearly defined flight path, nor do we have any knowledge of the pilot's control strategies as he attempted to complete the take-off. However, witness reports indicate that airborne segment was limited in absolute altitude to less than one wingspan, suggesting that the aircraft never climbed out of ground effect. The horizontal trajectory is defined by tree cut and wreckage location information after the first tree strike. Based on those data, simulations with moderate wing contaminant factors resulted in airborne segments which, in general terms, matched the witnesses' descriptions of the Dryden trajectory.

It is probably of significance that in those runs during which moderate to high levels of wing contamination were represented, stick shaker activation was a constant feature. The onset of this warning will usually trigger a highly trained response on the part of the pilot, who has been taught to use this indication as a means of achieving close to the maximum lifting performance of his wing when so needed. With the wing performance degraded by roughness this device can be misleading if used in an attempt to optimise lift since at stick shaker activation the wing may already be past the maximum C_L achievable in the presence of the contaminant. It should also be noted that the use of stick shaker triggering as an indication of maximum lifting capability must be essentially a *short term* procedure, even with the clean wing this operating point is well removed from the optimum lift/drag ratio for the aircraft and is not, therefore, a suitable operating condition for sustained climb. However, a pilot generally[7] has no other indication available to him and it is only to be expected that he would respond as trained.

NUMERICAL SIMULATIONS

The numerical simulations described in detail in Section 4 supported very strongly the observations made in the Fokker simulator. This indicates that the behaviour of that simulation may be taken, with some confidence, to represent closely the behaviour to be expected of an F-28 aircraft in actual flight.

---

[7] Note, however, that unlike the majority of current transport aircraft, the Fokker F-28 is equipped with an angle of attack indicator

Additionally, the off-line modelling complemented the dynamic simulations in that it permitted the investigators to examine a wide range of conditions in a very clinical manner and in a relatively short time. In particular it permitted the definition of two critical boundary conditions for contaminated take-off attempts, either of which would result in a catastrophic occurrence. Specifically, the region between the boundaries represents an entire range of slush and wing contamination conditions which could give rise to a trajectory of the kind described by witnesses to the Dryden accident.

A general observation based on the results of the numerical simulations is that the higher the rotation speed and the slower the rotation rate, the greater was the probability that the take off attempt would be successful. This is exactly what would be expected from an engineering evaluation of the effects of contamination on the aircraft's characteristics. Advice given in the F-28 handbook supports this observation.

GENERAL DISCUSSION

This statement immediately above raises two issues pertinent to this accident and worthy of comment here inasmuch as they bear on the act of attempting a take-off under the conditions pertaining at the time. It is not in the least likely that the average airline pilot would have sufficient theoretical knowledge to be able to assess in detail the effect on his aircraft's performance of these forms of contamination. Indeed, it is not possible to make such an assessment on the spur of the moment while already in the cockpit. The second issue concerns the pilot's awareness of his aircraft's external state under these kinds of conditions. Again, in some ways this is a function of the size and shape of aircraft of this class. By and large direct observation of the flying surfaces by the crew is either very difficult or impossible, once strapped in for take-off. In the F-28 approximately 50% of the wing can be viewed obliquely from the cockpit window with special effort, while by opening the window and leaning out the entire wing can be viewed. The automatic ice detection systems that presently exist are designed to detect and warn against the accretion of ice in flight rather than that due to the exposure of the aircraft to precipitation or frost formation while on the ground: the effects of the two types of airframe icing are quite different.

OTHER FACTORS

Wing Leading Edge Paint Deterioration

There have been reports that the wing leading edge of the F28 involved in this accident had a significant degree of paint cracking and deterioration. The paint thickness on the aircraft leading edge was measured at 0.016 inches, consisting of 3 or 4 layers of paint. This issue was brought up with Fokker's aerodynamics group who indicated that while the cracked paint certainly did not enhance performance, its effect on the maximum lift coefficient and stalling angle of attack was not judged to be significant.

There is a question of whether the deteriorated leading edge paint condition could have contributed to the degree that any contaminant would adhere to the wing. To date, there is no clear answer to that.

CONCLUSIONS

It is difficult when writing a report of this nature to be adequately mindful of the semantics or etymology of the words used. This is often the case when persons working in a specific discipline assign to a common word a precise or special meaning more limiting than that which applies in the vernacular. We have several times used the word 'cause' and phrases such as 'the cause of the accident'. It must be remembered that we use that word in a very technical sense to indicate a sequence of events which would or could give rise to a flightpath similar to the one reported at Dryden. The 'cause' to which we refer means a set of physical or engineering conditions which have a direct and predictable result (that is, we are describing a causal relationship). These are not of themselves the cause of the accident in the general sense, simply the result of a pilot attempting to take-off in a significantly contaminated aircraft.

It must be remembered that the conclusions of this subgroup report present possible causes of the flight path for the Dryden accident. It is critically important to remember that the assumptions listed in the beginning of this report must be clearly borne in mind in the final analysis of this accident. This report treats only the aerodynamics and aircraft handling aspects of this accident and assumes that there were NO other factors which could have been the related to the accident. There is no doubt that major failures of aircraft systems or other factors not mentioned in this report and not considered in this simulation could also have resulted in the accident flight profile, alone or in conjunction with the known wing contaminant.

With these caveats in mind, we are prepared to state:

1. The witness reported flight paths and "Dryden Scenario" which was based on those reports is physically possible from an engineering viewpoint.

2. The aerodynamic performance of the F28 in the Dryden accident was definitely degraded by the wing contamination which was reported by the witnesses on board the aircraft. This conclusion is based on knowledge of the sensitivity of aircraft lifting surfaces to contaminant and our analysis of the degree of contamination of the wings described by the witnesses. The work done by Fokker in their wind tunnel, general knowledge of aircraft aerodynamics and analyses of other accidents with F28's and similar aircraft clearly support the conclusion that the contaminants on the wings degraded the lifting capability and increased the drag on the accident aircraft.

3. The increased ground distance to the reported liftoff point could have been due to the following factors, individually or in combination:

   a) Small slush accumulations on the runway

   b) Selection of higher than normal rotation speed

4. An additional contributing factor to the increased ground distance to liftoff was the higher speed and/or pitch attitude required for liftoff as a result of wing

contaminant. This would have increased the takeoff run to the liftoff point, irrespective of any other factor. This was due to the additional time required to reach the required speed and/or to rotate the aircraft to the higher liftoff attitude. At the liftoff speed for the F28 in the Dryden case on the order of 130 knots, each additional second during rotation increased the ground run by approximately 200 feet.

5. The deteriorated condition of the paint on the wing leading edge probably did not affect the aerodynamic characteristics of the aircraft directly. However, the effect of the deteriorated paint on the adherence characteristics of contaminants at the leading edge is unknown, but could potentially have been a minor factor in the amount of contaminant that remained on the wing.

6. Simulation and analytical work done by this group has defined a range of conditions in terms of wing and runway contaminant levels which, alone, could have resulted in the accident profile.

7. Without FDR data, CVR data, the pilots themselves, and a mathematical description of the wing and runway contaminant levels, it can NOT be conclusively stated that wing or runway contamination alone caused the aircraft to crash.

REFERENCES

1. Wolters, S.R., Watch it in Winter, Operation and Maintenance of Fokker Aircraft, NO 3, Feb 1984

2. Jones, R., and Williams, D.H., The Effect of Surface Roughness on the Characteriestics of the Aerofoils NACA 0012 and RAF 34. NPL(UK) Reports and Memoranda No 1708, Feb 1936

3. Jane's All the World's Aircraft, 1975-76, p. 144

4. Schlichting, Boundary Layer Theory Pergamon Press, 1955

5. Schuringa, Tj., Aerodynamics of the Wing Stall of the Fokker F-28. AGARD CP-102, #20

6. Torenbeek, E., Synthesis of Subsonic Airplane Design Delft University Press

7. Warrink B.J., Simulation Report vs-28-25, Fokker Aircraft, June 1989, Order 22192

8. Anon F28 Simulation Data Base, Master File

9. Walter B. Horne et al. Studies of the Retarding Force Developed on an Aircraft Tire Rolling in Slush or Water. NASA TN D-552, September 1960

10. Slatter N.V. and Maltby R.L.,The Measurement of the Effects of Slush and Water on Aircraft During Take-Off. RAE R&M 3604, 1969.

11. loq. cit.

12. Cebeci, T., Effects of Environmentally Imposed Roughness on Airfoil [sic] Performance, Paper delivered at the Von Karman Institute for Fluid Dynamics, February 1987.

13. Zierten, T.A. and Hill E.G.,Effects of Wing Simulated Ground Frost on Airplane Performance. von Karman Institute Lecture Series on "Influence of Environmental Factors on Aircraft Perfromance", 1987.

14. loq. cit.

15. Abbott Ira H. and Von Doenhoff Albert E. The Theory of Wing Sections Dover Publications Inc. New York 1959, Ch 7, 7.5c pp157 et seq

16. Hoerner Dr-Ing S.F. Fluid-Dynamic Drag Published by the Author, 1965 Library of Congress No 64-19666 Ch 5.1

17. loq. cit.

Appendix 5

Wind Tunnel Investigation of a Wing-Propeller Model Performance Degradation due to Distributed Upper-Surface Roughness and Leading Edge Shape Modification

R.H. Wickens
V.D. Nguyen

April 1991

WIND TUNNEL INVESTIGATION OF A WING-PROPELLER MODEL PERFORMANCE DEGRADATION DUE TO DISTRIBUTED UPPER-SURFACE ROUGHNESS AND LEADING EDGE SHAPE MODIFICATION

R.H. Wickens and V.D. Nguyen
Applied Aerodynamics Laboratory
Institute for Aerospace Research
National Research Council Canada
Ottawa, Canada K1A 0R6

April 1991

SUMMARY

A wind tunnel investigation has assessed the effects of distributed upper surface roughness, and leading edge ice formation on a powered wing propeller model.

In the unpowered state, it was found that roughness reduces the lift slope, and maximum lift by 30 to 50 percent, depending upon particle size and Reynolds number. The leading edge region is especially sensitive to these disturbances, however removal of the roughness over a small portion of the nose restored the wing to close to its original performance.

The application of power to the wing, with an increase of slipstream dynamic pressure increases the lift slope and maximum lift; however this benefit is lost if the wing is roughened. Subtraction of the propeller reactions indicated that the slipstream interaction accounted for half the lift increase, and also resulted in reduced drag for the clean surface. This drag reduction was removed when the wing was roughened, indicating that the degradation of wing performance due to roughening is relatively greater when a slipstream is present, compared to the unpowered wing.

Leading edge ice accretion causes similar large losses in lift and increases of form drag although a comparison of the two types of contamination showed that leading edge ice produces a smaller reduction of lift slope prior to flow separation. In both types of contamination, Reynolds number is important, and emphasizes the necessity of testing under near full-scale conditions.

List of Symbols

C_L lift coefficient $\frac{L}{\frac{1}{2}\rho V^2 S_w}$

C_D Drag coefficient $\frac{D}{\frac{1}{2}\rho V^2 S_w}$

C_m moment coefficient $\frac{M}{\frac{1}{2}\rho V^2 S_w c}$

c wing chord

S_w wing area

C_{Tp} propeller thrust coefficient $\frac{T_p}{\rho N^2 D^4}$

C_{Np} propeller normal force coefficient $\frac{N_p}{\rho N^2 D^4}$

C_{mp} propeller pitching moment coefficient $\frac{M_p}{\rho N^2 D^5}$

C_c wing chord force coefficient $\frac{C_c}{\frac{1}{2}\rho V^2 S_w}$

C_{Do} parasite drag coefficient (unpowered)

C_{L_s}, C_{D_s}, C_{m_s} wing coefficients with the propeller reactions removed

C_s leading edge suction coefficient

D propeller diameter

N propeller rotation speed (RPS)

J propeller advance ratio $\frac{V}{ND}$

k roughness particle size

INTRODUCTION

Recent flying accidents resulting from adverse weather conditions in the form of freezing rain or snow, have focussed attention on the degradation of aerodynamic surfaces. One of the most recent accidents, involving a Fokker F-28, mk 1000 jet aircraft, and the subject of a Commission of Inquiry in Canada, dealt specifically with the degradation of such surfaces due to ice and snow contaminants on the wings. The information contained in this paper stems in part from the investigation conducted for the Commission of Inquiry into the Air Ontario Crash at Dryden, Ontario, March 10, 1989. (Ref. 10) Investigations of the effects of uniform roughness on airfoils shows clearly that stalling is premature, loss of maximum lift can be as high as 50%, (depending on Reynolds Number) and form drag reaches very high levels at angles of attack below normal clean wing stall.

The effect of upper surface roughness on complete aircraft configurations is less well known; however there is a long history of aircraft accidents related to flight in icing conditions, and several recent accidents, including the Air Ontario F-28 accident, involving swept-wing jet aircraft have highlighted the problem. In these situations it was observed that early flow separation and stalling was a characteristic result of ice and snow contaminants on the wing. Flow breakdown was accompanied not only by a loss of lift and an increase of drag, but also wing-dropping as a result of outer panel flow separation and wing tip stall prior to inboard wing stall. Experimental data on simulated upper surface contamination on a swept-wing model of a typical jet-commuter aircraft have confirmed what was suspected from flight experience, and have also demonstrated that large changes of trim will occur on the full-scale aircraft.

Figure (1a) from ref. (1) shows, for various two-dimensional airfoil configurations, losses in maximum lift and reductions the angle of attack for maximum lift that result from simulated hoar frost contamination. Large increases of drag also occur, and are attributed to form drag after separation and stall. Early wind tunnel tests on the effects of upper surface roughness on maximum lift of airfoils is also reported in reference (2), for conventional airfoils. This data shows that the loss of maximum lift is critically dependent on Reynolds Number, and also roughness particle size. For example at Reynolds Number greater than 10 million (typical for takeoff) the loss in maximum lift approaches 50% of the clean airfoil value. In comparison, at the

Reynolds number values typical of low speed wind tunnel testing the loss of maximum lift is much lower, thus highlighting the dangers of assessing wing contamination effects at other than full-scale conditions. There is little or no corresponding data for modern, supercritical airfoil shapes.

Wing drag also increases as a result of surface roughness. This is due to an increase in skin friction in unseparated flow, but mainly from increases in form drag after premature separation has occurred. If the roughness elements protrude above the laminar sublayer of the turbulent boundary layer in attached flow, the result is an increase of skin friction and the production of more turbulence. Increasing the Reynolds Number aggravates this effect and increases the probability of separation particularly around the nose, since the sub-layer will be thinner. This would presumably explain the higher losses in maximum lift incurred at high Reynolds number.

If the roughness height is large in comparison to the laminar sub-layer (as would be the case for freezing rain or ice accretion) then the frontal drag of these elements determines the average tangential force, and their shape, orientation and distribution become important, and increased turbulence and dissipation in the thickened boundary layer will lead to premature flow separation and stall.

Propeller-driven aircraft, where the slipstream passes over the wing surface, are thought to be less sensitive to the effects of upper surface contamination compared to the typical swept-wing configuration. This is due in part to the effects of sweep, that reduce the wing lift-slope, compared to a straight wing; and the effects of slipstream interaction, that augment span loading locally, increase wing lift slope, and also delay flow separation at high angles of attack. Thus the rotation angle on takeoff of a straight wing propeller-driven aircraft is likely to be less than that for an equivalent swept wing aircraft, with no slipstream interaction, and the likelihood of a premature stall may not arise.

Notwithstanding this apparent beneficial comparison, the propeller-driven aircraft may still experience significant losses of lift and large increases of drag if premature flow separation occurs when the wing upper surface is contaminated. Figure 1b from Ref. (1) for the Fokker F-27 turboprop transport wind tunnel model indicates however, that smaller losses in maximum lift may be expected from a contaminated wing, compared with the airfoil test results of Figure (1a). The corresponding reduction in critical angle of attack is also small and in some cases positive, and was attributed to a significant change in the wing-slipstream stall pattern. The extent to which the slipstream may remain attached to the wing surface is unknown but its influence may affect the overall stall pattern even when roughened by ice.

In view of the unknown nature of the complex interactions of wing boundary layer, propeller slipstream and distributed roughness, and the lack of experimental data, it was decided to use the half-wing propeller model of reference (3) to obtain some preliminary data on the effects of upper surface roughness in a slipstream and also the effects of typical in-flight ice accretion shapes on the leading edge. The utility of the data to aircraft design or performance estimation will be limited; the model configuration is not typical of current propeller transport configurations, and the test Reynolds Number was low (Re = 1.3 million).

MODEL

The general arrangement of the rectangular, unswept half-wing model is shown in figure 2. The wing, having a NACA 4415 airfoil section, was untwisted and was equipped with a 30 percent chord plain flap extending along the semi-span. The aspect ratio was 4.85. A nacelle containing a 20 hp water-cooled induction motor was underslung on the wing approximately one chord length above the floor. The four-bladed propeller was located 70% chord in front on the leading edge and was equipped with an adjustable pitch-setting mechanism. The two foot diameter propeller was the same model used in the investigations reported in references (3) and (4). In these reports full aerodynamic characteristics of the isolated propeller and also the interference effects of this wing model are reported. The relevant geometry of the propeller is listed as follows:

Propeller

Diameter	2.0 ft.
No. of blades	4
Solidity	0.127
Blade section at 0.75R	65 Series (design Cl = 0.7)

The complete model installation Figure, (2a), (2b), was mounted on the wind tunnel balance at the 30% chord location. The propeller motor was supported in a slender nacelle but did not have a separate thrust or normal force balance in this experiment. The wind tunnel balance thus measured the combined effects of wing and propeller reactions.

EXPERIMENTAL PROCEDURE

The wing was pitched through an angle of attack range from 6 to 26 degrees. A complete stall and flow breakdown was not achieved with this model due probably to the effects of the low aspect ratio, Reynolds number and the half-model configuration. Maximum lift was achieved however, and this was used as a basis of comparison for the effects of roughness. Model lift, drag and pitching moment were measured on the wind tunnel balance. Pitching moment was taken about the 30% chord location. The

measured forces include the propeller reaction comprised of thrust, normal force and pitching moment. The test Reynolds Number was 1.3 million (2.3 million for the unpowered wing only).

Propeller static thrust was measured on the wind tunnel balance under wind-off conditions. At the desired test conditions thrust was varied by adjusting the blade pitch settings to a value that corresponded approximately to the take off thrust coefficient of a typical turbo-prop aircraft. Under wind-on conditions at a dynamic pressure of 25 psf, and a propeller rotational speed of 3000 rpm, this thrust coefficient C_{T_p} was estimated from the data of ref. (5) to have a value of 0.115. Propeller thrust and normal force change with incidence, and the variation of these quantities, used in other section of this report, were also determined from the data of Ref. (5).

SIMULATED ROUGHNESS

Roughness, in the form of a uniform distribution of carborundum grit was applied over various portions of the chord. Three grades of standard grit were used: 150(.0041"), 80(.0083"), 46(.0165"). These correspond approximately to average roughness heights of .03", .06", and .11" respectively on a full-scale wing of 10 ft. chord. The roughness height/chord ratios for this test were 0.000227, .000461 and .000916 respectively. In addition a heavy grade (50 grit) of commercial sandpaper was applied to the wing surface. The roughness height and concentration of this application was considered to be significantly greater than the standard grit particles applied manually to the wing surface.

The roughness was applied initially to the upper surface from the leading edge stagnation region to the flap hinge line. Since only the forward portion of the chord was found to be sensitive however, most of the investigation was performed with only the first 25-30% of the chord roughened and the results presented in this report are for 30% coverage. The density of application was not varied or determined precisely.

In addition to distributed roughness application, shapes representing rime and glaze ice accretions were applied to the wing leading edge. The shapes were similar to those of ref. (6) and are shown in Figure (2c).

PRESENTATION OF RESULTS

Unpowered Wing

The unpowered wing data presents the effects of various grit sizes (46, 80, 150) deposited on the upper surface, and also a heavy grade of sandpaper attached to the upper surface. The amount of coverage along the chord corresponded to about 30%. Tests were also done at a higher Reynolds number (2.3 million), for the unpowered wing only.

Figure 3 shows the behaviour of Cl, Cd, and Cm for the unpowered wing in the clean and contaminated states for standard grit sizes at the test Reynolds number of 1.3 million, and for heavy sandpaper at Re = 2.3 million. The main effect of wing contamination is a reduction of lift slope and maximum lift by amounts that range between 20 - 25% for a Reynolds number of 1.3×10^6, and larger losses for the higher Reynolds number. The angle of attack for maximum lift (clean) was 20 degrees; this was reduced to about 15 degrees with contamination on the upper surface.

Drag is also increased at angles of attack below stall, and large increases of form drag occur when the flow separates. In general these losses, particularly at maximum lift, increase with particle size, with the highest loss occurring where sandpaper was applied to the wing (Fig. 3a). All reductions of lift increase with increasing Reynolds number as Reference (2) points out, and this is also the case in this test. The effect of roughness on pitching moment was small at angles of attack below stall; there appears to be a slight nose-up shift of the Cm versus α curve, and its magnitude increases slightly with grit size. The application of rough sandpaper at the high reynolds number increases this nose-up shift slightly.

The most significant parameters appear to be roughness size and Reynolds number, however it was observed that when a small portion (15%) of the leading edge was cleaned off, wing lift and drag was restored to close to its clean performance, however moment was not fully restored.

Powered Wing

With the blades installed and set to the angle for take-off thrust, the propeller was operated wind-on at an advance ratio of 1.4. This was much higher than a typical takeoff advance ratio, however it was the only way a high thrust coefficient could be achieved due to current and temperature limitations of the motor. As mentioned before propeller forces were not measured separately, however both thrust and normal force were inferred from the isolated propeller data of references (3) and (5) for further analysis of these results.

Figure (4) shows the effects of propeller thrust on lift, drag and pitching moment on the unpowered clean wing at a Reynolds number of 1.3 million. A higher Reynolds number test condition was not possible in the powered tests due to limitations of the motor. The application of power with the resulting slipstream interaction results in an increase of both the lift slope and the maximum lift by about 25%, and stalling angle is increased by about 4 degrees. The drag polar is shifted by an amount that corresponds to the thrust force plus a leading edge thrust on the wing due to increased suction. The drag equivalent of the estimated propeller thrust has a value of about 0.085, which, when subtracted from the total wing force at zero lift, apparently produces

a negative drag or thrust on the wing. This effect, known as the "Squire Effect", has been alluded to before (Ref. 7), and is attributed to the effects of flow rotation in the slipstream.

The pitching moment shown in figure (4c) exhibits an increased nose-up tendency due to the effects of the propeller and slipstream flow. The slope of the pitching moment curve vs α is increased with the application of power and beyond maximum lift there is a large nose-down shift of the pitching moment. The large change in moment is attributed mainly to the propeller normal force acting about the wing centre of rotation (Figure 2).

Effects of Roughness - Powered Wing

With roughness applied to the wing upper surface there appears to be a loss of lift slope and maximum lift of about 25 to 35% depending upon roughness element size. (Figure (5)). In effect, the benefits of powered lift, resulting from slipstream interaction, is lost. Drag also increases as the flow separates prematurely, and there also is an increase in the parasite drag at zero lift due to roughness, and increased dynamic pressure in the slipstream. The effect of roughness on wing pitching moment is small at angles of attack below stall, ($\alpha < 10°$) but the moment becomes more nose down as roughness size increases.

The application of the heavy sandpaper roughness further deteriorated the wing performance under power at the Reynolds number of 1.3 million. Maximum lift decreased slightly, as did the lift slope; although the stall was not sharply defined. Drag also increased near zero lift but the pitching moment did not change significantly, although the tendency continued to be nose-down.

A comparison was made between the powered and unpowered wing drag polars to show the relative effects of roughness with and without power (Figure 6). It is clear from these graphs that roughness, especially when it reaches the heavy proportions of sandpaper coverage, has a much more adverse effect on drag of the powered wing than for the unpowered wing in uniform flow. The lift curves exhibit about the same degree of degradation of performance between powered and unpowered configurations. The pitching moment change appears to be smaller when the wing is powered and is accompanied by an increase in slope (Cm vs alpha) and a small displacement in the nose up direction.

In order to simulate the scrubbing action of the slipstream, a portion of the roughness was removed at the propeller location. This resulted in a modest improvement of performance.

Wing-slipstream characteristics

In order to separate the propeller from the total wing forces, and to compare unpowered wing characteristics with those with the wing immersed in a slipstream, the isolated propeller data were estimated from Reference (5) and (Figure 7) and were removed from the wind tunnel balance data as follows:

$$C_{L_s} = C_L - (2/J^2)(D^2/S_w)[C_{T_p} \text{ Sin } \alpha + C_{N_p} \text{ Cos } \alpha] \quad (1)$$

$$C_{D_s} = C_D - (2/J^2)(D^2/S_w)[C_{T_p} \text{ Cos } \alpha - C_{N_p} \text{ Sin } \alpha] \quad (2)$$

$$C_{M_s} = C_M - (2/J^2)(D^2/S_w)\left[C_{N_p}\left(\frac{\bar{x}}{c}\right) + C_{T_p}\left(\frac{\bar{y}}{c}\right) + C_{M_p}\left(\frac{D}{c}\right)\right] \quad (3)$$

No attempt was made to correct the propeller data for the blockage and upwash effects of the wing; however the comments of Ref (8) and the experimental data of Ref (4) suggest that these interactions may be small.

The powered clean wing characteristics with the propeller reactions removed are shown in Figure (8). The lift curve lies between the powered and unpowered curves, suggesting that the slipstream interaction contributes about half of the powered lift increment to maximum lift, and lift-slope.

The drag polar (Figure 8) indicates significantly less drag due to the effects of the slipstream flow, particularly at low values of C_L (< 0.4), and near zero lift the wing actually produces a thrust. This has been attributed to the effects of slipstream rotation (Ref. 7), with the wing acting as a flow straightener. This result should probably be taken with caution, however, since no direct measurement of propeller thrust or normal force was available.

There appears to be a nose-down change in pitching moment when propeller forces are removed, since neither thrust or normal force are contributing (Figure 8c). The slipstream interaction evidently produces a lesser slope of the Cm vs α curve, and more nose-down moment, compared with the unpowered wing. A partial explanation of this change is given in Reference 4, and is attributed to changes in chordwise pressure distribution over the region of the wing covered by the slipstream.

Slipstream Interaction - Roughness

The loss of performance due to distributed roughness, for the wing-slipstream interaction, appears to be somewhat larger than that for the unpowered wing in steady uniform flow. This may be due to the high thrust coefficient of this test, and the resulting

augmentation of local pressures on the wing. Figure (9) shows lift ,drag and moment for the unpowered wing and for the wing immersed in a slipstream. Also shown is a shaded boundary that indicates the changes in drag due to increasing roughness in each case. The shaded areas in both graphs represent the maximum loss incurred by distributed roughness of varying grit size, including the heavy sand paper application. The negative drag generated on the wing near zero lift (Figure 9b) is all but removed by the action of the contamination on the nose and upper surface of the wing. In contrast the unpowered wing incurs a slightly lower drag loss due to roughness. At a lift coefficient Cls of about .36, the net drag is zero on the clean powered wing. For values of lift greater than this, drag rises rapidly, and eventually exceeds that of the unpowered wing since thrust is now no longer contributing a force in the streamwise direction and lift is reduced by the amount of the propeller normal force contribution. The effect of increasing roughness in both cases increases drag, particularly before stall.

The propeller contribution to pitching moment is mostly unstable (i.e. nose up). Therefore, removal of the propeller forces makes Cm more negative, and decreases the slope of the Cm vs α curve. The changes to pitching moment are relatively smaller when roughness is applied to the wing (Figure 9) compared to the clean condition. The slipstream interaction on the clean wing results in a slightly more stable pitching moment curve (Cms vs α) compared with the unpowered wing. The application of roughness causes, in both cases, a loss of stability in the pitching moment curves.

Leading edge ice accretion

In addition to uniform roughness on the wing upper surface, tests were also made with modifications to the leading edge that represented rime and glaze ice accretion (Figure 2). The data shown in Figure (10) for the unpowered wing show that such gross changes to the leading edge profile cause losses of maximum lift in the 30 to 50 percent range. Reynolds number is important and a further reduction of maximum lift of 15 to 20% will occur when reynolds number is increased to 2.3 million. Similar significant changes to pitching moment also arise from these leading edge shapes, particularly at high Reynolds numbers.

With the application of power, lift slope and maximum lift are increased but the wing performance is well below normal and the drag polars indicate high drag levels at all lift coefficients. Figure (11) shows a comparison between uniform contamination and leading edge accretion of heavy rime ice, for the drag polars and pitching moments of the ice-contaminated wing for the powered configuration. Leading edge ice results in less reduction of lift slope before stall, but a larger lift loss after stall.

Figure (11d) shows the effect of a slipstream interaction on the wing lift and drag for a medium and heavy leading edge rime accretion. As with distributed roughness,

leading edge ice contamination effectively removes the benefits of slipstream flow rotation.

Chord force and leading edge suction

The effective performance of an airfoil or wing depends on the production of negative pressures along the leading edge, and a leading edge suction force that ensures that the aerodynamic force becomes normal to the relative wind. The determination of the chord force coefficient C_c and the leading edge suction coefficient C_s indicate the degree to which lifting efficiency can be achieved.

C_c and C_s can be determined from experimental data as follows:

$$C_c = C_D \cos \alpha - C_L \sin \alpha \quad (4)$$

and for small angles

$$C_s = C_{D_o} - C_c \quad (5)$$

C_c and C_D can also be determined from the parabolic drag polar relationship (Ref. 9). Figure 12a shows the relationship between unpowered wing drag C_D and chord force C_c, and the effects of distributed roughness on both parameters, for the unpowered wing. It appears that roughness has a relatively larger effect on drag than on chord force.

Corresponding values of leading edge suction coefficient for the unpowered wing also show the effects of contamination. Below stall C_s is not greatly diminished by contamination around the nose, but drops suddenly beyond maximum lift.

Figure (12c) shows chord force vs. lift coefficient for the powered wing with leading edge ice and roughness, and with the propeller forces removed. The accretion of ice tends to lower the leading edge force at low values of C_{L_s} , but distributed roughness appears to have a more serious effect at higher lift coefficients.

CONCLUSIONS

1) The main effect of distributed upper surface roughness on an unpowered wing is to reduce lift slope and maximum lift by as much as 30 to 50 percent, depending upon roughness size, Reynolds number, and to a lesser extent, coverage.

2) The magnitude of the loss of maximum lift increases with roughness size, and also with Reynolds number and testing of roughened wings should be done at as high a Reynolds number as possible.

3) Roughness increases the parasite drag at zero lift and also results in a premature stall with resulting large increases of form drag.

4) The leading edge region is especially sensitive to distributed roughness regardless of particle size; there is a significant increase in drag and corresponding decrease of leading edge suction at angles of attack below stall. Conversely, removal of the roughness over a small portion of the nose restores the wing to almost clean performance.

5) If the wing is powered and clean, the slipstream interaction increases lift slope and maximum lift by 25 percent, for thrust coefficients appropriate to the take-off condition. If roughness is applied, maximum lift decreases by more than 25%, thus producing a lifting performance somewhat below the unpowered wing in the clean state. This may have significance in the event of an engine failure; the contaminated wing will suffer a further loss in maximum lift in the unpowered state.

6) An attempt was made to isolate the slipstream interaction on the wing by subtracting estimated propeller forces. When comparing the performance of the powered and unpowered wings, it was noted that roughness produced slightly higher losses on the wing immersed in the slipstream.

7) Loss of lift due to an accretion of rime or glaze ice on the leading edge of the wing may reach as high as 50 percent even when the wing is powered, and is sensitive to Reynolds number. Loss of maximum lift is greater for heavy rime ice than for heavy distributed roughness.

LIST OF REFERENCES

1. Wing Tips - Fokker product support division, #14, December 1989.

2. Jones, R., Williams, D.H. - The effect of Surface Roughness on the Characteristics of Airfoils. RAE R&M 1708, Feb. 1936.

3. Nishimura, Y. - An Experimental Investigation by Force and Surface Pressure Measurements on a Wing Immersed in a Propeller Slipstream. Part I: Force and Moment Measurements. NRC-CR-501, March 1968.

4. Nishimura, Y. - Surface Pressure Measurements Part II, NRC LR-525, June 1969.

5. Wickens, R.H. - Aerodynamic Force and Moment Characteristics of a Four-Bladed Propeller Yawed through 120 Degrees. NRC-LR-454. May 1966.

6. Olson, W., Shaw, R., Newton, J. - The Shapes and the Resulting Drag Increase for a NACA 0012 Airfoil, NASA TM 83556, 1984.

7. Squire, H.B., Chester, W. - Calculation of the Effect of Slipstream on Lift and Drag. ARC R&M 2368, 1950.

8. Durand, Vol II. Aerodynamic Theory.

9. Schlichting, H., Truckenbrodt, E. - Aerodynamics of the Airplane - McGraw-Hill 1979.

10. Morgan, J.M., Wagner, G.A., Wickens, R.H. - A Report of the Flight Dynamics of the Fokker F-28 mk 1000 as they pertain to the accident at Dryden, Ontario, March 1989. NRC/NAE misc. 64

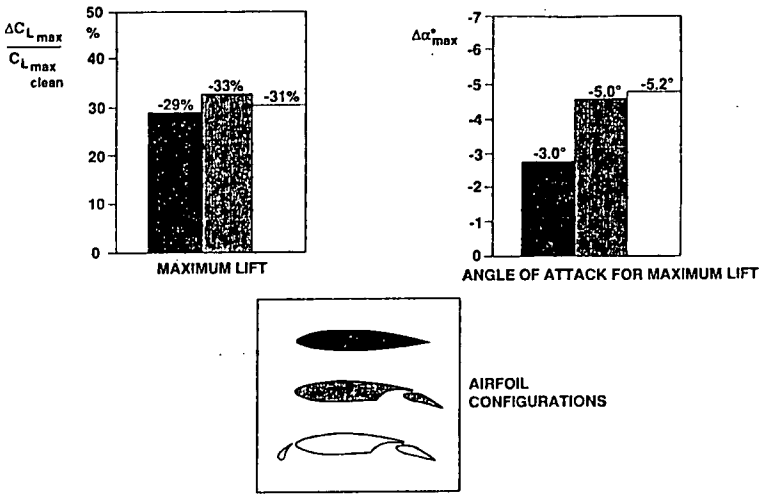

WING-ROUGHNESS-INDUCED LOSS OF MAXIMUM LIFT AND REDUCTION IN ANGLE OF ATTACK FOR MAXIMUM LIFT (REF. 1)

FIGURE 1

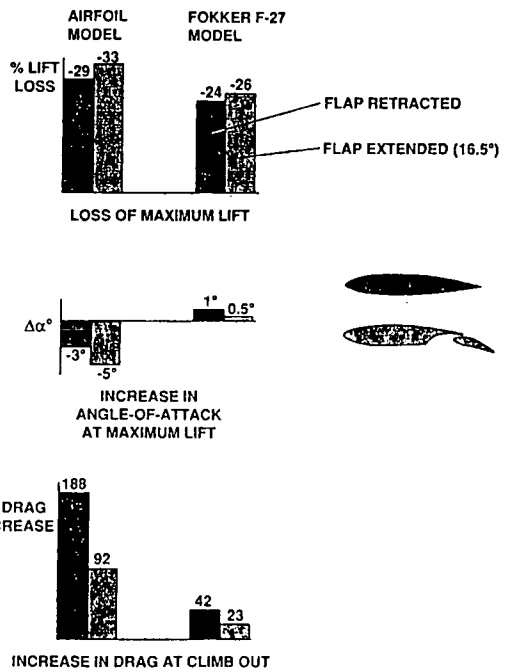

COMPARISON OF LIFT LOSS AND DRAG RISE FOR AIRFOIL AND PROPELLER-SLIPSTREAM MODELS

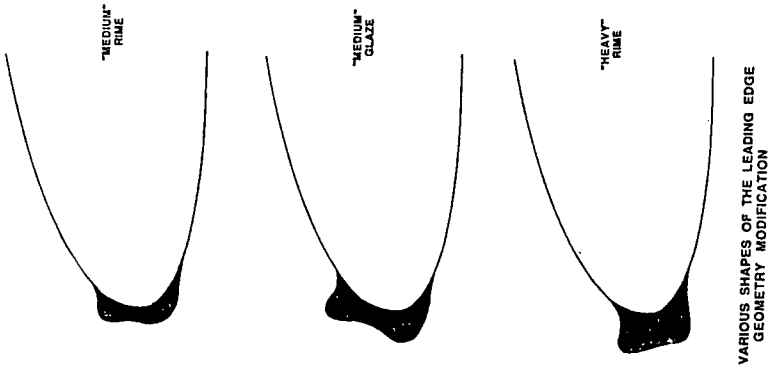

VARIOUS SHAPES OF THE LEADING EDGE GEOMETRY MODIFICATION

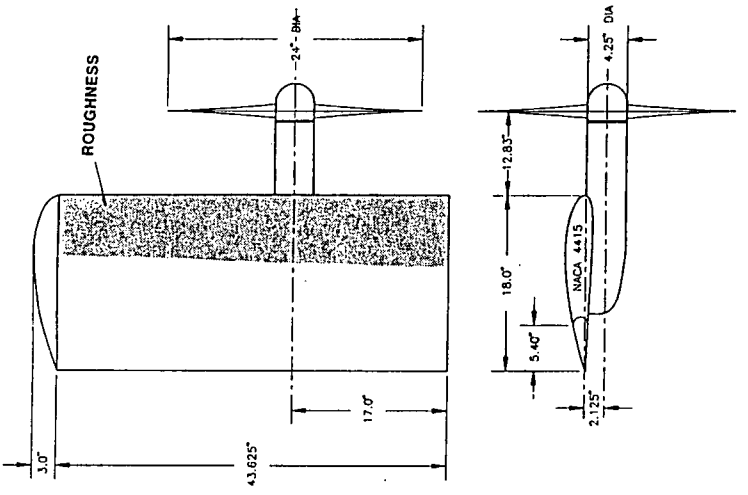

PLAN AND CROSS-SECTIONAL VIEW OF MODEL

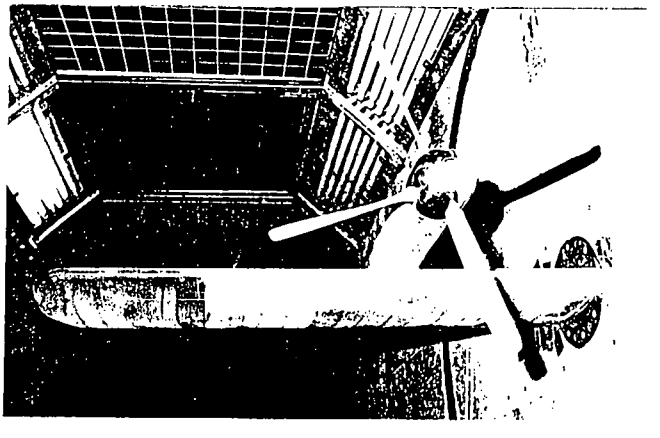

WING-PROPELLER MODEL WITH DISTRIBUTED ROUGHNESS

FIGURE 2

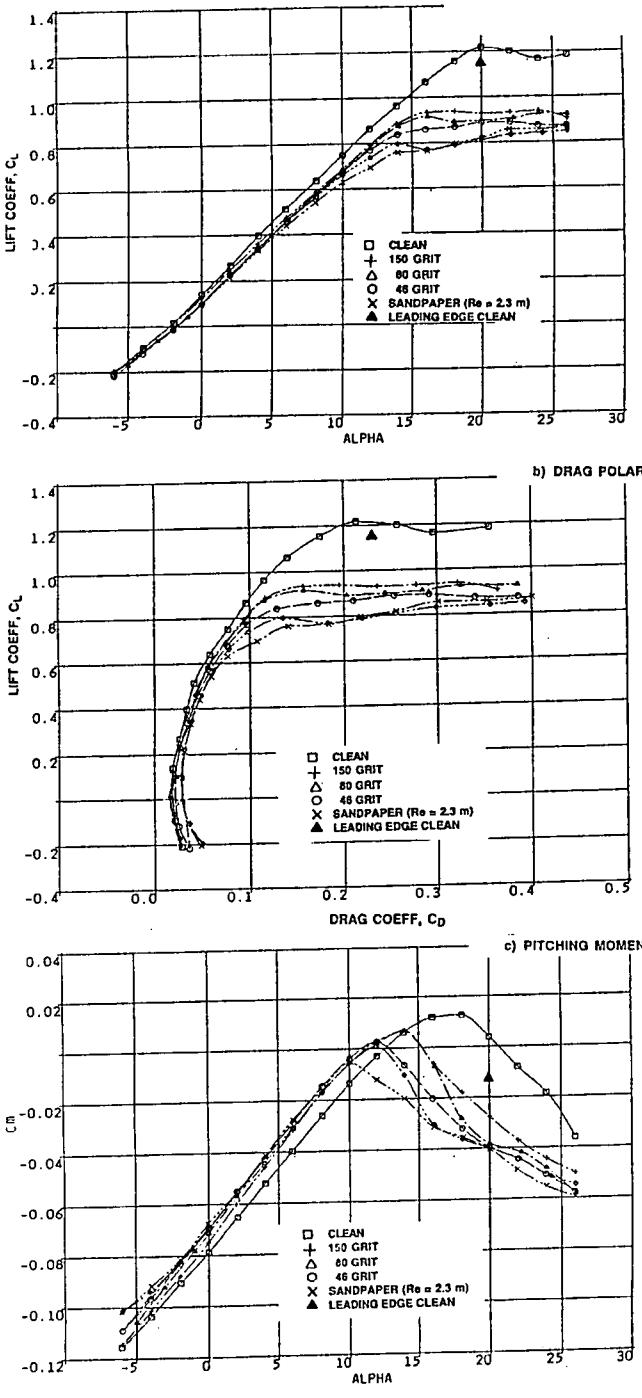

FIGURE 3

EFFECTS OF UNIFORM ROUGHNESS ON UNPOWERED WING PERFORMANCE, Re = 1.3 m, 30% COVERAGE

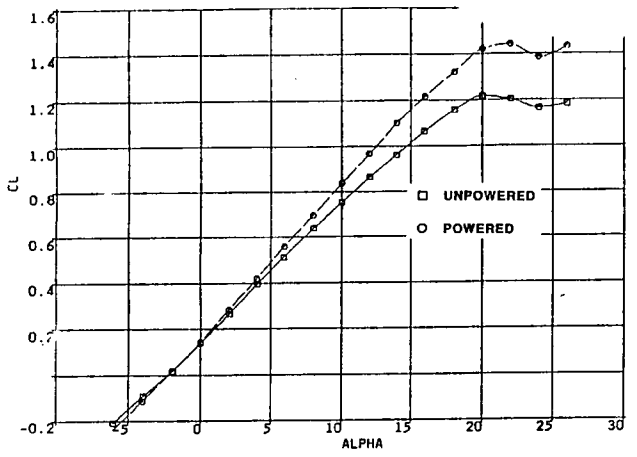

FIGURE 4

a) LIFT

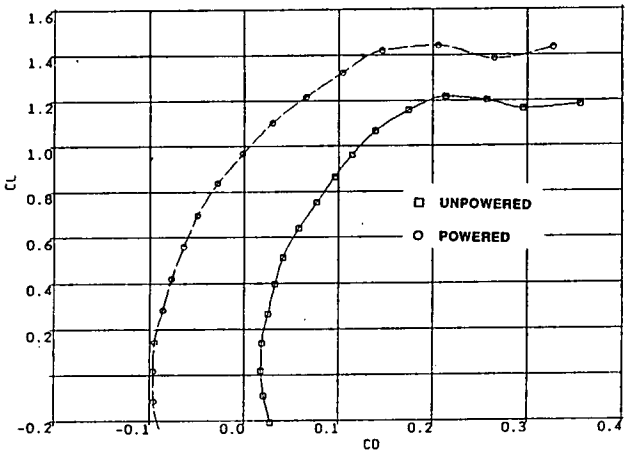

b) DRAG

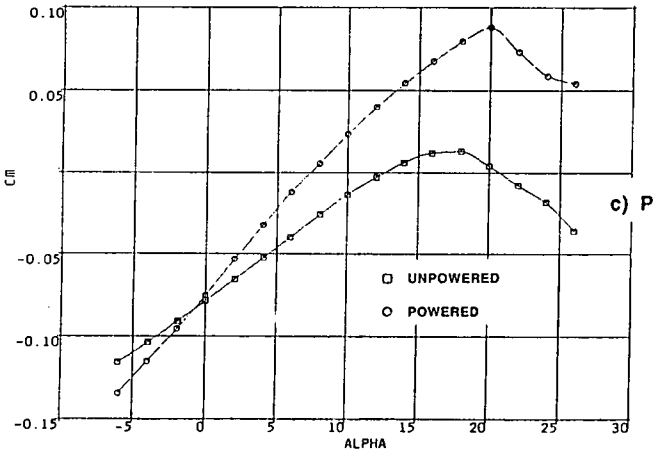

c) PITCHING MOMENT

COMPARISON OF POWERED AND UNPOWERED CLEAN WING PERFORMANCE C_{T_p} = 0.115, Re = 1.3 m

FIGURE 5

a) LIFT

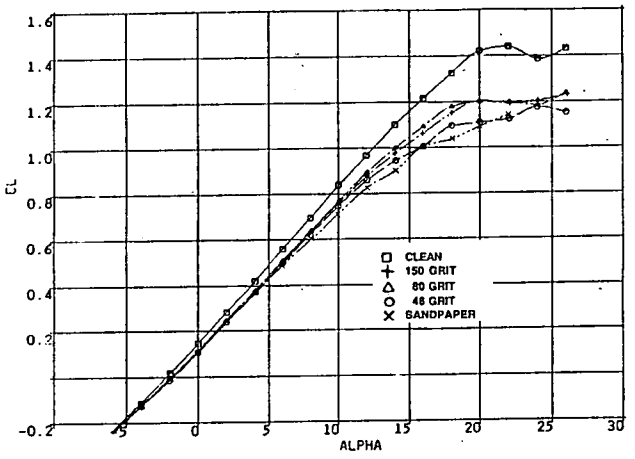

b) DRAG POLAR

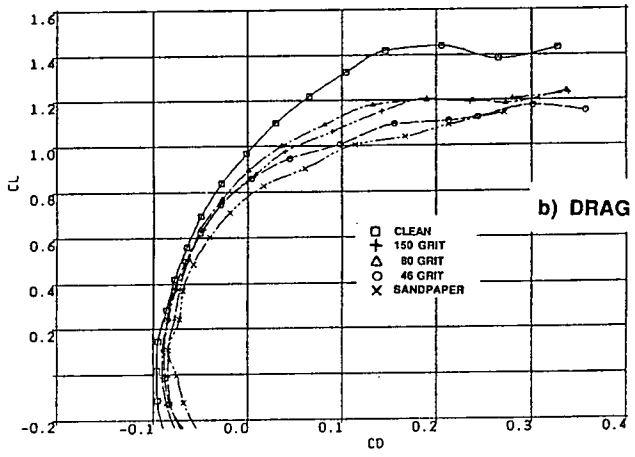

c) PITCHING MOMENT

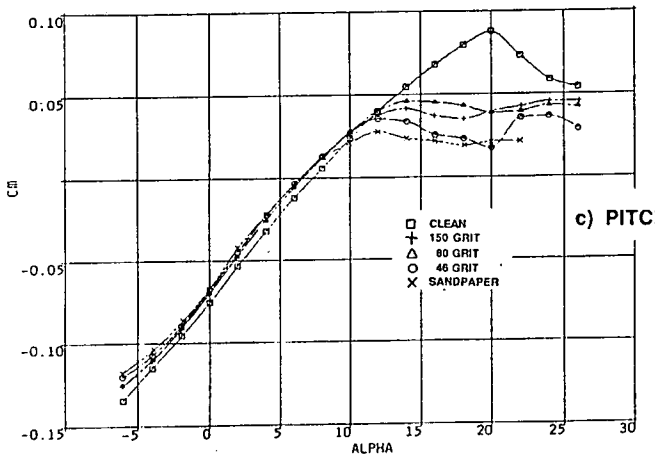

EFFECT OF UNIFORM ROUGHNESS ON POWERED WING PERFORMANCE, C_{T_p} = 0.115, Re = 1.3 m

FIGURE 6

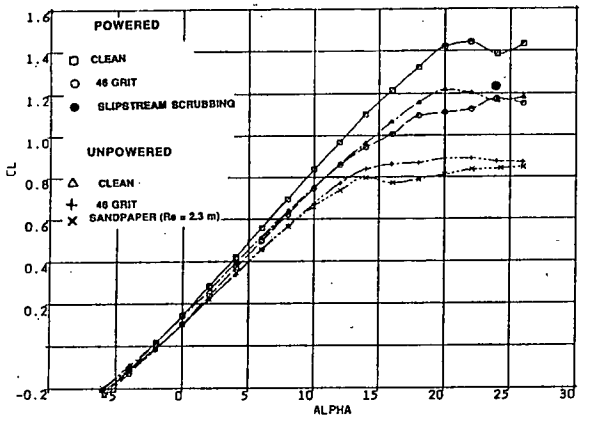

a) LIFT

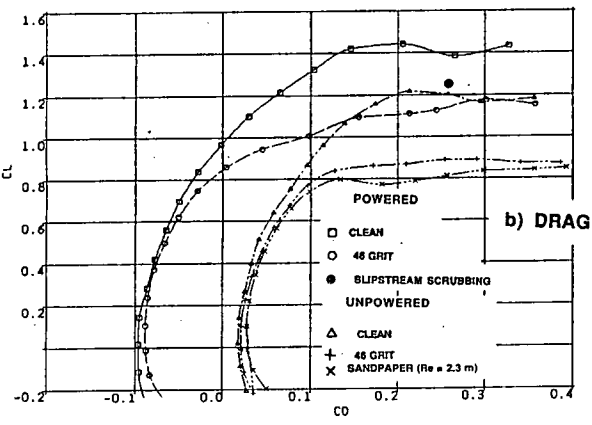

b) DRAG POLAR

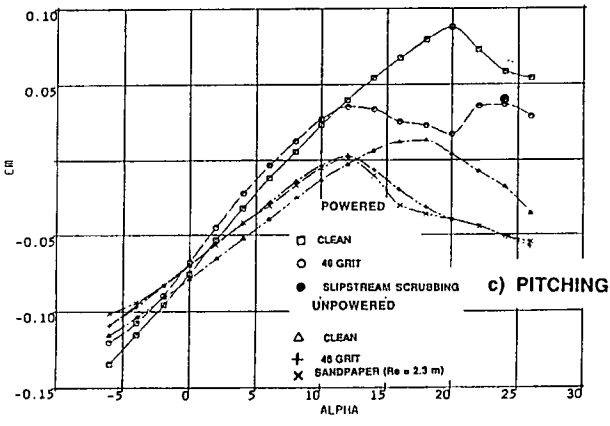

c) PITCHING MOMENT

COMPARISON OF EFFECTS OF UNIFORM ROUGHNESS ON POWERED AND UNPOWERED WING, 46 GRIT, 30% COVERAGE, C_{T_p} = 0.115, Re = 1.3 x 10^6

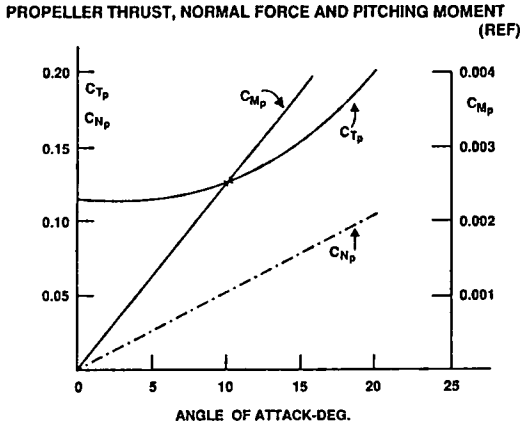

FIGURE 7

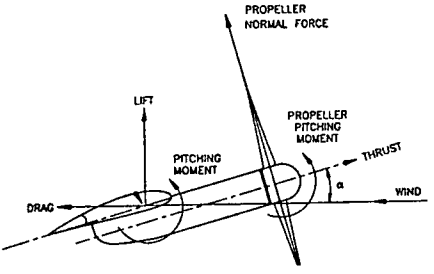

CONVENTION OF FORCES, MOMENTS AND ANGLE

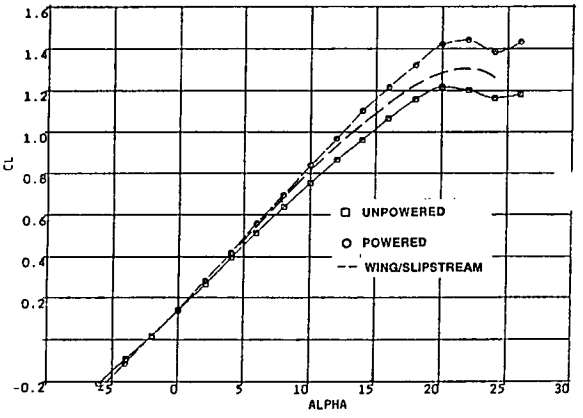

FIGURE 8

a) LIFT

REMOVAL OF PROPELLER REACTIONS FROM THE CLEAN, POWERED WING, C_{T_p} = 0.115, Re = 1.3 m

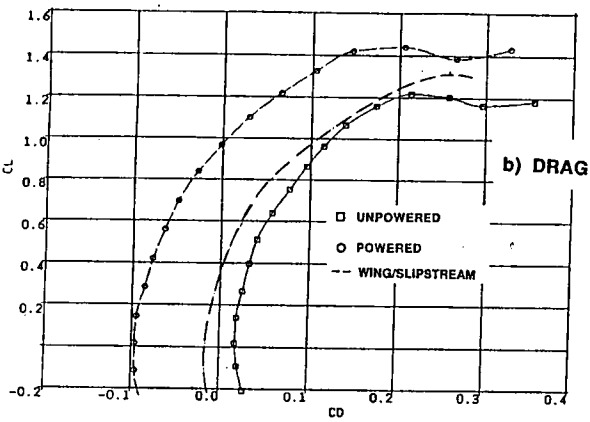

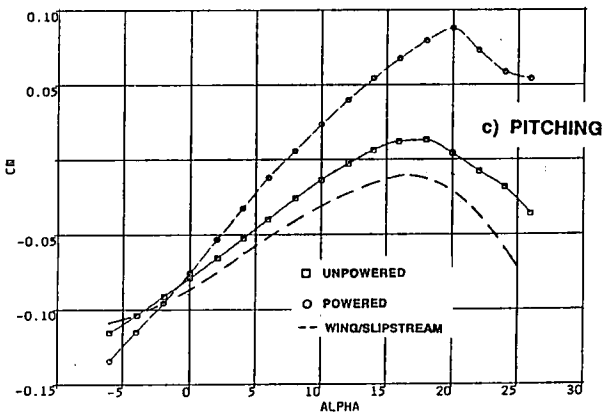

FIGURE 8

REMOVAL OF PROPELLER REACTIONS FROM THE CLEAN, POWERED WING, C_{T_p} = 0.115, Re = 1.3 m

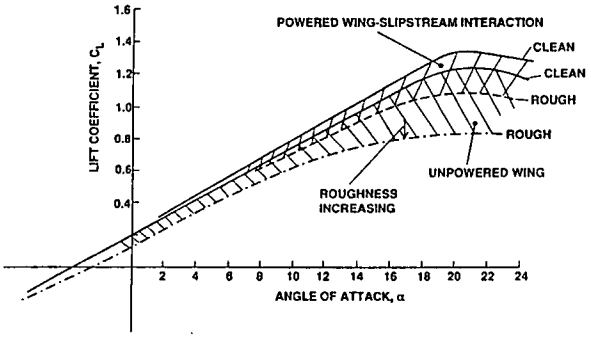

FIGURE 9

COMPARISON OF LIFT LOSS DUE TO DISTRIBUTED ROUGHNESS, OF AN UNPOWERED WING, AND A POWERED WING WITH PROPELLER REACTIONS REMOVED. C_{T_p} = 0.115, Re = 1.3 x 10^6

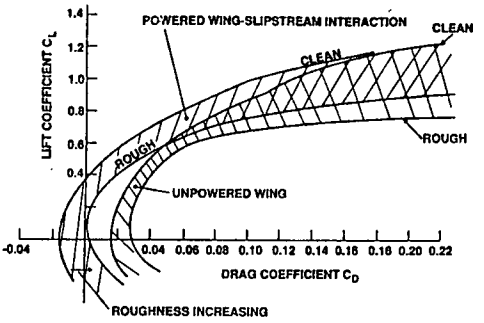

FIGURE 9

COMPARISON OF DRAG LOSSES DUE TO DISTRIBUTED ROUGHNESS, OF AN UNPOWERED WING AND A POWERED WING WITH PROPELLER REACTIONS REMOVED.
C_{T_p} = 0.115, Re = 1.3 x 10^6

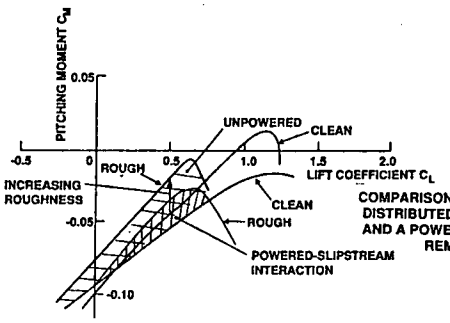

COMPARISON OF PITCHING MOMENT CHANGES DUE TO DISTRIBUTED ROUGHNESS, OF AN UNPOWERED WING AND A POWERED WING WITH PROPELLER REACTIONS REMOVED. C_{T_p} = 0.115, Re = 1.3 x 10^6

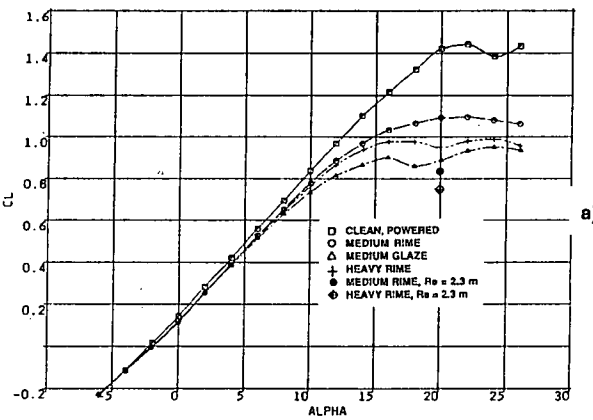

FIGURE 10

a) LIFT

EFFECT OF LEADING EDGE ICE ON POWERED WING PERFORMANCE,
C_{T_p} = 0.115, Re = 1.3 m

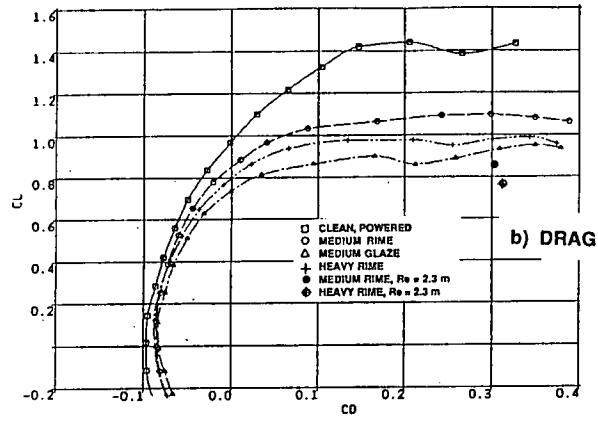

FIGURE 10

b) DRAG POLAR

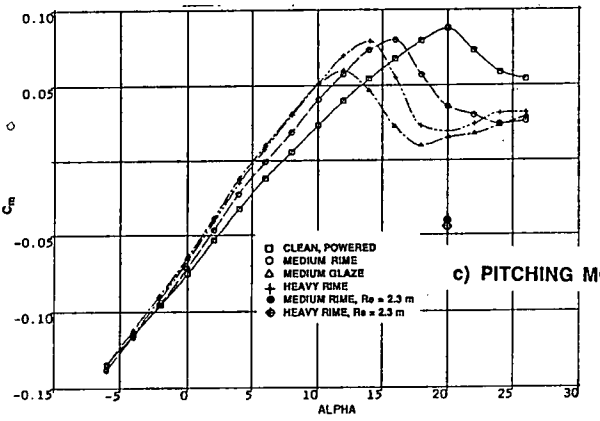

c) PITCHING MOMENT

EFFECT OF LEADING EDGE ICE ON POWERED WING PERFORMANCE, C_{T_p} = 0.115, Re = 1.3 m

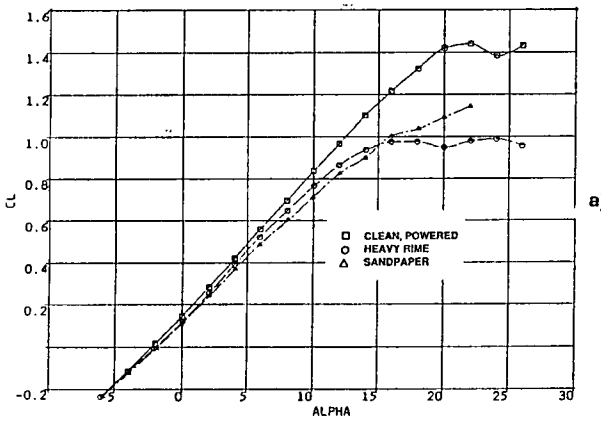

FIGURE 11

a) LIFT

COMPARISON OF LEADING EDGE ICE AND UNIFORM ROUGHNESS, C_{T_p} = 0.115, Re = 1.3 m

FIGURE 11

COMPARISON OF LEADING EDGE ICE AND UNIFORM ROUGHNESS, C_{T_p} = 0.115, Re = 1.3 m

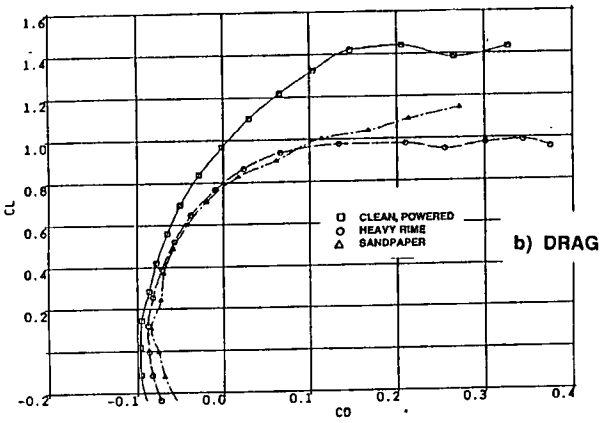

b) DRAG POLAR

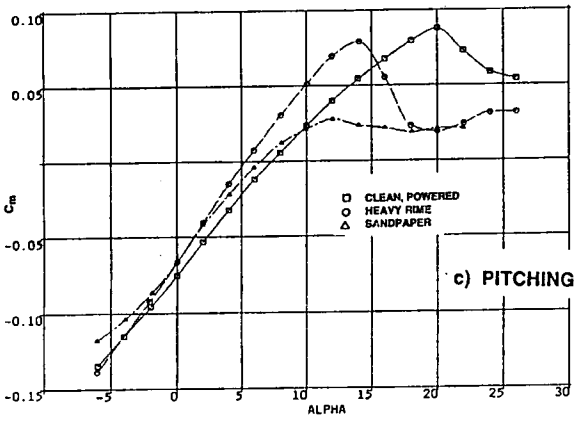

c) PITCHING MOMENT

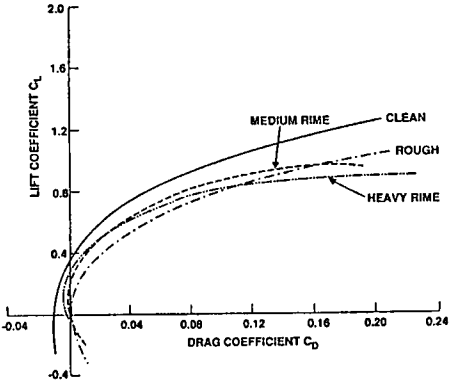

DRAG POLAR
COMPARISON OF DISTRIBUTED ROUGHNESS (50 GRIT SANDPAPER) AND LEADING EDGE ICE FOR POWERED WING-SLIPSTREAM INTERACTION (PROPELLER REACTIONS REMOVED) C_{T_p} = 0.115, Re = 1.3 x 10^6

FIGURE 12

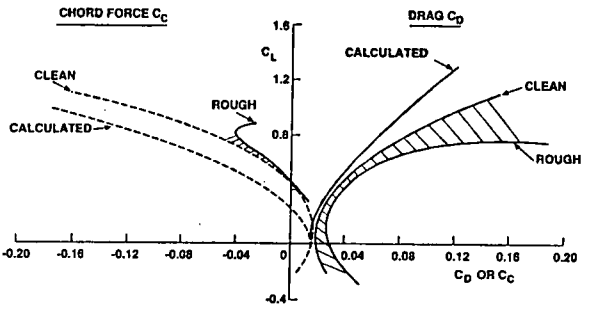

COMPARISON OF DRAG AND CHORD FORCE FOR CLEAN AND ROUGHENED UNPOWERED WING (50 GRIT SANDPAPER)

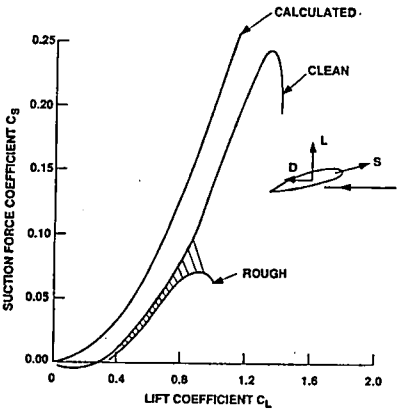

LEADING EDGE SUCTION FORCE COEFFICIENT FOR CLEAN AND ROUGHENED UNPOWERED WING

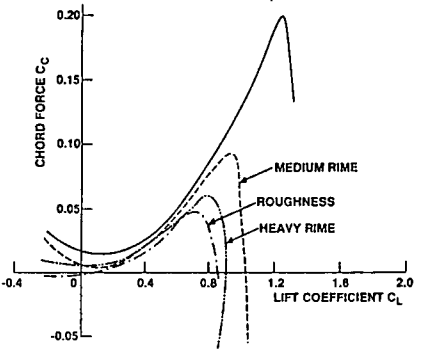

CHORD FORCE vs LIFT COEFFICIENT
COMPARISON AND LEADING EDGE ICE FOR POWERED WING-SLIPSTREAM INTERACTION (PROPELLER REACTIONS REMOVED) $C_{T_p} = 0.115$, $Re = 1.3 \times 10^6$